Ligand-functionalized and ligand-bridged or organyl-separated chalcogenido metalate-based clusters

Zhou Wu [1], Mirko Tallu [1], Gina Stuhrmann [1], Stefanie Dehnen [*]

Institute of Nanotechnology (INT) and Karlsruhe Nano Micro Facility (KNMF), Karlsruhe Institute of Technology (KIT), Hermann-von-Helmholtz-Platz 1, 76344 Eggenstein-Leopoldshafen, Germany

A R T I C L E I N F O

Keywords:
Chalcogenido metalate-based compounds
Cluster chemistry
Ligand-functionalization
Ligand-bridges
Organyl spacers

A B S T R A C T

Chalcogenido metalate-based clusters, comprising cluster cores with directly bonded metal cations and chalcogenide anions, have been a focus of inorganic and materials research for decades, owing to their structural elegance and captivating catalytic-related and optical-related properties. The introduction of a ligand sphere to functionalize, bridge, or separate these clusters can help to stabilize and control the topology as well as chemical and physical properties of such compounds owing to interactions between clusters and ligands. In addition, this multiplied the product spectrum in the chalcogenido metalate-based cluster family. In this article, we give an overview of the recent developments of ligand-functionalized and ligand-bridged or organyl-separated chalcogenido metalate-based compounds. For this, we selected some prototypical cluster families, ranging from supertetrahedral clusters and cluster of related compositions but other structural motifs, to coinage metal clusters and compounds based on octahedral transition metal arrangements. By summarizing the research on these species, this review will provide a general overview of the syntheses and structures of selected contemporary ligand-functionalized and ligand-bridged or organyl-separated cluster compounds, contribute to understand the

Abbreviations: ($C_{10}C_1Im$), 1-Decyl-3-methylimidazolium; (C_1im), 1-Methylimidazole; (C_2C_1Im), 1-Ethyl-3-methylimidazolium; (C_2im), 2-Ethylimidazole; ($C_4C_1C_1Im$), 1-Butyl-2,3-dimethylimidazolium; ($C_4C_1C_4Im$), 1,3-Dibutyl-2-methylimidazolium; (C_4C_1im), 1-Butyl-2-methylimidazole; ($C_4C_4C_1Im$), 1,2-Dibutyl-3-methylimidazolium; ($C_5C_1C_5Im$), 1,3-Dipentyl-2-methylimidazolium; ($C_6C_1C_6Im$), 1,3-Dihexyl-2-methylimidazolium; ($C_3C_1C_3Im$), 1,3-Dipropyl-2-methylimidazolium; (C_6C_1im), 1-Hexyl-3-methylimidazole; 0/1/2/3D, 0/1/2/3-dimensional; 1,2-dap, 1,2-Diaminopropane; 2,4-DMBT, 2,4-Dimethylbenzenethiolate; 2,5-DMBT, 2,5-Dimethylbenzenethiolate; 2-TBI, 2-Thiobenzimidazol; A/M/TM/Ch/X, Alkali metal/Metal/Trnanasition metal/Chalcogen/Halogen; BDT, 1,2-Benzenedithiolate; 5, 6-C_1C_1Bim, 5,6-Dimethyl-benzimidazole; BPE, 1,2-Bis(4-pyridyl)ethane; BPP, 1,3-Bis(4-pyridyl)propane; bpy, 4,4′-Bipyridine/-yl; bpy-CH_3, 3-Methyl-4,4′-bipyridine/-yl; bpy-NH_2, 3-Amino-4,4′-bipyridine/-yl; BTC, Benzenetricarboxylate; Bu, Butyl; Cat, Cation; CB, Carbon Black; cv, Crystal violet; CV, Cyclic voltammetry; dach, 1,2-Diaminocyclohexane; DBN, 1,5-Diazabicyclo[4.3.0]non-5-ene; DBU, 1,8-Diazabicyclo[5.4.0]undec-7-ene; DCM, Dichloromethane; Dec, Decyl; dien, Diethylenetriamine; DMA, Dimethylacetamide; DMF, N,N-Dimethylformamide; dmid, 1,3-Dithia-2-one-4,5-dithiolate; dmit, 1,3-Dithia-2-thione-4,5-dithiolate; dmmp, 2,6-Dimethylmorpholine; DOBzQA, 2-(1,3-dioxobenzo[de]isoquinolin-2-yl)acetate; DPE, 1,2-Bis(4-pyridyl)ethylene; dppb, Bis(diphenylphosphanyl)butane; dppbp, 4,4′-Bis(diphenylphosphanyl)biphenyl; dppm, Bis(diphenylphosphanyl)methane; dppp, 1,3-Bis(diphenylphosphanyl)propane; dppxy, 1,4-Bis(diphenylphosphinomethyl)benzene; dith, 1,3-Dithia-2-thione-4,5-diselenolate; en, Ethane-1,2-diamine; ESI, Electrospray ionization; fdc, Furan-2,5-dicarboxylate ligands; H_2DOT, 2,5-Dihydroxyterephthalic acid; H_3msa, Mercaptosuccinic acid; H_3nta, Nitrilotriacetic acid; H_4PTC4A, *p*-Phenyl-thiacalix[4]arene; H_4TC4A, *p*-Tert-butylthiacalix[4]arene; HER, Hydrogen Evolution Reaction; HSCy, Cyclohexanethiol; HTBP, Hexadecyltributylphosphonium; Hx, Hexyl; IL, Ionic Liquid; IM, Imidazolate; im, Imidazole; Im, Imidazolium; LSV, Linear Sweep Voltammogram; *m*-BDT, 1,3-Benzenedithiol; Me, Methyl; MeCN, Acetonitrile; mo, Methyl Orange; MS, Mass Spectrometry; NHC, *N*-heterocyclic carbene; NMR, Nuclear Magnetic Resonance; ORR, Oxygen Reduction Reaction; ox, Oxalate; *p*-BDT, 1,4-Benzenedithiol; PDI, 1,4-Phenylene diisocyanide; PEG-400, Polyethylene glycol 400; PFBT, Pentafluorobenzenethiol; Ph, Phenyl; PL, Photoluminescence; Pn, Pentyl; Pr, Propyl; ^{p}Tos, *p*-Toluenesulfonate; py, Pyridine; pyz, Pyrazine; rt, Room temperature; SCCAM, Supertetrahedral chalcogenolate cluster-based assembled material; SCIF, Supertetrahedral cluster imidazolate framework; SCTF, Supertetrahedral cluster-based triazolate framework; SC-XRD, Single-crystal X-ray diffraction; SDS, Sodium dodecyl sulfate; solv, Solvent molecules; TBT, Tertiarybutylthiolate; TCNQ, Tetracyanoquinodimethane; TCPP, Tris(4-chlorophenyl)phosphine; TEPA, Tetraethylenepentamine; TFA, Trifluoroacetate; Tfd, Bis(trifluoromethyl)-1,2-dithiolate; TMDC, Transitional metal dichalcogenide; TMDP, 4,4′-Trimethylenedipiperidine; TMSD, (Diazomethyl)trimethylsilane; Tos, Toluenesulfonate; TPOM, tetrakis(4-pyridyloxymethylene)methane; TPPA, Tris(4- pyridylpheny)amine; tppe, 1,1,2,2-Tetrakis(4-(pyridine-4-yl)phenyl)-ethene; tpt, 2,4,6-Tri-4-pyridyl-1,3,5-triazine; TPyP, 5,10,15,20-Tetra(4-pyridyl)porphyrin; trien, Triethylenetetraamine; TZ, 1,2,4-Triazolate; UV–vis, Ultraviolet–visible.

* Corresponding author.
E-mail address: stefanie.dehnen@kit.edu (S. Dehnen).

[1] These authors contributed equally to this work.

formation of the molecular structures and give some further insights into the effects of their functional modifications.

1. Introduction

Cluster molecules are often regarded as atomically precise intermediates between small(er) molecular compounds and nano particles or bulk solids, both lacking the atomic precision [1–3]. The development of cluster chemistry is therefore of significance to understand the nature of chemical bonding and reactivity at molecular scale, and leading to unique fundamental properties and practical applications of solid-state compounds that can be precisely controlled [4–8]. The last half century has witnessed the explosive growth of a wide spectrum of cluster families ranging from non-metal clusters to clusters comprising only metal atoms or a mixture of both. Examples are fullerenes [9], boranes [10], chalcogenido metalates [11], polyoxo metalates [12], and Zintl clusters [13], amongst many others. Owing to a combination of their structural beauty, a rich variety of compositions and structures, as well as a number of appealing catalytic and optical properties, chalcogenido metalate-based clusters have stood out [14–16]. Therefore, they are in the focus of this article.

Chalcogenido metalate-based clusters are composed of either transition metal [17] or main-group metal cations [18], or a mixture of both [19], which are linked by chalcogenide ligands. They may be classified in a variety of ways, one of which is a classification by the type of the cluster architecture. This review mainly focuses on the families of supertetrahedral chalcogenido metalate clusters, silver chalcogenide nanoclusters, and octahedral Chevrel-type cluster molecules.

The most prominent supertetrahedral chalcogenido metalate clusters belong to the T*n*, P*n*, and C*n*(,*m*) families (for a definition of the respective cluster types, see Section 2) [20]. They are constructed by corner-sharing or corner-linked $[MCh_4]^{q-}$ subunits (M = metal cations; Ch = S^{2-}, Se^{2-}, Te^{2-}). Selected examples are shown in Fig. 1.

Coinage metal nanoclusters can be described as a combination of "M_2Ch" or M (M = Cu, Ag, Au) in a cluster core of rather spherical symmetry, which is surrounded by chalcogenolate ligands [15,21–25],

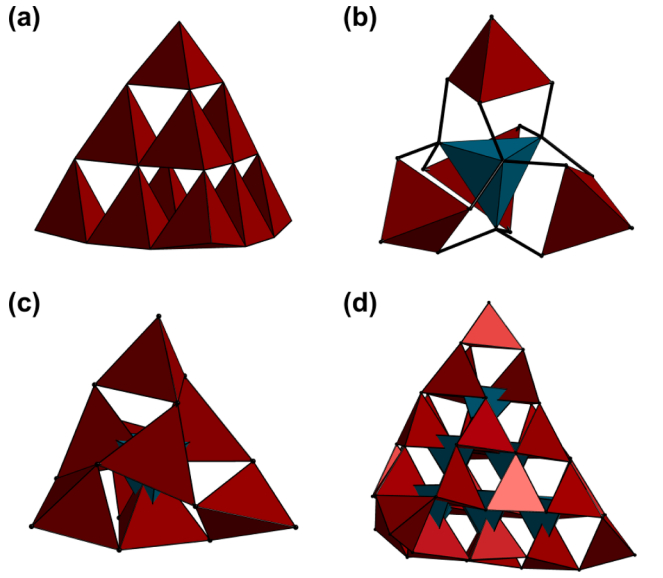

Fig. 1. Selected examples of the T*n*, P*n*, and C*n*(,*m*) supertetrahedral chalcogenido metalate cluster families. (a) T3-$[M_{10}Ch_{16}X_4]^{q-}$. (b) P1-$[M_8Ch_{13}X_4]^{q-}$. (c) C0-$[M_8Ch_{13}X_4]^{q-}$. (d) C2,1-$[M_{32}Ch_{50}X_4]^{q-}$. M metal atoms, Ch chalcogen atoms, X terminal anions or ligands, q charges. T1-type $[MCh_4]^{q-}$ units are shown as a dark-red colored polyhedra, anti-T1-type $[ChM_4]^{q+}$ units are shown as teal colored polyhedra.

with many of the prototypic examples being based on silver chalcogenides. Clusters that refer to Chevrel phases [26] are based on molecules with the general formula of $[M_6Ch_8]^{q-}$ as building units. In this structure, octahedra of metal atoms are enclosed by eight face-capping chalcogenide ligands. All of these cluster types are discussed in more detail in the respective chapters within this article.

Although there are reports on naked chalcogenido metalate-based clusters, including record holders in size [27–29], most reported molecules based on polynuclear M/Ch motifs are decorated with ligands for functionalizing, bridging, or separating the cluster moieties and are in the focus of this review [30–32]. Ligand functionalization not only stabilizes the chalcogenido metalates, but also plays a significant role to control the size and assembly/packing of the compounds in the solid materials [15]. Furthermore, their properties can be effectively modified through introducing specific ligands. For instance, the attachment of redox-active ferrocene-based groups to the clusters endows them with an electrocatalytic activity, and the decoration with amine groups has been shown to trigger fluorescence [33]. Their addition is also helpful to improve the solubility of chalcogenido metalate-based clusters in standard organic solvents, which opens up the door to many analytical methods, such as mass spectrometry (MS), nuclear magnetic resonance (NMR) spectroscopy, and transmission electron microscopy (TEM) for instance, to better understand the molecular structures and investigate the formation mechanisms of such clusters in specific cases [34,35]. Overall, such organic–inorganic hybrid materials show a promising application potential within nano-chemistry and reticular chemistry.

As a comprehensive overview of all known and reported chalcogenido metalate-based clusters would rather fill a book than a review article, we concentrate on some types of corresponding cluster compounds, which turned out to be particularly topical in recent years. We discuss the syntheses and structures of selected ligand-functionalized and ligand-bridged or organyl-separated chalcogenido metalate-based compounds (Scheme 1) of the types briefly introduces above, and properties that stem from their specific compositions and structures. We split the contents into the following chapters: 2. Ligand-functionalized and ligand-bridged supertetrahedral chalcogenido metalate-based compounds; 3. Ligand-functionalized and organyl-separated chalcogenido metalate-based compounds exhibiting other cluster architectures—ranging from discrete to polymeric units with more unusual (sub) structures; 4. Ligand-functionalized silver chalcogenide cluster-based compounds—ranging from chalcogenide/chalcogenolate-functionalized species to polymers; 5. Ligand-functionalized and ligand-bridged transition metal chalcogenides based on $\{Re_6Se_8\}$, $\{Co_6Se_8\}$, $\{Mo_3Ch_x\}$ (x = 4, 7), $\{Fe_4S_4\}$, or $\{Co_4S_4\}$ units. In chapter 6, we refer to the persisting challenges and give an outlook for this specific area of cluster chemistry, as we hope that this review contributes to the continuous developments of these fields in the near future.

2. Ligand-functionalized and ligand-bridged chalcogenido metalate-based compounds

2.1. Ligand-functionalization of discrete supertetrahedral chalcogenido metalate-based clusters

Supertetrahedral chalcogenido metalate-based clusters (*vide supra*) are considered as ideal candidates for modelling the structures, as well as the properties, of bulk metal chalcogenide semiconductors [36]. However, issues still remain. Limited solubility and chemical sensitivity (mostly against O_2) or limited thermal stability, especially for selenido- and tellurido-metalates, hinder an in-depth understanding of the behavior of these compounds in solution. To deal with these issues,

ligand-functionalization offers itself as a promising solution.

To describe the build-up of supertetrahedral clusters that refer to the sphalelite architecture, the T*n* nomenclature is commonly used [37–39]. It formally considers the overall tetrahedral molecule to be built up from small tetrahedral $[MCh_4]^{q-}$ subunits condensed at their corners, where *n* is the number of such units to be found on an edge of the supertetrahedron. As examples, $[SnS_4]^4$ would be classified as a T1 cluster, while the cluster core of adamantane-like compounds such as $[(PhSi)_4S_6]$ (**1**, Fig. 2a) are fall into the T2 category [40]. A T3-type cluster is found with the anion in $(H^+–NC_7H_9)_2[Ga_{10}S_{16}(NC_7H_9)_4]$ (**2**, Fig. 2b) [41]. The anion $[In_{16}Cd_4S_{31}(DBN)_4]^6$ (in **3**, DBN = 1,5-diazabicyclo[4.3.0]non-5-ene**)** is an example of a T4-type cluster (Fig. 2c) [42] and the anion $[Cu_5Ga_{30}S_{52}(SH)_2(C_4C_1im)_2]^{11-}$ (in **4**, C_4C_1im = 1–Butyl-2-methylimidazole) represents a T5 cluster decorated with imidazole (im) groups (Fig. 2d) [43]. All four compounds will be discussed in more detail below. In ligand-functionalized compounds, typically the terminal chalcogenide atoms at the supertetrahedron corner of a prototypic supertetrahedral cluster is replaced with an (anionic) organic group, such as alkyl or aryl, or a neutral donor-type ligand, such as pyridyl-based functionalities or imidazoles. If not otherwise stated, this is the substitution pattern for all compounds described in this chapter.

Of all the T*n* cluster types of chalcogenido metalate-based clusters, T2-type clusters have been investigated most extensively. An example for this is T2-$[(PhSi)_4S_6]$ (**1**, Fig. 2a), in which phenyl groups bound to a sulfido silicate-based adamantane-type cluster. It is noteworthy to mention that every part of this molecule can be varied. The Si and S sites can be replaced by Sn or Ge and Se or Te respectively, and almost any organic ligand can be attached, leading to multiple possibilities to modify and affect the stability and properties of the compounds. This generally applies to most of the T*n* clusters, and is not specific to the T2 type. Hence, the following discussion highlights the synthetic methods to prepare clusters of all T*n* type.

The ionothermal synthesis method has recently emerged as a very convenient method for the synthesis of chalcogenido metalate clusters decorated with ligands. The reactions take place in ionic liquids at elevated temperatures (and concomitant pressure increase). In most cases, alkylimidazolium-based ionic liquids (ILs) of the general type $(C_m(C_n)C_oIm)X$ (m, n, o = number of C atoms in the alkyl chains at position 1, 2, and 3 of the imidazolium ring (Im); X = anion) are used [44,45]. There are some prominent examples of the ionothermal treatment of precursor salts and/or elements with ILs to form ligand-decorated T*n*-type chalcogenido metalate-based clusters.

The first ionothermally synthesized clusters with ligand decoration were the T5 clusters $[Cu_5Ga_{30}S_{52}(SH)_2(C_4C_1im)_2]^{11-}$ (in **4**, Fig. 2d) and $[Cu_5Ga_{30}S_{52}(SH)_{1.5}Cl(C_4C_1im)_{1.5}]^{11.5-}$ (in **5**), where the IL $(C_4C_1C_1Im)Cl$ decomposes *in situ* to generate (C_4C_1im) ligands that coordinate to two (in **4**) or one and a half (in **5**) of the gallium atoms at the corners of the cluster. Both compounds were synthesized by the reaction of $(H^+–en)_2[Ga_4S_7(en)_2]$ with $Cu(NO_3)_2{\cdot}3H_2O$ in $(C_4C_1C_1Im)Cl$ at 160 °C in a stainless steel autoclave for 5 (**4**) or 7 (**5**) days, respectively [43]. In subsequent work, the T3 clusters $[In_{10}Ch_xCl_3(C_4C_1im)]^{5-}$ ($Ch_x = S_{16}$, in **6a**; $S_{7.12}Se_{8.88}$, in **6b**; Se_{16}, **6c**; and $Se_{13.80}Te_{2.20}$, in **6d**) were generated this way, which contain a coordinating (C_4C_1im) ligand on one indium atom with the other corners being substituted by chlorine atoms. These compounds were synthesized from the elements (In, Ch) in $(C_4C_1C_1Im)Cl$ and methylamine [46]. Further variation of the reaction conditions allowed the formation of three novel Cu–In- and Cd–In-based T5 clusters with different chalcogen moieties, $[Cu_5In_{30}S_xSe_{52-x}Cl_3(im)]^{12-}$ with x = 0 (in **7a**), 3.5 (in **7b**); $[Cd_6In_{28}S_xSe_{52-x}Cl_3(C_1im)]^{11-}$ (C_1im = 1–methylimidazole) with x = 0 (in **8a**), 23.5 (in **8b**), 36 (in **8c**), and $[Cd_6In_{28}S_{44}Se_8Cl(C_1im)_3]^{9-}$ (in **9**). They were obtained by a microwave-assisted ionothermal process starting from the elements, CuSCN (for **7**), or $CdCl_2$ (for **8** and **9**) in $(C_4C_1C_1Im)Cl$ under addition of diluting solvents, namely thiourea, and/or amines. Here, imidazole in **7** or 1–methylimidazole in **8** and **9** serve as ligands that coordinate to the terminal metal atoms (i.e., In) [35].

Another strategy of ionothermal synthesis uses alkali metal chalogenido (semi)metalates (e.g., $A_x[M_yCh_z]$, A = Li – K; M = Ge, Sn; Ch = S, Se) in/with alkylimidazolium-based ionic liquids (*vide supra*) in the absence or presence of amines such as ethane-1,2-diamine (en) or 2,6-dimethylmorpholine (dmmp) as auxiliaries in sealed borosilicate glass ampoules between 60 °C and 180 °C. According to the large number of variables possible in the starting materials and reaction temperatures, many different clusters have been isolated in this manner. In most cases, the ionic liquids serve as counterions or, in some other cases, protonated en or dmmp compensate the charge of such chalcogenido metalate clusters. In the following section we present different ways to obtain such ligand-functionalized cluster anions from $A_x[M_yCh_z]$ salts [44,45].

Recently, methylated sulfido-oxido stannate clusters based on a (filled) T3-type architecture were obtained in salts of the general formula $(C_4C_1C_1Im)_{4+x}[Sn_{10}S_{16}O_4(SMe)_4][An]_x$ (Fig. 3a, with x = 0, 1; **10a**, as example). For their syntheses, the ionic liquid used as the reaction medium has taken part in the reaction as source of the methyl group [47]. The cluster cores can be derived from a hypothetical, neutral T3 supertetrahedron of the composition "$\{Sn_{10}S_{20}\}$", which incorporates four additional O^{2-} anions that link the four Sn atoms. The purely inorganic version of this cluster, $[Sn_{10}S_{20}O_4]^{8-}$ has been known since many years in several different salts, which were obtained by wet-chemical synthesis techniques [48–50]. Notably, all attempts to alkylate this—or any related—chalcogenido metalate cluster molecule by application of the common (harsh) alkylation procedures using common

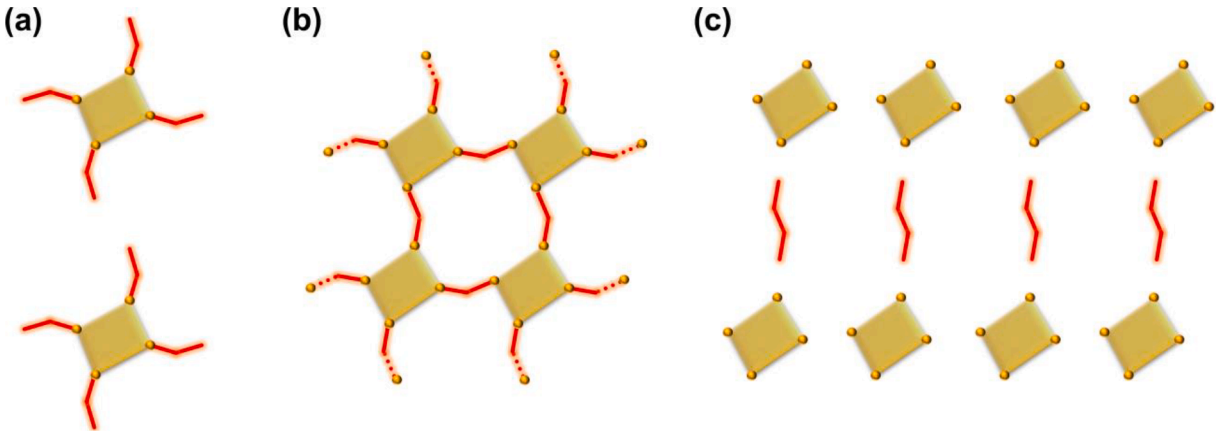

Scheme 1. Schematical illustrations of the types of compounds discussed in this article. (a) Ligand-functionalized clusters (b) Ligand-bridged clusters. (c) Organyl-separated clusters. The yellow cuboids represent cluster molecules, and the ligands, linkers or spacer molecules are shown as red solid lines; the latter can be either purely organic groups, or organic molecules with donor atoms/groups, or purely inorganic molecules (N_2H_4).

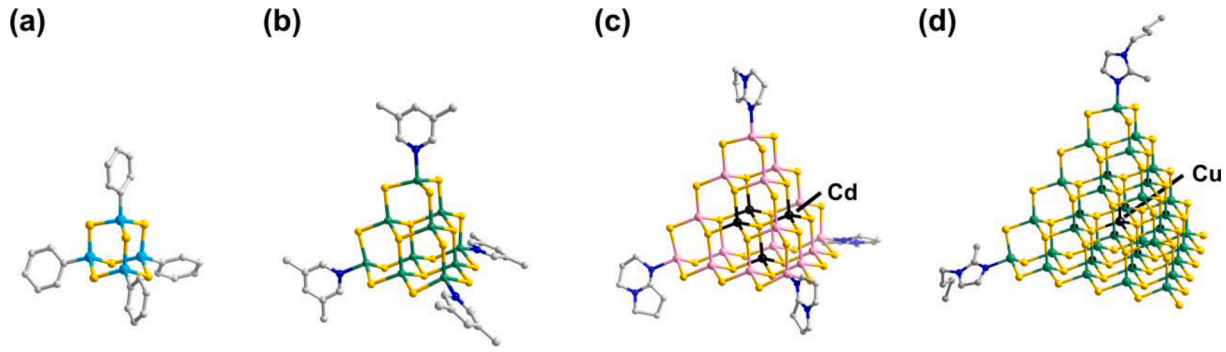

Fig. 2. Molecular structures of selected ligand-functionalized T*n* clusters. (a) T2-$[(PhSi)_4S_6]$, functionalized with phenyl groups. (b) T3-$[Ga_{10}S_{16}(NC_7H_9)_4]^{2-}$ decorated with 3,5-dimethylpyridine. (c) T4-$[In_{16}Cd_4S_{31}(DBN)_4]^{6-}$ capped with neutral DBN molecules. (d) T5-$[Cu_5Ga_{30}S_{52}(SH)_2(C_4C_1im)_2]^{11-}$ decorated with (C_4C_1im). H atoms are omitted for clarity.

solvents and conventional, usually toxic, alkylation reagents (e.g., Meerwein salt or MeI) previously failed owing to the compounds' very small nucleophilicity. Upon the mild treatment in ionic liquid, however, *in situ* methylation was achieved effectively and selectively. All corners of the supertetrahedron were functionalized. The same methylated cluster anion $[Sn_{10}S_{16}O_4(SMe)_4]^{4-}$ (in **10b**), can also be generated by using an IL based on $(C_4C_4C_1Im)^+$ cations, which confirms that methylation is preferred over a butylation in these cases [51]. Though both anions in **10a** and **10b** are the same, the overall compounds differ in the crystal structure, as the crystal lattice is somewhat templated by the extra steric bulk provided by the butyl group in $(C_4C_4C_1Im)^+$. Switching the cation in the IL to the isomeric $(C_4C_1C_4Im)^+$, resulted in the butylation of the cluster (in $(C_4C_1C_4Im)_{4+x}[Sn_{10}S_{16}O_4(SBu)_4]Br_x$, **11**; Fig. 3b); this result also confirmed that the N-bonded ligand is the source of the alkyl substituent to be transferred [34]. Finally, an expansion of the study to ILs containing the cations $(C_xC_1C_xIm)^+$ (x = 3, 5, 6), led to a series of alkylated T3-based sulfido-oxido stannate cluster anions, $[Sn_{10}O_4S_{16}(SC_x)_4]^{4-}$, in **12** – **14**. The clusters differ by the variation in the alkyl substituent on the terminal sulfur atoms depending on which IL is used, and by the different alkyl groups' effects on the packing scheme of the cluster molecules in the corresponding crystal structures [52]. The most remarkable effect of the attachment of the alkyl groups to the four corners of the cluster is a significant increase in solubility upon both charge reduction and addition of unpolar groups. As a result, the butylated cluster dissolved readily in organic solvents like MeCN, remarkably without loss of the wide-band semiconductor properties of the underlying inorganic cousin. Mass spectrometry (Fig. 3c) and NMR spectroscopy (Fig. 3d) confirmed the retainment of the clusters in solution. The optical absorption properties were studied by ultraviolet–visible (UV–vis) spectroscopy and time-dependent density functional theory (TD-DFT) studies, which confirmed similar band gaps in solution and the solid state, and marginal effects in comparison with the inorganic analog and between methylated and butylated species (Fig. 3e).

Moving away from ionothermal synthesis, an alternative strategy was the use of organic superbases, such as DBN or 1,8-diazabicyclo [5.4.0]undec-7-ene (DBU). The synthesis of a supertetrahedral cluster is a challenge due to the fact that the negative charge of the cluster increases dramatically when the cluster gets bigger. Efforts have therefore been made to reduce the negative charge. For instance, higher-valent metal ions, such as In^{3+} or Sn^{4+}, were included [53], or metal complex cations were used as cluster corners or to form an anionic 3D framework [54]. In this context, the superbases can have two different functions at a time: they can terminate the cluster corners and/or serve as counterions upon protonation. The clusters $[In_{16}M_4S_{31}(DBN)_4]^6$ (M = Cd^{2+}, in **3a**, Fig. 2c; Mn^{2+}, in **3b**; Co^{2+}, in **3c**; Fe^{2+}, in **3d**) and $[In_{10}S_{16}(DBN)_4]^2$ (in **15**) are examples of a T3-type and a T4-type unit, respectively, obtained from reactions in DBN [42]. The base acts in both roles here: neutral DBN terminates the cluster anion by coordinating to the metal cation in the corners (thus reducing the cluster's overall charge) and simultaneously, DBN serves also as charge-balancing species in the protonated form. By adding a ligand, such as imidazole or its derivatives, to the synthesis with superbases, the superbase will just act as charge-balancing species, while the imidazole serves to terminate the cluster corners owing to this base's higher nucleophilicity. The first cluster to be prepared from the superbase DBU in such a way was the T5-type supertetrahedral anion $[In_{22}Cd_{13}S_{52}(C_1im)_4]^{12}$ (in **16**). Prior to that study, T5-type clusters were only known to occur in 2D and 3D frameworks [55,56]. In compound **16**, however, the central $\{Cd_{13}S_4\}$ core is embedded in an $\{In_{22}S_{48}\}$ shell, which is capped by four neutral organic molecules through N → In coordination. The (protonated) superbase acts just as counterions, (H^+–DBU), here. Therefore, these specific cluster architectures can only be prepared upon using both the superbase and the imidazole derivative, and consequently, the superbase used has a marked effect on the reaction outcome: DBN could be used as terminating species and charge balancing species while (the larger) DBU was only found to act as a charge-balancing species. More details of the effect of the nature of the superbase are yet to be explored and remain an open avenue of investigation.

Most of the compounds mentioned above have also been investigated with regards to their promising physical and optical properties, such as photoluminescence, photoconductivity, and photocatalytic ability. The investigation of the optical properties of chalcogenido metalate cluster-based compounds is mostly carried out to find out whether the corresponding compounds are suitable for application as innovative materials. Varying the metal and/or chalcogen atoms leads to different optical band gaps and thus allows fine-tuning of the properties [57].

UV–vis spectroscopy of compounds **4** and **5** showed an absorption edge of 3.68 and 3.62 eV, respectively, hence blue-shifted in comparison to that of the purely inorganic anion $[Cu_5Ga_{30}S_{52}(SH)_4]^{13-}$ (3.04 eV). However, the ligands have no effect on the photoluminescence spectra [43]. UV–Vis spectra of compounds **6a** – **6d** (Fig. 4a) showed that the absorption edge of the spectrum is red-shifted as the chalcogen is exchanged from lightest to heaviest (**6d**: 2.65 eV; **6a**: 3.31 eV; Fig. 4b). Compounds **7** – **9** also show a similar trend, as the band gap elevates with increasing S:Se ratio (**7**: 2.15 eV, cf., **9**: 3.01 eV). Changing from indium to gallium in the copper-based T5-type clusters also led to a larger band gap (**4** *vs.* **8** or **9**).

The catalytic activity of chalcogenido metalate-based compounds in decomposition reactions of photodegradable organic pollutants, such as dye impurities, e.g., methyl orange (mo) and crystal violet (cv), under ultraviolet-light and visible-light irradiation has also become an important area of research [35,46]. In the case of ligand-decorated clusters, these studies have remained very rare though, and the first investigations were performed on the discrete T3-type clusters **6**, for the photodegradation of mo. The sulfide compound **6a** was found to have a higher photodegradation efficiency under UV illumination than the S/Se-, Se- or Se/Te-containing clusters (**6b** – **6d**). After 80 min, cluster **6a**

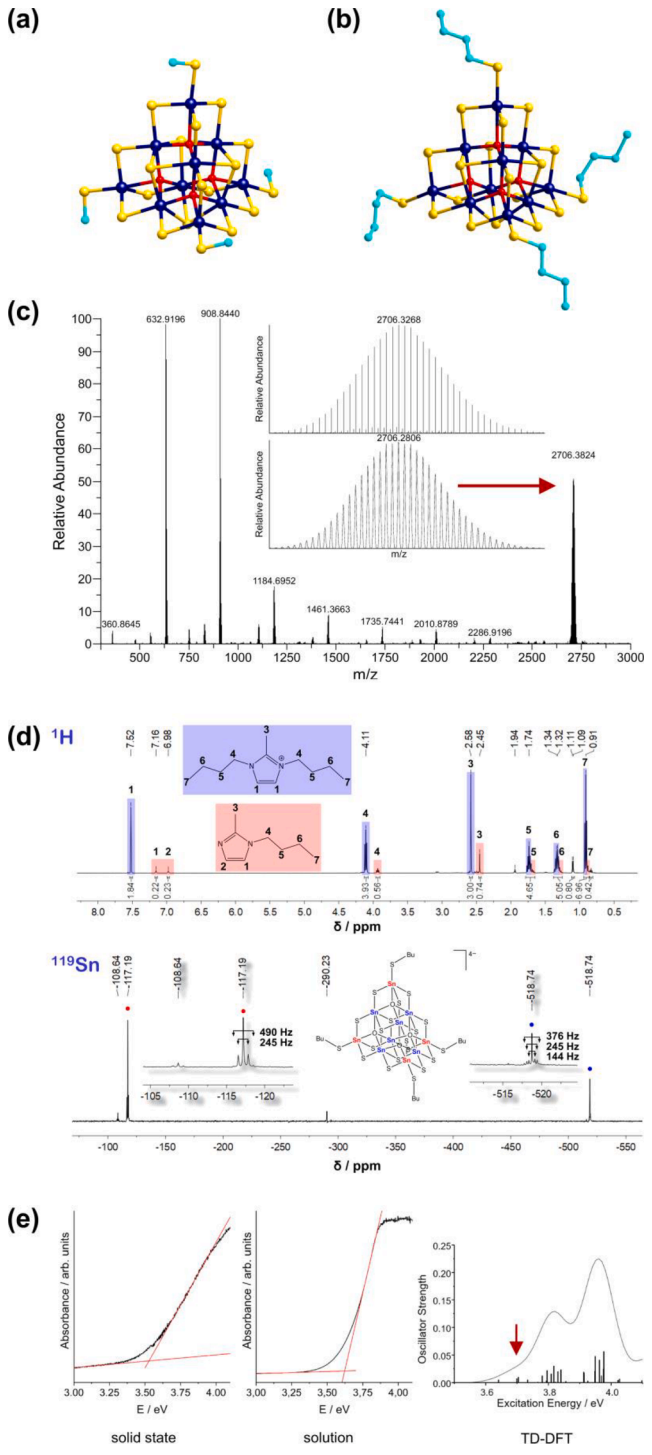

Fig. 3. Molecular structures and properties of alkylated T3-type sulfido-oxido stannate cluster anions, obtained by *in situ* alkylation in ionic liquids that served simultaneously as reaction media and alkylation reagents. (a) The methylated cluster $[Sn_{10}S_{16}O_4(SMe)_4]^{4-}$. (b) The butylated cluster $[Sn_{10}S_{16}O_4(SBu)_4]^{4-}$. C atoms of the alkyl groups are highlighted in turquoise color. H atoms are omitted for clarity. (c) Proof of the presence of the $[Sn_{10}S_{16}O_4(SBu)_4]^{4-}$ cluster in MeCN solution by means of ESI(–) mass spectrometry. (d) Proof of the presence of the $[Sn_{10}S_{16}O_4(SBu)_4]^{4-}$ cluster in MeCN solution by means of NMR-spectroscopy (right). (e) Comparison of the solid-state UV–vis spectrum of the salt $(C_4C_1C_4Im)_{4+x}[Sn_{10}S_{16}O_4(SBu)_4]Br_x$, the solution UV–vis spectrum of a solution of $(C_4C_1C_4Im)_{4+x}[Sn_{10}S_{16}O_4(SBu)_4]Br_x$ in MeCN, and DFT calculations. Reproduced from Ref. [34] with permission from Wiley-VCH.

had a photodegradation efficiency of 95.4%, while for **6b** and **6c**, it was not until 120 min had passed for an efficiency of 95.7%. For compound **6d**, only a degradation efficiency of approximately 69.4% was obtained after 120 min. Changing the wavelength of the incident radiation from UV to visible light resulted in the opposite findings. Overall, all samples showed better catalytic activities under UV light irradiation (Fig. 4c–d) [35,46].

The photodegradation of cv was probed using **7a** and **7b** as catalysts. The mixed sulfide-selenide cluster compound (**7b**) exhibits higher a photodegradation efficiency than the pure selenium compound (**7a**). **7b** required 80 min to photodegrade nearly 99% of the cv, whereas the **7a** required 120 min to degrade approximately 93%. This is due to the more negative conduction band of **7b** as compared to that of **7a**.

Due to the suitable band position, crystalline metal chalcogenides also play an important role in photocatalytic H_2 generation from water, e.g., the hydrogen evolution reaction (HER). Nevertheless, very low H_2 generation rates are observed for bulk crystalline metal chalcogenides due to insufficient exposure of the active sites to the H_2O molecules. The discrete T5 clusters in **8** and **9** were investigated for photocatalytic H_2 production using the solid-state compounds in heterolytic processes. H_2 production increased with irradiation time, and the H_2 production activity increased with increasing sulfur content of the clusters. In addition, the transient photocurrent densities of these compounds were measured to demonstrate the separation efficiency of photoexcited electron-hole pairs upon visible-light irradiation. Solutions or dispersions of these compounds have not been reported, most likely due to the inherently poor solubility of salts containing these highly-charged anions [35]. An overview of the described properties of these T5 clusters is shown in Fig. 5.

Apart from T*n* clusters, a second member of the supertetrahedral chalcogenide family is represented by penta-supertetrahedral clusters (P*n*, $n = 1$ or 2). Structurally speaking, P*n* clusters can be viewed as attachment of four T*n* clusters onto the faces of an anti-T*n* cluster, which exhibit the same geometry but inversed metal and chalcogen atomic positions—for example $[ChM_4]^{q+}$, in comparison with $[MCh_4]^{q-}$ [58]. Overall, they possess structural characteristics of the Wurtzite structure type, but in a fashion that cannot be expanded to a 3D structure (in contrast to the T*n* series, which can be viewed as exact fractions of the Sphalerite structure type). Herein, we will only mention ligand-functionalized P*n* clusters. As opposed to T*n* clusters, the known P*n* cluster usually comprise ligands on all chalcogen atoms, hence on the edges and the corners of the cluster molecules, which increasing the coordination sphere of those moieties and has a notable impact on chemical and physical properties. The difference is not an inherent property of the cluster family, but refers to their usually different synthetic approaches. To obtain functionalized P*n* clusters, chalcogenolates were commonly used as starting materials and Ch sources. For instance, by reacting NaSePh with CdI_2, Na_2S or NaSH and $[Et_4N]Cl$ in MeOH and MeCN, the phenyl-decorated P1 cluster anion $[SCd_8(SePh)_{16}]^{2-}$ (in **17**, Fig. 6a), which consists of four T1-type $[CdSe_4]^{6-}$ units and one anti-T1-type $[SCd_4]^{6+}$ unit, is obtainable [59]. Both metal and chalcogen atoms, as well as ligands can be varied, and thus enable a wide variety of similar functionalized P1 clusters. Larger P2-type clusters, like $[Cu_{11}In_{15}Se_{16}(SePh)_{24}(PPh_3)_4]$ (**18**, Fig. 6b), have also been isolated. In **18**, the four corners are occupied by phosphines instead of chalcogenolates, which may generally offer opportunities for further transformation by substituting the phosphine [60]. Although this first ligand-functionalized P2 cluster was documented in 2000, none larger than P2 have been synthesized to date, and remains a goal in the future development of P*n* cluster chemistry.

The ionothermal route used for T*n* clusters has also been successfully applied to the synthesis of ligand-functionalized P1 clusters, however, this (probably post-synthetic) approach has allowed a selective, partial alkylation of the corner Ch atoms only, as described above for the T3-based sulfido-oxido stannate cluster. For instance, the ionothermal reaction of $K_2[Sn_2Se_5]$ and $MnCl_2$ in $(C_4C_1Im)[BF_4]$, in the presence of small amounts of dmmp, led to the formation of the first methylated selenido stannate cluster $[Mn_4Sn_4Se_{13}(SeMe)_4]^{6-}$ (in **19**, Fig. 6c). Unlike

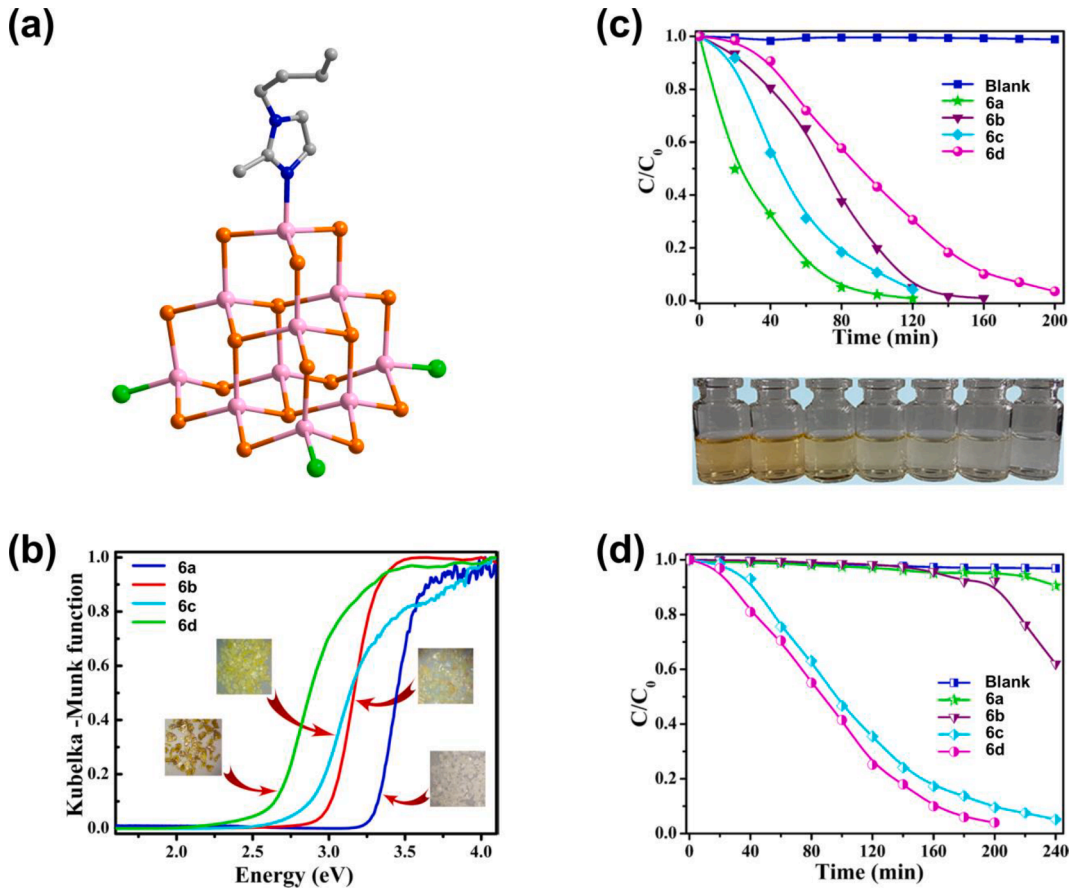

Fig. 4. (a) Molecular structure of the anionic cluster $[In_{10}Se_{16}Cl_3(C_4C_1im)]^{5-}$ with one (C_4C_1im) terminal ligand and three Cl ligands; H atoms are omitted for clarity. (b) Solid-state UV–vis spectra of $[In_{10}Ch_xCl_3(C_4C_1im)]^{5-}$ (Ch_x S_{16} in 6a; $S_{7.12}Se_{8.88}$ in 6b; Se_{16} in 6c; $Se_{13.80}Te_{2.20}$ in 6d). (c) Photodegradation of mo catalyzed by $[In_{10}Ch_xCl_3(C_4C_1im)]^{5-}$ (6a–6d) monitored as normalized concentration change as a function of illumination time under UV light, and images of the color change of the solutions during irradiation. (d) Photodegradation of mo catalyzed by $[In_{10}Ch_xCl_3(C_4C_1im)]^{5-}$ (6a–6d) monitored as normalized concentration change as a function of illumination time under visible light. Reproduced from Ref. [46] with permission from the American Chemical Society.

in **14a**, for example, not IL cations serve as counterions in **19**, but protonated dmmp molecules [47].

All ligand-functionalized discrete supertetrahedral chalcogenido metalate cluster-based presented in section 2.1 are summarize in Table 1.

2.2. Ligand-bridged and ligand-functionalized chalcogenido metalate-based supertetrahedra

As alluded to earlier, compensating for the high charge of supertetrahedral clusters is a significant synthetic challenge. In this section, the linkage of anionic clusters by bridging ligands will be presented as another approach into this direction.

In 2008, 1,2-bis(4-pyridyl)ethylene (DPE) and its derivatives were used as bridges to synthesize gallium-sulfide-based supertetrahedral clusters, in which the sulfur atoms at the vertices had been replaced by a ligand [61]. The anion in $(H^+–NC_6H_7)_2[Ga_{10}S_{16}(NC_6H_7)_2(DPE)]$ (**20**, Fig. 7a) consists of one-dimensional zigzag chains of alternating T3-type clusters and dipyridyl-ligands, with the two remaining vertices of the supertetrahedral clusters terminated by monodentate 4-methylpyridine molecules. The anion in $(H^+–NC_7H_9)_2[Ga_{10}S_{16}(NC_7H_9)(DPE)_{3/2}]$ (**21**) also contains supertetrahedral clusters of the T3 type, but in this structure, three of the terminal S^{2-} anions have been replaced by DPE, while the remaining vertex is terminated by a 3,5-dimethylpyridine molecule. Using the DPE group, which acts as the bridge, led to the formation of layers with a honeycomb-like topology of the cluster framework with a pore diameter of ca. 30 Å (Fig. 7b).

In addition to networks, the first dimer-type anions of ligand-functionalized supertetrahedra have been prepared. Here, both DPE and 4,4′-bipyridine (bpy) molecules were used as bridges, with the amine groups of the linker in both structures covalently bound to a supertetrahedral T3-type cluster, while the remaining vertices were also functionalized by ligands [62]. In the dimeric anion of the salt $(H^+–NC_7H_9)_6[Ga_{20}S_{34}H_2(NC_7H_9)_4(DPE)]$ (**22**), two vertices of each supertetrahedral cluster are terminated by 3,5-dimethylpyridine, and one is protonated to form a $(SH)^-$ group. Two different types of cluster units are observed in the anionic substructure of the salt $(H^+–NC_7H_9)_6[Ga_{10}S_{16}(NC_7H_9)(bpy)_3][Ga_{20}S_{32}(NH_3)_2(NC_6H_7)_4(bpy)]$ (**23**). One of them, $[Ga_{20}S_{32}(NH_3)_2(NC_6H_7)_4(bpy)]^{4-}$, is a dimer of two supertetrahedral clusters that are bridged *via* a bpy molecule. Two terminal S^{2-} anions of each supertetrahedral cluster in the dimer were replaced by monodentate amine linkers, and the remaining vertex is terminated by NH_3. The other anion is a monomeric supertetrahedral anion, $[Ga_{10}S_{16}(NC_7H_9)(bpy)_3]^{2-}$, terminated by one 3,5-dimethylpyridine and three bpy molecules.

A new level of structural hierarchy could be achieved with the compound $(H^+–NC_5H_5)_8[(Ga_{10}S_{16})_7(NC_2H_7)_4(NC_6H_7)_8(N_2C_{12}H_{12})_8]$ (**24**) [63]. Again, the salt is based on the T3-type $[Ga_{10}S_{16}(NC_6H_7)_4]^{2-}$ cluster units introduced above, yet with different connection modes (Fig. 7c).

Four T3 clusters are bridged *via* bpy ligands to a central T3 subunit in a tetrahedral fashion. Each of these assemblies of five clusters is connected *via* additional bpy bridges to four further T3-type clusters, which in turn serve as bridges to the next four assemblies—this way extending

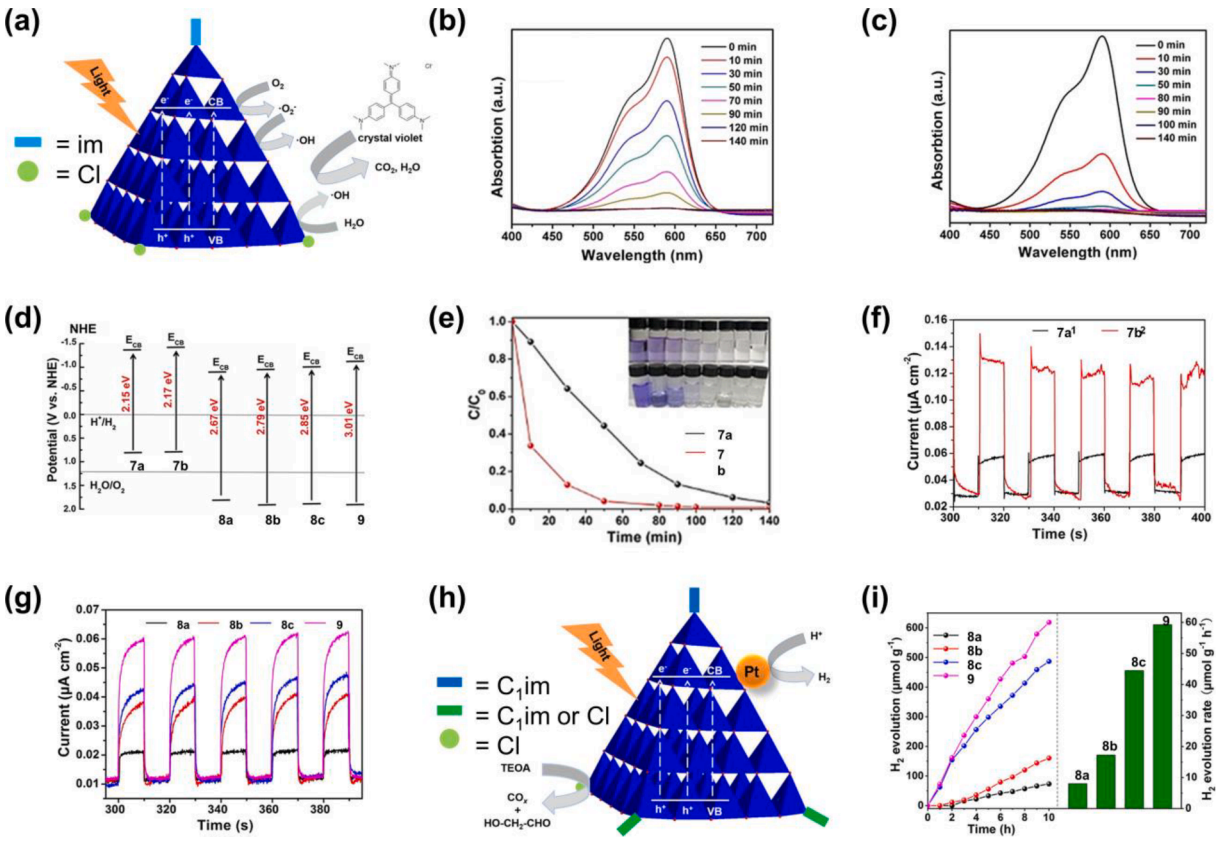

Fig. 5. (a) Illustration of the proposed photocatalytic mechanism for photodegradation of cv by $[Cu_5In_{30}S_xSe_{52-x}Cl_3(im)]^{12-}$; only the inorganic cluster core is shown in polyhedral form for clarity. (b) Photodegradation of cv using $[Cu_5In_{30}Se_{52}Cl_3(im)]^{12-}$ under visible-light irradiation, monitored by optical absorption spectroscopy. (c) Photodegradation of cv using $[Cu_5In_{30}S_{3.5}Se_{48.5}Cl_3(im)]^{12-}$ under visible-light irradiation, monitored by optical absorption spectroscopy. (d) Band structures of $[Cu_5In_{30}S_xSe_{52-x}Cl_3(im)]^{12-}$ with x 0, 3.5, $[Cd_6In_{28}S_xSe_{52-x}Cl_3(C_1im)]^{11-}$ with x 0, 23.5, 36, or $[Cd_6In_{28}S_{44}Se_8Cl(C_1im)_3]^{9-}$, determined through impedance/potential measurements. (e) Photodegradation of cv under catalysis of $[Cu_5In_{30}Se_{52}Cl_3(im)]^{12-}$ (black line) and $[Cu_5In_{30}S_{3.5}Se_{48.5}Cl_3(im)]^{12-}$ (red line) monitored as normalized concentration change as a function of irradiation time under visible light and images of the color change of the solutions during the irradiation. (f) Transient photocurrent density versus time for $[Cu_5In_{30}S_xSe_{52-x}Cl_3(im)]^{12-}$ with x 0, 3.5 and (g) for $[Cd_6In_{28}S_xSe_{52-x}Cl_3(C_1im)]^{11-}$ with x 0, 23.5, 36 or $[Cd_6In_{28}S_{44}Se_8Cl(C_1im)_3]^{9-}$. (h) Schematic representation of the proposed mechanism of the photocatalytic H_2 production from H_2O and catalysts $[Cd_6In_{28}S_xSe_{52-x}Cl_3(C_1im)]^{11-}$ with x 0, 23.5, 36 or $[Cd_6In_{28}S_{44}Se_8Cl(C_1im)_3]^{9-}$, only the inorganic cluster core is shown in polyhedral form for clarity. (i) Comparison of the photocatalytic H_2 evolution from H_2O in the presence of $[Cd_6In_{28}S_xSe_{52-x}Cl_3(C_1im)]^{11-}$ with x 0, 23.5, 36 or $[Cd_6In_{28}S_{44}Se_8Cl(C_1im)_3]^{9-}$ upon illumination with Xe lamp with a cut off filter. Reproduced from Ref. [35] with permission from Wiley-VCH.

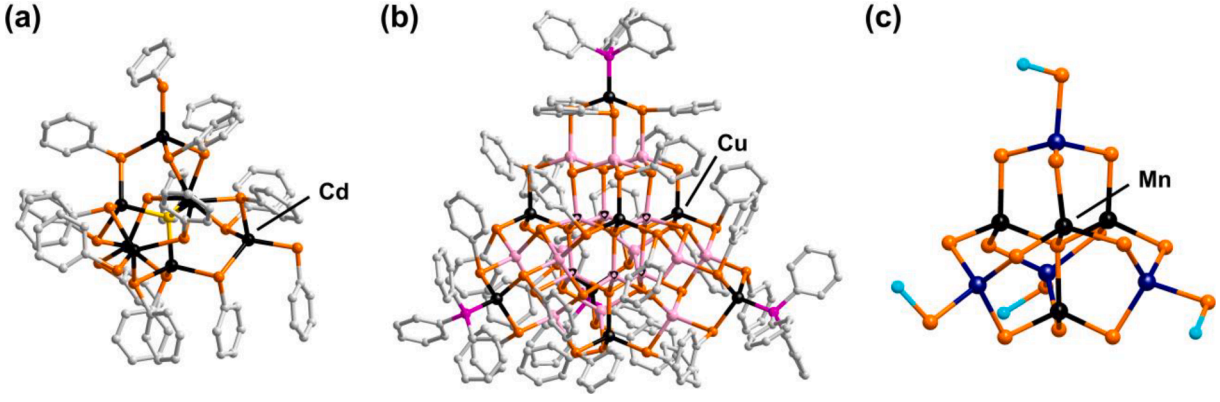

Fig. 6. Molecular structures of selected ligand-functionalized P*n*-type chalcogenido metalate clusters (*n* 1–2). (a) Ph-decorated supertetrahedral P1-type cluster anion $[SCd_8(SePh)_{16}]^{2-}$. (b) Triphenylphosphine-terminated P2-type cluster $[Cu_{11}In_{15}Se_{16}(SePh)_{24}(PPh_3)_4]$. (c) Methylated P1-type cluster $[Mn_4Sn_4Se_{13}(SeMe)_4]^{6-}$ obtained from ionothermal reactions. H atoms are omitted for clarity.

into a 2D network. The two remaining vertices of the bridging T3 clusters are bound to en molecules. The structure of the compound represents a new complexity in this class of materials. The individual $[GaS_4]^{5-}$ tetrahedra can be considered as the primary building blocks, while the three crystallographically distinct T3 clusters form secondary building blocks. The assemblies of five cluster molecules tethered together by bpy linkers are tertiary building blocks that form the next level of the structural hierarchy.

Table 1
Summary of the ligand-functionalized discrete supertetrahedral chalcogenido metalate-based clusters presented in section 2.1.

Compound	Reactants	Temperature (°C)	Ref.
$[(PhSi)_4S_6]$ (**1**)	Na_2S, $PhSiCl_3$ in THF	0 to rt	[40]
$(H^+–NC_7H_9)]_2[Ga_{10}S_{16}(NC_7H_9)_4]$ (**2**)	Ga and S in 3,5-dimethylpyridine	170	[41]
$(Cat)_6[In_{16}M_4S_{31}(DBN)_4]$ (**3**)	Li_2S, $In(NO_3)_3{\cdot}xH_2O$, $MX{\cdot}yH_2O$ in 2-amino-1-butanol, DBN or DBU, and MeCN (MX = Cd $(NO_3)_2$, $Mn(Ac)_2$, $CoCl_2$, $FeSO_4$)	150	[42]
$(C_4C_1C_1Im)_8[Cu_5Ga_{30}S_{52}(SH)_2(C_4C_1im)_2][NH_4]_3$ (**4**)	$(H^+–en)_2[Ga_4S_7(en)_2]$, $Cu(NO_3)_2{\cdot}3H_2O$, thioacetamide, 4,4′–bipyridyl in $(C_4C_1C_1Im)Cl$ with dimethylamine	160	[43]
$(C_4C_1C_1Im)_{9.5}[NH_4]_2[Cu_5Ga_{30}S_{52}(SH)_{1.5}Cl(C_4C_1im)_{1.5}]$ (**5**)	$(H^+–en)_2[Ga_4S_7(en)_2]$, $Cu(NO_3)_2{\cdot}3H_2O$, S, Na_2CO_3 in $(C_4C_1C_1Im)Cl$	160	[43]
$(C_4C_1C_1Im)_5[In_{10}Ch_xCl_3(C_4C_1im)]$ (**6**)	In, Ch in $(C_4C_1C_1Im)Cl$ and methylamine ($Ch_x = S_{16}$, $S_{7.12}Se_{8.88}$, Se_{16}, $Se_{13.80}Te_{2.20}$)	160	[46]
$(C_4C_1C_1Im)_{12}[Cu_5In_{30}S_xSe_{52-x}Cl_3(im)]$ (**7**)	In, Se, CuSCN in $(C_4C_1C_1Im)Cl$ with MeCN, C_1im, (thiourea) and DBU (x = 0, 3.5)	150	[35]
$(C_4C_1C_1Im)_{11}[Cd_6In_{28}S_xSe_{52-x}Cl_3(C_1im)]$ (**8**)	In, S, Se in $(C_4C_1C_1Im)Cl$ with C_1im, $CdCl_2$ and thiourea (x = 0, 23.5, 36)	150	[35]
$(C_4C_1C_1Im)_9[Cd_6In_{28}S_{44}Se_8Cl(C_1im)_3]$ (**9**)	In, S, Se in $(C_4C_1C_1Im)Cl$ with C_1im, $CdCl_2$ and thiourea	150	[35]
$(C_4C_1C_1Im)_{4+x}[Sn_{10}S_{16}O_4(SMe)_4][An]_x$ (**10a**)	$A_4[SnS_4]{\cdot}zH_2O$, $(MnCl_2)$ in $(C_4C_4C_1Im)Cl/[BF_4]$ with en or dmmp (x = 0, 1, AM/z = Li/13, Na/14)	150 or 180	[47]
$(C_4C_4C_1)_4[Sn_{10}O_4S_{16}(SMe)_4]$ (**10b**)	$K_4[SnS_4]{\cdot}4H_2O$ in $(C_4C_4C_1Im)Cl$ with dmmp	180	[51]
$(C_4C_1C_4Im)_{4+x}[Sn_{10}O_4S_{16}(SBu)_4]Br_x$ (**11**)	$K_4[SnS_4]{\cdot}4H_2O$ in $(C_4C_1C_4Im)Br$ with dmmp	180	[34]
$(C_3C_1C_3Im)_4[Sn_{10}O_4S_{16}(SPr)_4]$ (**12**)	$Na_4[SnS_4]{\cdot}14H_2O$ in $(C_3C_1C_3Im)Br$	180	[52]
$(C_5C_1C_5Im)_4[Sn_{10}O_4S_{16}(SPn)_4]$ (**13**)	$Na_4[SnS_4]{\cdot}14H_2O$ in $(C_5C_1C_5Im)Br$	180	[52]
$(C_6C_1C_6Im)_4[Sn_{10}O_4S_{16}(SHx)_4]$ (**14**)	$Na_4[SnS_4]{\cdot}14H_2O$ in $(C_6C_1C_6Im)Br$	180	[52]
$(H^+–DBN)_2[In_{10}S_{16}(DBN)_4]{\cdot}(MeCN){\cdot}(H_2O)$ (**15**)	Li_2S, $In(NO_3)_3{\cdot}xH_2O$ mixed with 2-amino-1-butanol, MeCN and DBN	150	[42]
$(H^+–DBU)_9Li_3[In_{22}Cd_{13}S_{52}(C_1im)_4]{\cdot}2(MeCN){\cdot}31H_2O$ (**16**)	Li_2S, $In(NO_3)_3{\cdot}xH_2O$, $Cd(NO_3)_2{\cdot}4H_2O$ mixed with 1-methylimidazole, 2-amino-1-butanol, MeCN and DBU	150	[42]
$[Et_4N]_2[SCd_8(SePh)_{16}]$ (**17**)	NaSePh, $CdCl_2$, and Na_2S or NaSH in MeCN/MeOH	rt	[59]
$[Cu_{11}In_{15}Se_{16}(SePh)_{24}(PPh_3)_4]$ (**18**)	CuCl, $InCl_3$, $PhSeSiMe_3$, $Se(SiMe_3)_2$, and PPh_3 in THF	rt	[60]
$(H^+–dmmp)_6[Mn_4Sn_4Se_{13}(SeMe)_4]$ (**19**)	$K_2[Sn_2Se_5]$, $MnCl_2$ in $(C_4C_1Im)[BF_4]$ with dmmp	120	[47]

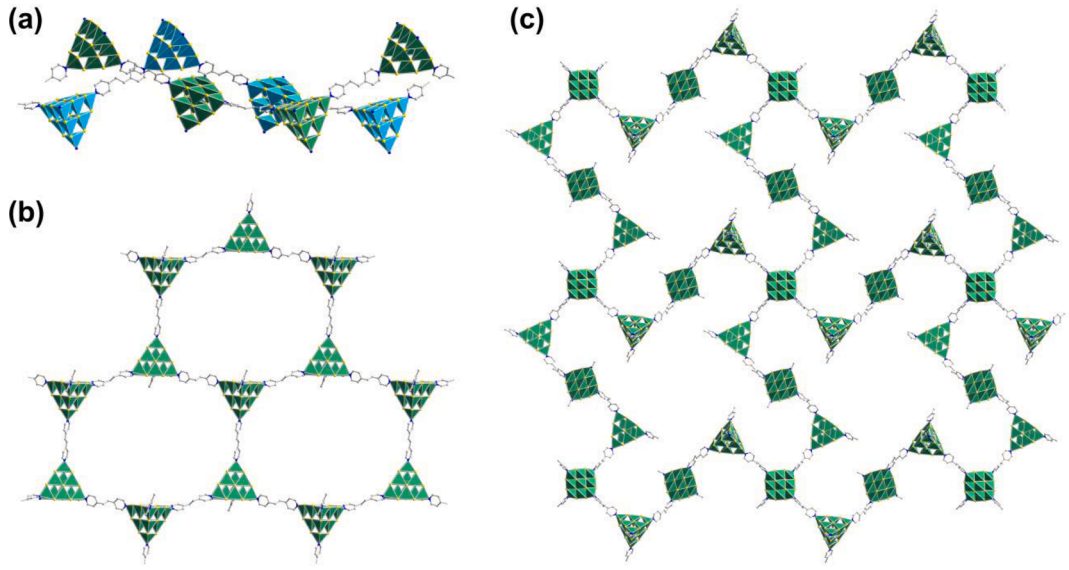

Fig. 7. Polyhedral representation of different assemblies of bpy ligand-bridged T3 clusters. (a) Intertwined helical chains (discriminated by green and blue polyhedra, respectively) of 1D-$\{[Ga_{10}S_{16}(NC_6H_7)_2(DPE)]^{2-}\}$ in **20** (b) Honeycomb layers in 2D-$\{[Ga_{10}S_{16}(NC_7H_9)(DPE)_{3/2}]^{2-}\}$ in **21**. (c) Interrupted 2D networks in $(H^+–NC_5H_5)_8[(Ga_{10}S_{16})_7(NC_2H_7)_4(NC_6H_7)_8(DPE)_8]$ in **24**. Each individual polyhedron represents a $[GaS_4]^{5-}$ motif. H atoms are omitted for clarity.

To achieve a new type of ordering, 4,4′-trimethylenedipyridine (TMDP) was used as an additional linker along with DPE to synthesize discrete nanotubes of $(H^+–NC_2H_7)_2[Ga_{10}S_{16}(N_2C_{12}H_{12})(NC_2H_7)_2]$ (**25**). The anion in **25** is built up from chiral helical chains of alternating supertetrahedral T3 clusters and DPE ligands. Four single-stranded helical chains are intertwined to form a four-stranded helical nanotube with an outer diameter of 30 Å and an inner diameter of 2 Å. While smaller DPE ligands thus enabled the generation of single-walled chiral nanotubes, larger TMDP ligands gave rise to the formation of $(H^+–NC_5H_5)_3[Ga_{10}S_{16}(OH)_2(TMDP)_2]$ (**26**), in which, for the first time, organic and inorganic ligands coexisted between supertetrahedral clusters in the same structure. The 2D structure is built of T3-$[Ga_{10}S_{16}(OH)_2(N_2C_{13}H_{14})_2]^{4-}$ clusters, and each T3 cluster is bridged *via* μ_2-$(OH)^-$ groups to two neighboring clusters. These chains in turn are bridged *via* TMDP ligands to form the final 2D network [64].

The supertetrahedral cluster T3-$[Cd_6Ag_4(SPh)_{16}(DMF)(H_2O)(DPE)]$ (DMF = N,N-dimethylformamide) was used as a building block for the synthesis of crossbridged discrete supertetrahedral chalcogenolate clusters with conjugated bipyridine linkers. The strategy to control the dimensions of the coordination polymers utilized here was to tune the ratio between $[Cd_6Ag_4(SPh)_{16}]$ clusters and DPE linkers. Two equivalents of DPE in the synthesis resulted in the formation of the diamond-like framework 3D-$[Cd_6Ag_4(SPh)_{16}(DPE)_2)]$ (**27**, Fig. 8c) [65], while the use of smaller relative amounts of DPE resulted in the formation of a strands-like assembly in 1D-$[Cd_6Ag_4(SPh)_{16}(DMF)(H_2O)(DPE)]$ (**28**, Fig. 8a) [66]. Both structures comprise the initial T3-$[Cd_6Ag_4(SPh)_{16}]$

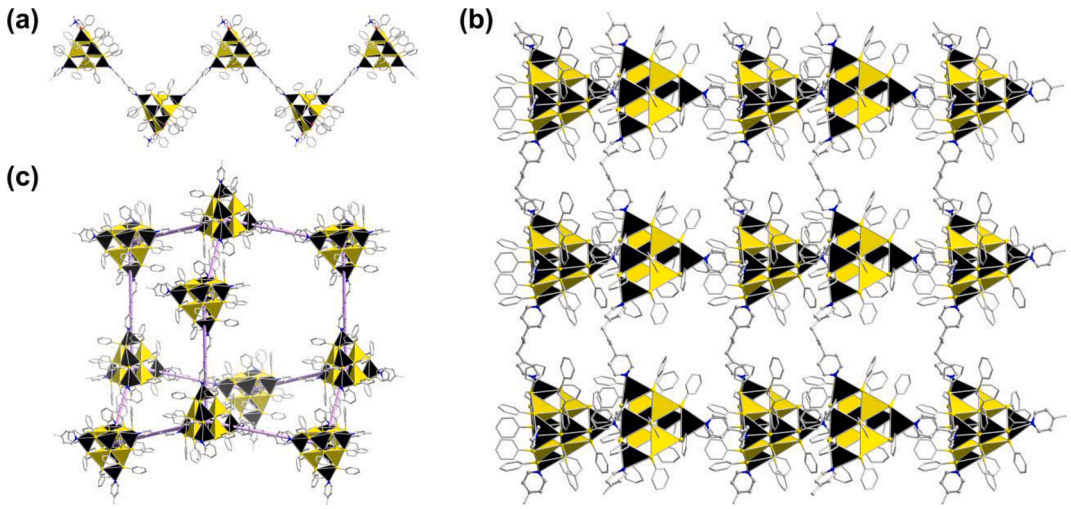

Fig. 8. Extended structures based on T3-$[Cd_6Ag_4(EPh)_{16}]$ cluster units. (a) 1D-$[Cd_6Ag_4(SPh)_{16}(DMF)(H_2O)(DPE)]$ chain. (b) 2D-$[Cd_6Ag_4(ChPh)_{16}(TMDP)_2]$ (Ch S, Se) layers. (c) 3D-$[Cd_6Ag_4(SPh)_{16}(DPE)_2)]$ framework (an adamantane unit within the network highlighted by lavender lines as a guide to the eye). Black polyhedra represent $[CdS_4]^{6-}$, yellow polyhedra represent $[AgS_4]^{7-}$ units.

building unit, but with different connection modes. In **27**, each T3 cluster is coordinated by four DPE ligands, which in turn connect two T3 clusters each. In compound **28**, only two vertices of the T3 cluster are decorated by DPE ligands, while the remaining two vertices are coordinated by solvent molecules. By changing the bridge from the linear and rigid DPE bridge to the more flexible TMDP, the layered structure of 2D-$[Cd_6Ag_4(ChPh)_{16}(TMDP)_2]$ (**29**, Ch = S, Se, Fig. 8b) was obtained [67]. In **29**, T3-$[Cd_6Ag_4(EPh)_{16}]$ clusters act as building units again, and each T3 cluster is connected to four TMDP bridges. Each of them in turn is connected to two T3 clusters, which results in a wave-like network architecture. All three compounds show photocatalytic activity in the degradation of organic dyes.

The chromophoric ligand tris(4-pyridylpheny)amine (TPPA) allowed for the synthesis of two new supertetrahedral chalcogenolate cluster-based assembled materials (SCCAMs), namely 1D-{$[Cd_{12}Ag_8(SPh)_{32}$(TPPA)$(DMF)_3(H_2O)_2]\cdot 2DMF$} (**30**) and 2D-$[Cd_{12}Ag_8(SPh)_{32}(TPPA)_2(DMF)(H_2O)]$ (**31**). The two compounds are formed depending on the ratio between the bridges and the starting material $Cd(SPh)_2$ used in the synthesis. A ratio of 1:6 equivalents of TPPA and $Cd(SPh)_2$, respectively, yielded **30**. Here, one TPPA linker connects three clusters such that two clusters connect to four others, while the third one only exhibits a connection *via* one ligand to two other clusters. As a result, a 1D structure is obtained. If the ratio is increased to 1:3 (TPPA:$Cd(SPh)_2$), compound **31** is obtained instead. Here, all cluster nodes are three-connected through the TPPA ligands, resulting in a 2D sheet with a 6^3 honeycomb network [68].

The structures discussed above demonstrate that the incorporation of bridge molecules based on N-donor heterocycles as ligands can vastly extend the architectures of chalcogenide networks. Besides pyridine-based bridges, imidazolates can also be used to bridge supertetrahedral clusters. 3D networks consisting of μ_4-supertetrahedral T3-type or T4-type clusters connected by various imidazolate bridges, so called supertetrahedral cluster imidazolate frameworks (SCIFs), were synthesized [69]. The special feature of these structures is that the size and geometry of their pore space can be influenced by the size of the cluster and the type of substituents on the imidazolate bridges. For example, the anionic substructures 3D-{$[In_{16}Cd_4S_{31}(2\text{-}C_2im)_2]^{8-}$} (in **32**, 2-$C_2$im = 2-ethylimidazole) and 3D-{$[In_{16}Cd_4S_{31}(5,6\text{-}C_1C_1Bim)_2]^{8-}$} (in **33**, 5,6-$C_1C_1$Bim = 5,6-dimethyl-benzimidazole) were the first examples of covalently ligand-bound assemblies of T4 clusters.

In 2018, the use of a mixture of imidazolate bridges and superbases led to the formation of two new metal chalcogenide imidazolate frameworks, $(H^+\text{–}DBU)_5[(In_{10}S_{17})(IM)]$ (**34**) and $(H^+\text{–}DBU)_{8.75}[(Cd_4In_{16}S_{31.5})(IM)_{1.75}]$ (**35**, IM = imidazolate) [70]. In **34**, each T3-$[(In_{10}S_{17})(IM)]$ cluster is connected to four surrounding T3 clusters by sharing two IM units and two μ_2-S^2 ligands at the corners of the supertetrahedron, thereby building a 3D architecture with a distorted doubly-interpenetrated diamond-like structure (Fig. 9a). Compound **35** contains an interrupted 3D-network with a unique topology based on 3-connected and 4-connected T4-$[(Cd_4In_{16}S_{31.5})(IM)_{1.75}]$ clusters, with the former featuring a terminal $(SH)^-$ group at one of the four corners. The two kinds of differently connected clusters are distributed at regular intervals in a 1:1 ratio. Together, they form a 3D framework that evolves from 2D wave-like layers, which are connected to each other by the four-connected T4 clusters (Fig. 9b).

In addition to imidazolate bridges, 1,2,4-triazolate (TZ) bridges are also widely used, although these show some differences from imidazolate bridges. 1,2,4-Triazolate has more N-atoms compared to imidazolate, and a lower Lewis basicity. Two new supertetrahedral cluster-based triazolate frameworks (SCTFs) were prepared by incorporation of TZ ligands [71]. Both reported structures are built from condensed T3 $\{In_{10}S_{20}\}$ clusters and TZ bridges to form hybrid structures, $(H^+\text{–}DBN)_{5.5}[(In_{10}S_{17.5})(TZ)_{0.5}]$ (**36**) and $(H^+\text{–}DBN)_5[(In_{10}S_{17})(TZ)]$ (**37**). In **37**, one corner of the T3-InS cluster is bound to one TZ bridge, while the remaining three corners are connected to neighboring clusters *via* μ_2-S^2 bridges. Altogether, this results in a distorted diamond-like architecture (Fig. 9c). **36** has a similar structure, but with a μ_2-S^{2-}/TZ ratio of 2:2, which yields 1D zigzag chains of T3 clusters that are connected *via* TZ bridge.

So far, all structures shown have been based upon N-donor ligands. In addition, chalcogenide frameworks in which the clusters are bridged by O-donor bridges were reported—in 2018 for the first time. They form assemblies from clusters ranging from T3-type to T5-type architectures [72]. The anion 1D-{$[(In_{10}S_{16})(H_2O)_2(BTC)]^{4-}$} (in **38**, BTC = benzenetricarboxylate) is built of a T3-$\{In_{10}S_{16}O_2\}$ cluster, in which two sulfur atoms at the vertices are replaced by oxygen atoms from water molecules. The two remaining vertices are bridged *via* BTC ligands to form a 1D chain (Fig. 10a). $[(Fe_4In_{16}S_{31})(H_2O)_3(BTC)_{1/3}]^{7-}$ (in **39**) is based on a T4-$[Fe_4In_{16}S_{31}O_3]$ cluster, where three vertices were replaced by oxygen atoms from water molecules. The last remaining vertex is bound to one BTC ligand, and one BTC ligand in turn is connected to three other T4 clusters to form a discrete anionic supramolecular assembly (Fig. 10b). The T5-type secondary building units of 2D-$\{[(In_{35}S_{48}O_8)(H_2O)(BTC)]^{10}\}$ (in **40**) represent the largest supertetrahedral sulfido-oxido nanoclusters of the T*n* series, while all other reported examples if T*n*-type sulfido-oxido clusters exhibited n = 2, 3, 4 [73,74]. In **40**, the T5

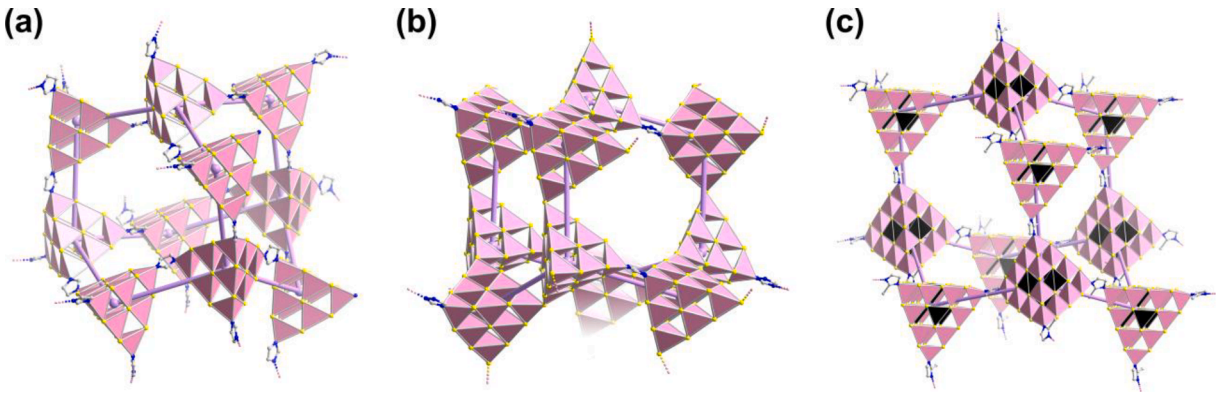

Fig. 9. Polyhedral representation of sulfido metalate clusters bridged by IM or TZ bridges. (a) $(H^+–DBU)_5[(In_{10}S_{17})(IM)]$. (b) $(H^+–DBU)_{8.75}[(Cd_4In_{16}S_{31.5})(IM)_{1.75}]$. (c) $(H^+–DBN)_{5.5}[(In_{10}S_{17.5})(TZ)_{0.5}]$. Rose polyhedra represent $[InS_4]^{5–}$ units, black polyhedral represent $[CdS_4]^{6–}$ units.

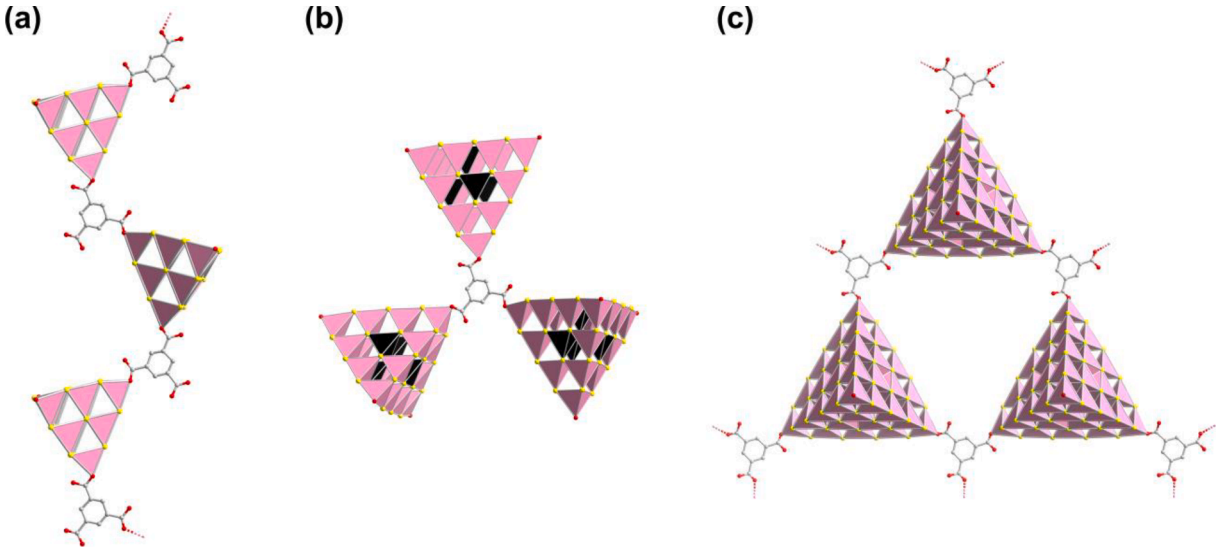

Fig. 10. BTC-bridged assemblies of supertetrahedral chalcogenido metalate clusters. (a) one dimensional T3-$\{[(In_{10}S_{16})(H_2O)_2(BTC)]^{4–}\}$. (b) discrete T4-$[(Fe_4In_{16}S_{31})(H_2O)_3(BTC)_{1/3}]^{7–}$. (c) two dimensional T5-$\{[(In_{35}S_{48}O_8)(BTC)(H_2O)]^{10–}\}$. Rose polyhedra represent $[InS_4]^{5–}$, black polyhedra represent $[FeS_4]^{6–}$.

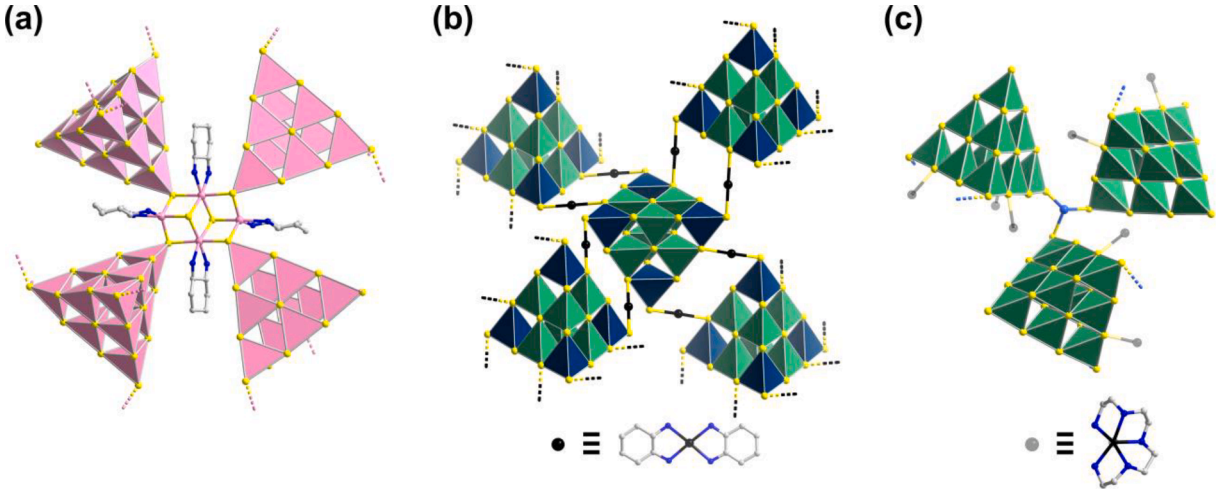

Fig. 11. Polyhedral representation of assemblies of In/S and Ga/S-based clusters. (a) $(H_2^+–dach)\{[Ni(dach)_3][In_{12}S_{20}(dach)_2]\}\cdot 3H_2O$ with $[In_4S_2(dach)_4]^{8+}$ units bridging T3-type $\{In_{10}S_{20}\}$ clusters. (b) $[Mn(dach)_2]^{2+}$-linked heterometallic T3-$\{Mn_2Ga_4Sn_4S_{20}\}$ clusters. (c) $[TM(TEPA)]_3[Ga_{10}S_{19}SHSb]$. Rose, sea-green, and dark-blue polyhedra represent $[InS_4]^{5–}$, $[GaS_4]^{5–}$, and $[SnS_4]^{4–}$, respectively. H atoms are omitted for clarity.

cluster can be described as a T5-{$In_{35}S_{52}$} with four of the sulfide ligands in the cluster core being replaced by oxide ligands, and four additional oxide atoms being inserted into four of the central admantane-type cages. The T5-type units are assembled in a plane and oriented in the same fashion. Each of them connects to three bridging BTC molecules (and *vice versa*) to form a 2D-superlattice with a honeycomb-like topology if T5-type cluster and BTC ligands are viewed as three-connected nodes (Fig. 10c).

Using 1,2-diaminocyclohexane (dach), (H_2^+–dach){[Ni(dach)$_3$][$In_{12}S_{20}$(dach)$_2$]}·3H_2O (**41**) was synthesized. It contains a polyanionic 3D-{[$In_{12}S_{20}$(dach)$_2$]$^{4-}$} framework, which is constructed by T3-{$In_{10}S_{20}$} clusters mentioned above and a {In_4(dach)$_4S_6$} cluster subunit condensed at four corners of the T3 clusters in a 2:1 ratio [75]. In this second subunit, two defect hetero cubane moieties {In_3S_4} are condensed to share one face, which results in a centrosymmetric assembly. The In atoms possess two different coordination environments: trigonal bipyramidal {InS_3N_2} and octahedral {InS_4N_2}. Each In atom of the cluster is coordinated by one chelating dach molecule (Fig. 11a).

A neutral 3D chalcogenide framework containing dach molecules is [Mn(dach)$_2$]$_4$[$Mn_2Ga_4Sn_4S_{20}$] (**42**). The compound is built up from a regular supertetrahedral T3 cluster and [Mn(dach)$_2$]$^{2+}$ complexes, which act as linkers to connect neighboring supertetrahedral T3 subunits by S–Mn–S bonds (Fig. 11b) [76]. In the bridge, the Mn atom has a six-coordinate environment with four N atoms of the two dach ligands at the equatorial sites and two S atoms from the edge or the corner of the T3 clusters at the axial sites. Overall, each T3 cluster is bridged to four other T3 clusters *via* eight [Mn(dach)$_2$]$^{2+}$ complexes, resulting in a 3D open framework with a diamond-like topology.

In 2022, three new 3D chalcogenide frameworks of the general formula [TM(TEPA)]$_3$[$Ga_{10}S_{19}$SHSb] (TM = Mn, **43a**; Ni, **43b**; Fe, **43c**) were introduced upon the use of tetraethylenepentamine (TEPA) [77]. The compounds are isostructural and consist of three-coordinated sulfido gallate-based supertetrahedral T3 clusters, which are connected to three adjacent, three-connected Sb^{3+} ions by their corners. Additionally, each of the T3 cluster is decorated with a different type of [TM(TEPA)]$^{2+}$ (TM = Mn/Ni/Fe) complexes at their edges. The T3 clusters are connected to Sb^{3+} ions in a way that results in left-handed and right-handed helices along the crystallographic *a*-axis. (Fig. 11c).

Ligands do not only serve to bridge and/or decorate cluster from corners and/or edges of supertetrahedra, but can also stabilize subunits in the cavities of cluster aggregates. An example is given by the selenido metalate cluster, (C_2C_1Im)$_{10}$[Na_5(CN)$_6$@Cu_6(Ge_4Se_{10})$_4$(Cu)] (**44**, in which the Cu atoms carry $(CN)^-$ ligands [11]. It was obtained by ionothermal treatment of Na_4[$GeSe_4$]·14H_2O, CuCN/Cu(OAc)$_2$·H_2O, and dmmp in (C_2C_1Im)[B(CN)$_4$]. This compound consists of four T2-type [Ge_4Se_{10}]$^{4-}$ units, which are linked by six Cu^I atoms bearing $(CN)^-$ ligands. The resulting (defect) supertetrahedron is connected on three of its corners to Cu^I units which serve as bridges to the neighboring clusters, ultimately forming a two-dimensional layer (Fig. 12a). The $(CN)^-$ groups point towards the center of the inner cavity of this cluster and coordinate to a Na^+centered (non-bonding) Na_4 tetrahedron (Fig. 12b).

In addition to assemblies comprising bridged T*n* clusters, there was also success in linking P*n* clusters by bipyridyl ligands to form one-dimensional polymeric chains in three cases. All three compounds, 1D-[Zn_8S(SPh)$_{14}$(DPE)] (**45**), 1D-[Zn_8S(SPh)$_{14}$(BPP)] (**46**) and 1D-[Zn_7CoS(SPh)$_{14}$(BPP)] (**47**), were synthesized by hydrothermal reactions and comprise P1 cluster units [78]. The P1-type {Zn_8S_{14}} cluster in **45** is connected to two N atoms of one *trans*-1,2-bis(4-pyridyl) ethylene ligand each, that links the clusters into one-dimensional zig-zag chains of alternating P1 clusters and dipyridyl moieties. Compound **46** is based on the same P1 {[Zn_8S_{14}]} cluster as in **45**, but the P1 clusters are bridged *via* 1,3-bis(4-pyridyl)propane molecules here. The P1 clusters in **47** are also linked *via* 1,3-bis(4-pyridyl)propane molecules, but in the P1 cluster core, one Zn atom was replaced by a Co atom. This could not be determined through crystallographic refinement, so inductively coupled plasma spectrometry was used to prove the Zn:Co ratio. In addition to bipyridyl bridges in P*n* clusters, there was also success in using the quadridentate linker tetrakis(4-pyridyloxymethylene)methane (TPOM) to build the P1 cluster [Cd_8S(SPh)$_{16}$(TPOM)$_2$] (**48**). In each P1-type {[Cd_8S(SPh)$_{16}$]} cluster core, two corners are occupied by SPh^- groups while the two other corners are terminated by N atoms from TPOM. In turn, one TPOM ligand is connected to three other P1-type clusters to form a 1D structure [79].

Besides T*n* and P*n* clusters, there is a third family of tetrahedral clusters, the so-called capped supertetrahedral clusters (C*n*). In C*n* clusters, each cluster consists of a regular T*n* unit in the cluster core, the four faces of which are capped by barrelanoid cages characteristic of the hexagonal Wurtzite-type structure. Each face of the T*n* core unit is covered with a single atomic layer, the T(n + 1) layer, and each corner of this cluster is covered with an MCh group (M = metal, Ch = chalcogen). One distinct structural feature is that there is an open cleft along each edge of the cluster. In 2005, three C*n* clusters bridged *via* bifunctional linkers were synthesized. 1D-[Cd_8S(SPh)$_{14}$(TMDP)$_2$] (**49**) is built of a C0-{[Cd_8S(SPh)$_{14}$]} cluster (Fig. 13a), at two vertices of which the S atoms were replaced by TMDP linker molecules. Every bridge, in turn, is connected to two C0 clusters, resulting in a 1D chain. In 1D-

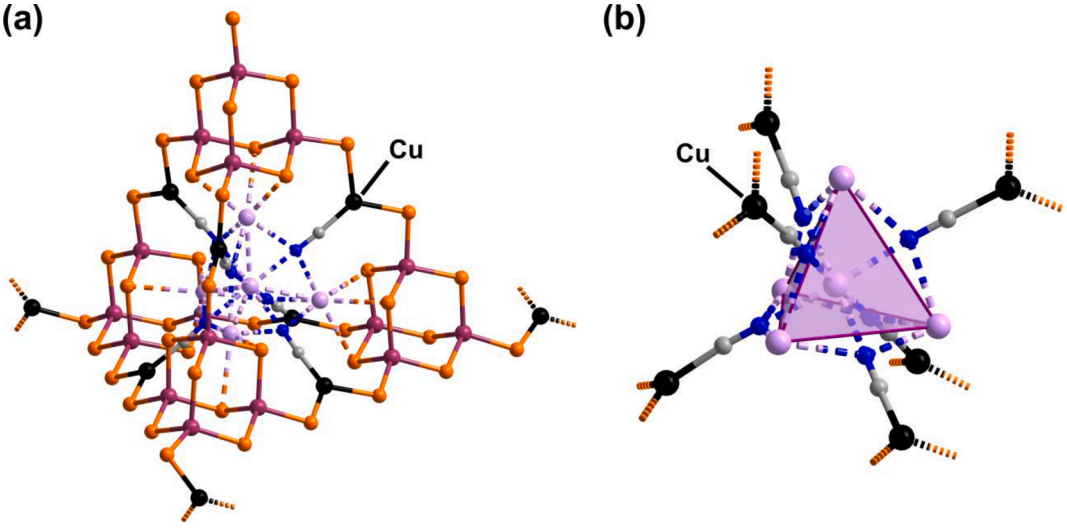

Fig. 12. Crystal structure of (C_2C_1Im)$_{10}$[Na_5(CN)$_6$@Cu_6(Ge_4Se_{10})$_4$(Cu)]. (a) The supertetrahedral cluster [Na_5(CN)$_6$@Cu_6(Ge_4Se_{10})$_4$(Cu)]$^{10-}$. (b) Central unit with cyanide ligands linking copper and sodium cations in the inner cavity of the cluster. H atoms and counterions are omitted for clarity.

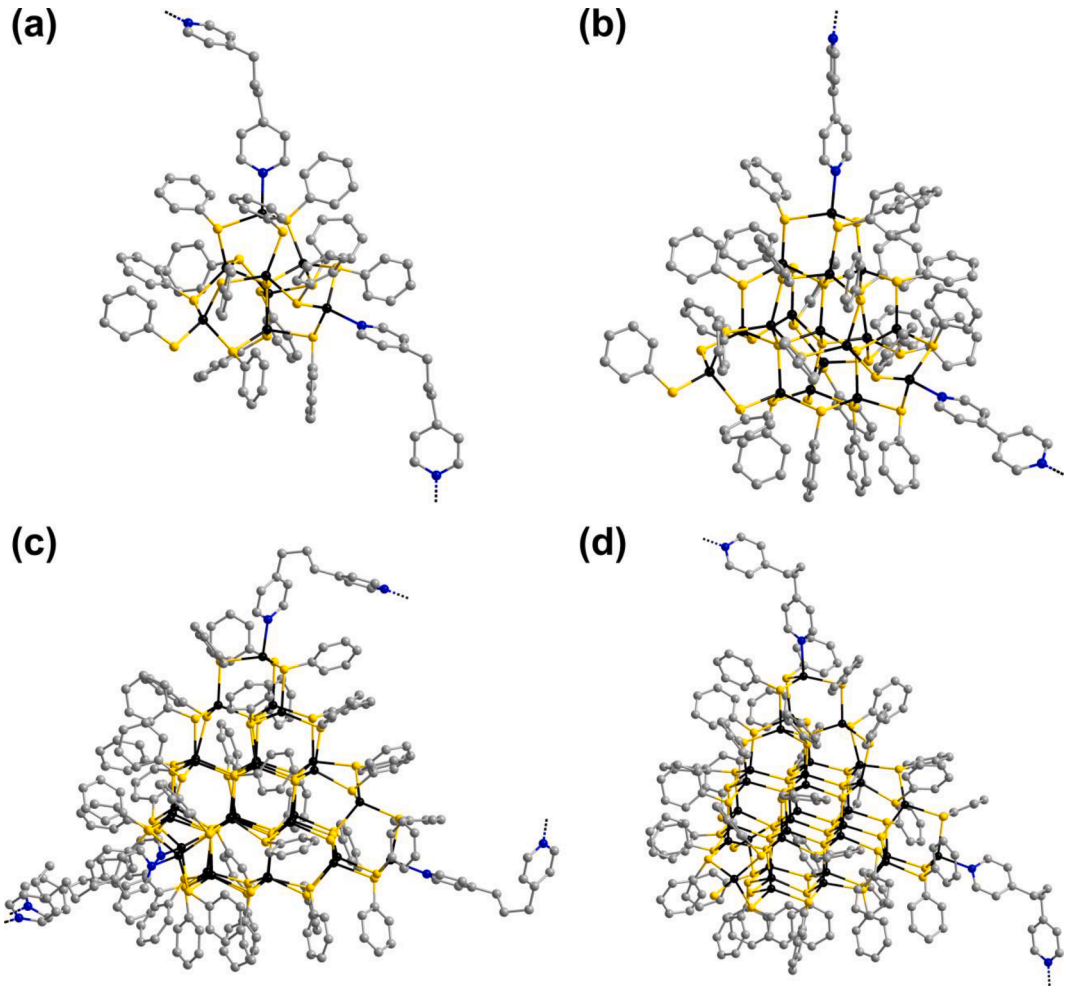

Fig. 13. Structures of the C*n* and C*n,m* clusters. (a) C0-[$Cd_8S(SPh)_{14}$] cluster core in 1D-[$Cd_8S(SPh)_{14}(TMDP)_2$]. (b) C1-[$Cd_{17}S_4(SPh)_{26}$] cluster core in 1D-[$Cd_{17}S_4(SPh)_{26}(bpy)_2$], (c) C2,1-[$Cd_{32}S_{14}(SPh)_{36}$] in 1D-[$Cd_{32}S_{14}(SPh)_{36}(TMDP)_4$]. (d) C2,2-[$Cd_{32}S_{14}(SPh)_{38}$] in 1D-[$Cd_{32}S_{14}(SPh)_{38}(TMDP)_2(PPh_4)_2$]. Cd atoms are drawn in black. H atoms are omitted for clarity.

[$Cd_{17}S_4(SPh)_{26}(bpy)_2$] (**50,** Fig. 13b), the C1-type [$Cd_{17}S_4(SPh)_{26}$] cluster is bridged *via* the more rigid bpy molecule to form a 1D zigzag chain [75]. There was also success in bridging a C1-type cluster by using the quadridentate linker TPOM. In [$Cd_{17}S_4(SPh)_{28}(TPOM)_2$] (**51**) two corners per C1-type {[$Cd_{17}S_4(SPh)_{28}$]} cluster unit are terminated by TPOM linkers. For linking into a 1D chain, every TPOM linker is connected to two C1-type clusters [79].

In addition to C*n* clusters, there are also C*n,m* clusters. These have the same composition as the corresponding C*n* type, while *m* of the four {M_4Ch_5} corner units are rotated by 60°. Each of the four corner units can be rotated independently, so *m* ranges from 1 to 4 [58]. Two C*n,m* clusters, 1D-[$Cd_{32}S_{14}(SPh)_{36}(TMDP)_4$] (**52**) and 1D-[$Cd_{32}S_{14}(SPh)_{38}(TMDP)_2(PPh_4)_2$] (**53**), which are bridged *via* TMDP molecules, were obtained under solvothermal conditions. Compound **52** has one barrelanoid cage rotated, which leads to a C2,1-type cluster (Fig. 13c), while in compound **53**, two corners are rotated (C2,2 type, Fig. 13d). In **52**, the C2,1-[$Cd_{32}S_{14}(SPh)_{36}$] cluster is connected by two TMDP bridges into doubly-bridged chains, while in **53**, each C2,2-[$Cd_{32}S_{14}(SPh)_{38}$] cluster alternates with one TMDP molecule to build singly-bridged chains. These materials exhibit size-dependent optical properties, as the absorption edge shifts to longer wavelengths when larger clusters are used as building blocks [80].

Before publication of these clusters, only a few C*n,m* clusters were known, and almost all C*n* clusters were synthesized in the form of molecular crystals or covalent superlattices by corner-bound thiolates. A few examples of covalent assemblies of chalcogenide nanoclusters and ligands have been reported [81]. Regarding the optical properties of C*n* and C*n,m* clusters comprising various semiconducting nanoclusters as building blocks, it was reported again that the optical absorption of the material is red-shifted when larger clusters are used as building blocks [80]. In comparison to solutions containing discrete clusters of the similar size and composition, the extended compounds exhibit broader absorption spectra, with the onset of their absorption red-shifted; this refers to electronic communication between clusters within the unique arrangements described here [82].

All ligand-bridged and ligand-functionalized, supertetrahedral chalcogenido metalate cluster-based compounds presented in section 2.2 are summarized in Table 2.

3. Ligand-functionalized or organyl-separated chalcogenido metalate-based compounds exhibiting other cluster architectures

3.1. Ligand-functionalized chalcogenido metalate-based clusters exhibiting other cluster architectures

In this section, we present chalcogenido metalate-based clusters prepared by an ionothermal synthetic route and composed of other building blocks than the supertetrahedral ones described above, and octahedral ones discussed below. This means that the clusters are composed of different subunits such as tetrahedral and trigonal pyramidal or trigonal planar units, rather than an assembly of tetrahedra only.

Table 2
Summary of the ligand-bridged and ligand-functionalized chalcogenido metalate-based supertetrahedra in Section 2.2.

Compound	Dimensionality	Reactants	Temperature (°C)	Ref.
$(H^+–NC_6H_7)_2[Ga_{10}S_{16}(NC_6H_7)_2(DPE)]$ **(20)**	1D	Ga, S, DPE and 4-methylpyridine	170	[61]
$(H^+–NC_7H_9)_2[Ga_{10}S_{16}(NC_7H_9)(DPE)_{3/2}]$ **(21)**	2D	Ga, S, DPE and 3,5-dimethylpyridine	200	[61]
$(H^+–NC_7H_9)_6[Ga_{20}S_{34}H_2(NC_7H_9)_4(DPE)]$ **(22)**	0D	Ga, S, DPE, $FeCl_2{\cdot}4H_2O$ and 3,5-dimethylpyridine	200	[62]
$(H^+–NC_7H_9)_6[Ga_{10}S_{16}(NC_7H_9)(bpy)_3]$ $[Ga_{20}S_{32}(NH_3)_2(NC_6H_7)_4(bpy)]$ **(23)**	0D	Ga, S, bpy and 3,5-dimethylpyridine	200	[62]
$(H^+–NC_5H_5)_8[(Ga_{10}S_{16})_7(NC_2H_7)_4(NC_6H_7)_8(N_2C_{12}H_{12})_8]$ **(24)**	2D	Ga, S, 1,3-benzodiazole and 4-methylpyridine	200	[63]
$(H^+–NC_2H_7)_2[Ga_{10}S_{16}(DPE)(NC_2H_7)_2]$ **(25)**	2D	Ga, S, DPE, tetraphenylphosphonium bromide and pyridine	200	[64]
$(H^+–NC_5H_5)_3[Ga_{10}S_{16}(OH)_2(TMDP)]$ **(26)**	2D	Ga, S, TMDP and pyridine	200	[64]
$[Cd_6Ag_4(SPh)_{16}(DPE)_2]]$ **(27)**	3D	$Cd_6Ag_4(SPh)_{16}(DMF)_4$ in DPE	rt	[65]
$[Cd_6Ag_4(SPh)_{16}(DMF)(H_2O)(DPE)]$ **(28)**	1D	$Cd_6Ag_4(SPh)_{16}(DMF)_3(CH_3OH)$ in DMF, DPE	rt	[66]
$[Cd_6Ag_4(ChPh)_{16}(TMDP)_2]$ **(29)**	2D	$Cd_6Ag_4(EPh)_{16}(DMF)_3(CH_3OH)$ in DMF, TMDP (Ch = S, Se)	rt	[67]
$[Cd_{12}Ag_8(SPh)_{32}(TPPA)(DMF)_3(H_2O)_2]{\cdot}2DMF$ **(30)**	1D	$AgNO_3$, $Cd(PhS)_2$ in DMF, TPPA	rt	[68]
$[Cd_{12}Ag_8(SPh)_{32}(TPPA)_2(DMF)(H_2O)]$ **(31)**	2D	$AgNO_3$, $Cd(PhS)_2$ in DMF, TPPA	rt	[68]
$(Cat)_8[In_{16}Cd_4S_{31}(2\text{-}C_2im)_2]$ **(32)**	3D	Li_2S, $In(NO_3)_3{\cdot}xH_2O$, $Cd(NO_3)_2{\cdot}4H_2O$, 2-ethylimidazole, 2-amino-1-butanol, DBU	150	[69]
$(Cat)_8[In_{16}Cd_4S_{31}(5,6\text{-}C_1C_1Bim)_2]$ **(33)**	3D	Li_2S, $In(NO_3)_3{\cdot}xH_2O$, $Cd(NO_3)_2{\cdot}4H_2O$, 5,6-dimethylbenzimidazole, 2-amino-1-butanol,acetontril, DBU	150	[69]
$(H^+–DBU)_5[(In_{10}S_{17})(IM)]$ **(34)**	3D	In, S, IM, toluene, (R)-(-)-2-amino-1-butanol, DBU	180	[70]
$(H^+–DBU)_{8.75}[(Cd_4In_{16}S_{31.5})(IM)_{1.75}]$**(35)**	3D	$In(NO_3)_3{\cdot}4.5H_2O$, $Cd(NO_3)_2{\cdot}4H_2O$, IM, thiourea, MeCN, cyclohexylamine, DBU	150	[70]
$(H^+–DBN)_{5.5}[(In_{10}S_{17.5})(TZ)_{0.5}]$ **(36)**	1D	$In(NO_3)_3{\cdot}4.5H_2O$, S, TZ, DMF, DBN	180	[71]
$(H^+–DBN)_5[(In_{10}S_{17})(TZ)]$ **(37)**	3D	$In(NO_3)_3{\cdot}4.5H_2O$, thiourea, TZ, MeCN, DBU	150	[71]
$(Cat)_4[(In_{10}S_{16})(H_2O)_2(BTC)]$ **(38)**	1D	$In(NO_3)_3{\cdot}xH_2O$, H_3BTC, thiourea, DBU, DMF	180	[72]
$(Cat)_7[(Fe_4In_{16}S_{31})\cdot(H_2O)_3(BTC)_{1/3}]$ **(39)**	3D	$In(NO_3)_3{\cdot}xH_2O$, H_3BTC, thiourea, $Fe_2(SO_4)_3{\cdot}xH_2O$, DBU, DMF	180	[72]
$(Cat)_{10}[(In_{35}S_{48}O_8)(H_2O)(BTC)]$ **(40)**	2D	$In(NO_3)_3{\cdot}xH_2O$, H_3BTC, thiourea, DBU, DMF	180	[72]
$(H_2^+\text{-dach})\{[Ni(dach)_3][In_{12}S_{20}(dach)_2]\}{\cdot}3H_2O$ **(41)**	3D	Ni, In, L-cysteine, $(C_4C_1Im)Br$, GeO_2 in a water solution of 1 mL 65 % dach	160	[75]
$[Mn(dach)_2]_4[Mn_2Ga_4Sn_4S_{20}]$ **(42)**	3D	S, Ga_2O_3, Sn, $Mn(Ac)_2{\cdot}4H_2O$, H_2O, dach	180	[76]
$[Mn(TEPA)]_3[Ga_{10}S_{19}SHSb]$ **(43a)**	3D	$Mn(Ac)_2{\cdot}4H_2O$, S, Ga_2O_3, Sb_2S_3, TEA, TEPA and water	180	[77]
$[Ni(TEPA)]_3[Ga_{10}S_{19}SHSb]$ **(43b)**	3D	$Ni(Ac)_2{\cdot}4H_2O$, S, Ga_2O_3, Sb_2S_3, TEA, TEPA and water	180	[77]
$[Fe(TEPA)]_3[Ga_{10}S_{19}SHSb]$ **(43c)**	3D	$Fe(Ac)_2{\cdot}4H_2O$, S, Ga_2O_3, Sb_2S_3, TEA, TEPA and water	180	[77]
$(C_2C_1Im)_{10}[Na_5(CN)_6@Cu_6(Ge_4Se_{10})_4(Cu)]$ **(44)**	2D	$[Na_4(H_2O)_{14}][GeSe_4]$, CuCN/$Cu(OAc)_2{\cdot}H_2O$ in $(C_2C_1Im)[B(CN)_4]$ with dmmp	150	[11]
$[Zn_8S(SPh)_{14}(DPE)]$ **(45)**	1D	$Zn(OAc)_2{\cdot}2H_2O$, DPE, thiourea, thiophenol, water	150	[78]
$[Zn_8S(SPh)_{14}(BPP)]$ **(46)**	1D	$Zn(OAc)_2{\cdot}2H_2O$, BPP, thiourea, AgOAc, thiophenol, water	165	[78]
$[Zn_7CoS(SPh)_{14}(BPP)]$ **(47)**	1D	$Zn(OAc)_2{\cdot}2H_2O$, BPP, thiourea, $Co(NO_3)_2{\cdot}6H_2O$, thiophenol, water	150	[78]
$[Cd_8S(SPh)_{16}(TPOM)_2]$ **(48)**	1D	Thiourea, $Cd(SPh)_2$, TPOM, MeCN, methanol	85	[79]
$[Cd_8S(SPh)_{14}(TMDP)_2]$ **(49)**	1D	Thiourea, $Cd(SPh)_2$, PPh_4Br, TMDP, MeCN, water	85–150	[80]
$[Cd_{17}S_4(SPh)_{26}(bpy)_2]$ **(50)**	1D	Thiourea, $Cd(SPh)_2$, PPh_4Br, bpy, MeCN	85–150	[80]
$[Cd_{17}S_4(SPh)_{28}(TPOM)_2]$ **(51)**	1D	Thiourea, $Cd(SPh)_2$, TPOM, DMF, water	85	[79]
$[Cd_{32}S_{14}(SPh)_{36}(TMDP)_4]$ **(52)**	1D	Thiourea, $Cd(SPh)_2$, PPh_4Br, TMDP, MeCN	110	[80]
$\{Cd_{32}S_{14}(SPh)_{38}(TMDP)_2[PPh_4]_2\}$ **(53)**	1D	Thiourea, $Cd(SPh)_2$, PPh_4Br, TMDP, MeCN	85–150	[80]

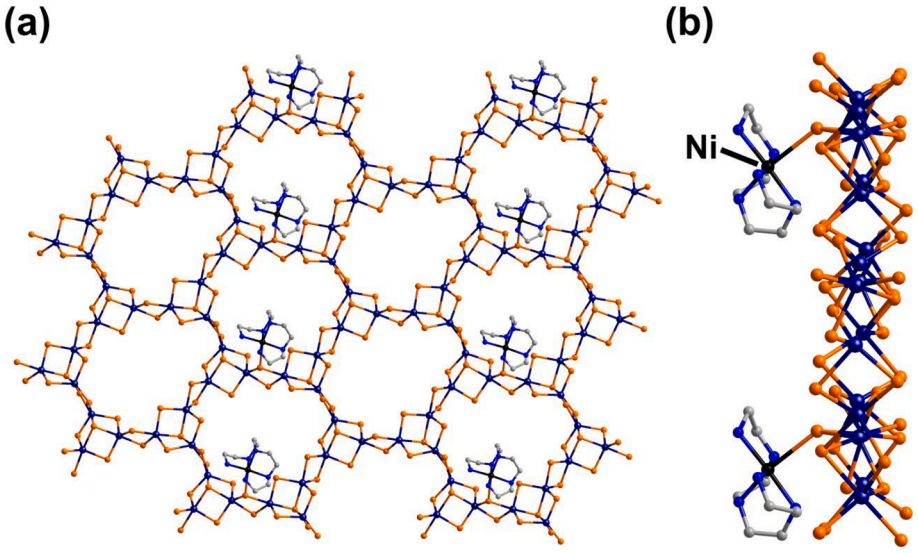

Fig. 14. (a, b) Two different crystallographic views of the ligand-functionalized layered selenido stannate anion 2D-$\{[Ni(TEPA)Sn_{12}Se_{28}]^{6-}\}$ anion. Counterions and H atoms are omitted for clarity.

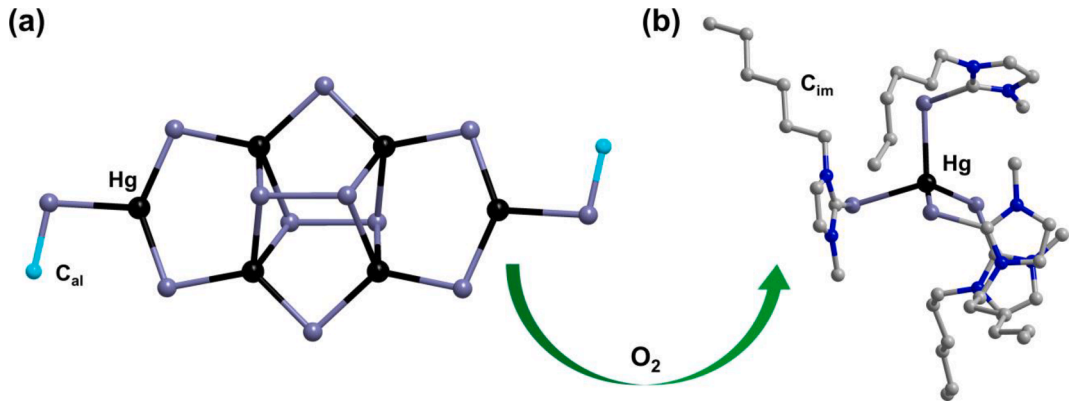

Fig. 15. Molecular structures of organyl-functionalized tellurido mercurate compounds. (a) Methylated $[Hg_6Te_6(Te_2)_2(TeMe)_2]^{6-}$ anion. (b) Carbene-functionalized cation $[Hg(TeC_6C_1im)_4]^{2+}$. C_{al} alkylated carbon atoms at the cluster, C_{im} carbon atom of imidazole ligands; H atoms are omitted for clarity.

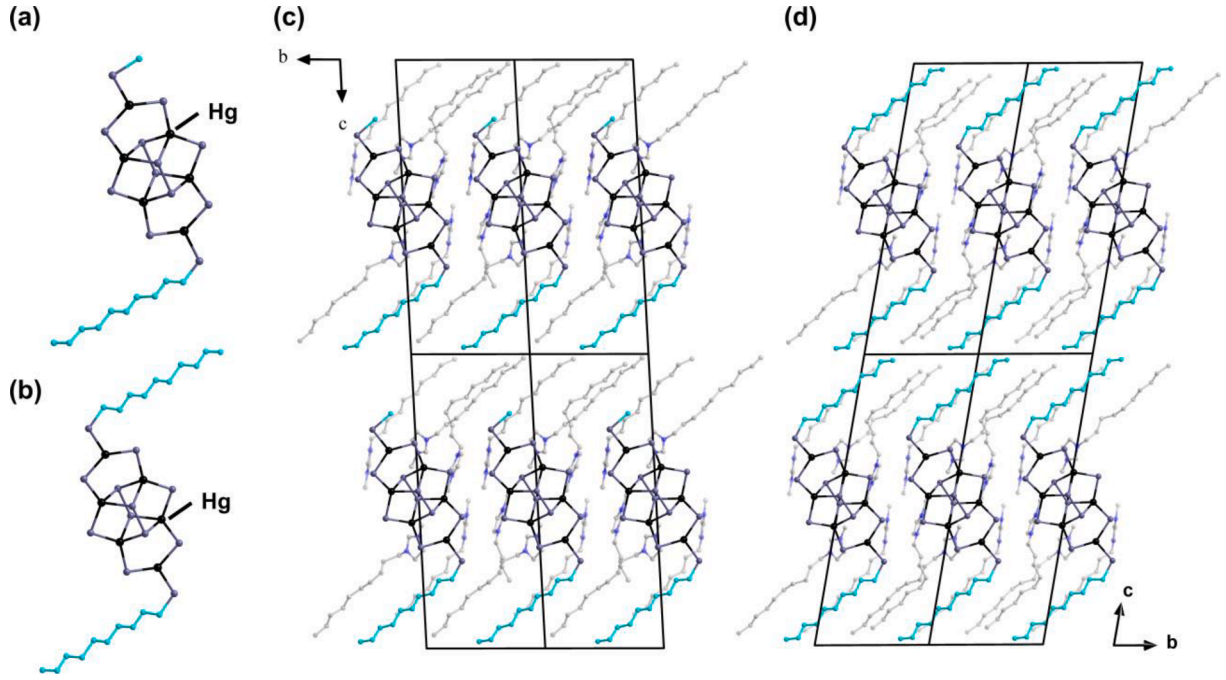

Fig. 16. Alkylated tellurido mercurate cluster anions embedded in a lamellar crystal structure. (a) Molecular structure of the $[Hg_6Te_6(Te_2)_2(TeMe)(TeDec)]^{6-}$ anion terminated by one methyl group and one decyl group at the terminal telluride positions. (b) Molecular structure of $[Hg_6Te_6(Te_2)_2(TeDec)_2]^{6-}$, homoleptically decylated at its terminal telluride positions. (c) $2 \times 2 \times 2$ supercell of the first, viewed along the crystallographic *a*-axis (d) $2 \times 2 \times 2$ supercell of the latter, viewed along the crystallographic *a*-axis. Carbon atoms from the alkyl groups are drawn in turquoise color to distinguish them from the carbon atoms of the counterions drawn in grey color. H atoms are omitted for clarity.

The first organically decorated, layered selenido stannate anion 2D-$\{[Ni(TEPA)Sn_{12}Se_{28}]^{6-}\}$ (in **54**; Fig. 14a–b) was synthesized from ionic liquids in 2016. It was obtained upon reaction of elemental Sn and Se with $Ni(NO_3)_2{\cdot}6H_2O$ in $(C_4C_1C_1Im)Cl$ with TEPA. The anion consists of two double-defect hetero cubane structures that extend two-dimensionally to form a six-membered annular layered architecture [83].

The ionothermal synthesis of heavier chalcogenido metalate precursors, such as $A_x[M_yCh_z]$ with A = Na, M = Hg, and Ch = Te, has seen a lot of success. The first functionalized tellurido mercurate anion, homoleptically methylated, was found in the compound $(C_nC_1Im)_6[Hg_6Te_6(Te_2)_2(TeMe)_2]$ (n = 6 (**55a**), 8 (**55b**); Fig. 15a). It is an extremely air- and moisture-sensitive compound which was synthesized from $Na_2[HgTe_2]$ in the ionic liquids $(C_nC_1Im)[BF_4]$ (n = 6, 8). The $[Hg_6Te_6(Te_2)_2(TeMe)_2]^{6-}$ anion consists of four (distorted) tetrahedral $[HgTe_4]^{6-}$ units and two trigonal planar $[HgTe_3]^{4-}$ units, with methyl groups attached to the two terminal telluride atoms [47]. Briefly exposing compounds of the anion $[Hg_6Te_6(Te_2)_2(TeMe)_2]^{6-}$ to air and resealing them under argon yields the new species $[Hg(TeC_nC_1im)_4]^{2+}$ (n = 6 (in **56a**), 8 (in **56b**); Fig. 15b) with a cation built up from a mercury atom tetrahedrally coordinated by four carbene-functionalized tellurones that formed *in situ*. UV–vis spectroscopic measurements of these two compounds showed that the longer chain length resulted in a slightly narrower optical band gap (2.50 eV for **56a**; 2.45 eV for **56b**) [84].

All ligand-functionalized chalcogenido metalate cluster-based compounds presented in Section 3.1 are summarized in Table 3.

3.2. Ligand-functionalized and organyl-separated discrete chalcogenido metalate-based clusters exhibiting other cluster architectures

Tellurido mercurate clusters can also be derivatized with longer alkyl

Table 3
Summary of the ligand-functionalized chalcogenido metalate-based cluster compounds presented in Section 3.1.

Compound	Dimensionality	Reactants	Temperature (°C)	Ref.
$(C_4C_1C_1Im)_4[Ni(TEPA)Cl_2]$ $[Ni(TEPA)Sn_{12}Se_{28}]$ (**54**)	2D	Sn, Se, $Ni(NO_3)_2{\cdot}6H_2O$ in $(C_4C_1C_1Im)Cl$ with TEPA	160	[83]
$(C_nC_1Im)_6[Hg_6Te_6(Te_2)_2(TeMe)_2]$ (**55**)	0D	$Na_2[HgTe_2]$ in $(C_nC_1Im)[BF_4]$ (n = 10, 12)	80	[47]
$[Hg(TeC_nC_1Im)_4][BF_4]_2$ (**56**)	0D	$(C_nC_1Im)_6[Hg_6Te_6(Te_2)_2(TeMe)_2]$ in $(C_nC_1Im)[BF_4]$ (n = 6, 8), under ambient conditions	rt	[84]

chains in the tellurolate groups. Two examples featuring the same inorganic core as described for **55** are the heteroleptically decorated anion $[Hg_6Te_6(Te_2)_2(TeMe)(TeDec)]^{6-}$ (in **57**, Fig. 16a) and another homoleptically functionalized cluster $[Hg_6Te_6(Te_2)_2(TeDec)_2]^{6-}$ (in **58**, Fig. 16b). Compound **57** was synthesized from $Na_2[Hg_3Te_4]$ with $(C_{10}C_1Im)[BF_4]$ and small amounts of en as auxiliary at 80 °C for 20 h. It is the first chalcogenide metalate compound to feature two different alkyl chains upon alkylation by an IL. **58** is obtained from the reaction of $Na_2[HgTe_2]$ with $(C_{10}C_1Im)[BF_4]$ and small amounts of $ZnCl_2$ at 80 °C for 20 h. Both compounds show lamellar arrangements in their crystal structure, where the anionic substructures are embedded in a lamellar pattern of the alkyl chains provided by the cluster termini and the IL cations (Fig. 16c–d); this is reminiscent of soap/surfactant micelles or to lipid double layers, e.g., in cell membranes. Consequently, the crystals contain layers comprising the ionic part, with strong interactions between the anionic clusters and the cationic imidazolium rings of the IL component, and non-polar interlayers formed by the long alkyl chain of the ILs and the tellurolate group on the clusters. This arrangement may be viewed as both, a ligand-functionalized and an organyl-separated chalcogenido metalate-based cluster compound [85].

Besides compounds with direct covalent bonds between the cluster atoms and ligands, it is also possible to isolate compounds, in which purely inorganic chalcogenido metalate clusters are organyl-separated by ILs or surfactants as spacer molecules in an ordered fashion in the solid state.

One example is the compound $(C_{10}C_1Im)_4[Hg_4Te_2(Te_2)_2(Te_3)_2]$ (**59**). Its anion, $[Hg_4Te_2(Te_2)_2(Te_3)_2]^{4-}$, contains two folded $[Hg_2Te(Te_2)]$ rings and two additional lateral Te_3^{2-} "handles" (Fig. 17a–b). The cluster has a similar inorganic architecture as the anion in **58** for example, except that two $[HgTe_2(TeDec)]^{3-}$ units have been replaced by two $(Te_3)^{2-}$ fragments [85]. Another example is the anion $[Hg_8Te_8(Te_2)_4]^{8-}$ (in **60**), a purely inorganic porphyrin analogue, which differs from the organic cousin by the absence of an electronic π-system, thus preventing the occurrence of "global" aromaticity. Owing to missing multiple bonds and a larger inner diameter, the macrocycle has a non-planar structure in the salt, therby being perfectly adjusted to the environment of embedding imidazolium cations (Fig. 17c–d) [86]. Both of these anions were synthesized ionothermally in the long-alkyl chain IL $(C_{10}C_1Im)[BF_4]$, using inorganic reactants $Na_2[Hg_3Te_4]$ (for **59**) or $Na_2[HgTe_2]$ (for **60**) and en as auxiliary. UV–Vis spectroscopy showed that the presence of larger polytelluride units leads to a narrower band gap (1.26 eV for **59**; 2.16 eV for **60**).

Apart from the ionothermal synthesis of organyl-separated chalcogenido metalate clusters, similar compounds can also be obtained by a surfactant-thermal synthetic route. This method exploits the properties of surfactants by using solutions of surface-active substances as solvents. These include compounds such as polyethylene glycol (PEG), hexadecyltributylphosphonium bromide, [HTBP]Br, or alkylammonium-based salts of general composition $[C_nH_{2n+1}N(CH_3)_{3-m}H_m]X$ (n = 10, 12, 14, 16, 18; m = 0, 1, 3; X = Cl, Br). These surfactants were instrumental for the formation of the following compounds, since no crystals formed in their absence under the otherwise same reaction conditions [87].

The first example of an explicit synthesis in alkylammonium-based surfactants was that of $[H^+–C_{12}H_{25}NH_2]_4[Sn_2S_6]{\cdot}2H_2O$ (**61**), in which the $[Sn_2S_6]^{4-}$ anion, consisting of two edge-sharing $[SnS_4]^{4-}$ tetrahedra, is embedded in a lamellar arrangement of long-chain alkylammonium surfactants (Fig. 18a) [88]. **61** was prepared by treatment of $SnCl_4{\cdot}5H_2O$ with $Na_2S{\cdot}9H_2O$ in an H_2O/MeOH solution of the surfactant dodecylamine. A cation exchange of $A_4[Ge_4Ch_{10}]$ (A = Na, K; Ch = S, Se) with the surfactant $[C_nH_{2n+1}N(CH_3)_{3-m}H_m]X$ (n = 10, 12, 14, 16, 18; m = 0, 1; X = Cl, Br), treated at varying temperatures (from room temperature to 120 °C) depending on the spacer molecules used, also yielded lamellarly arranged compounds containing the T2-type $[Ge_4Ch_{10}]^{4-}$

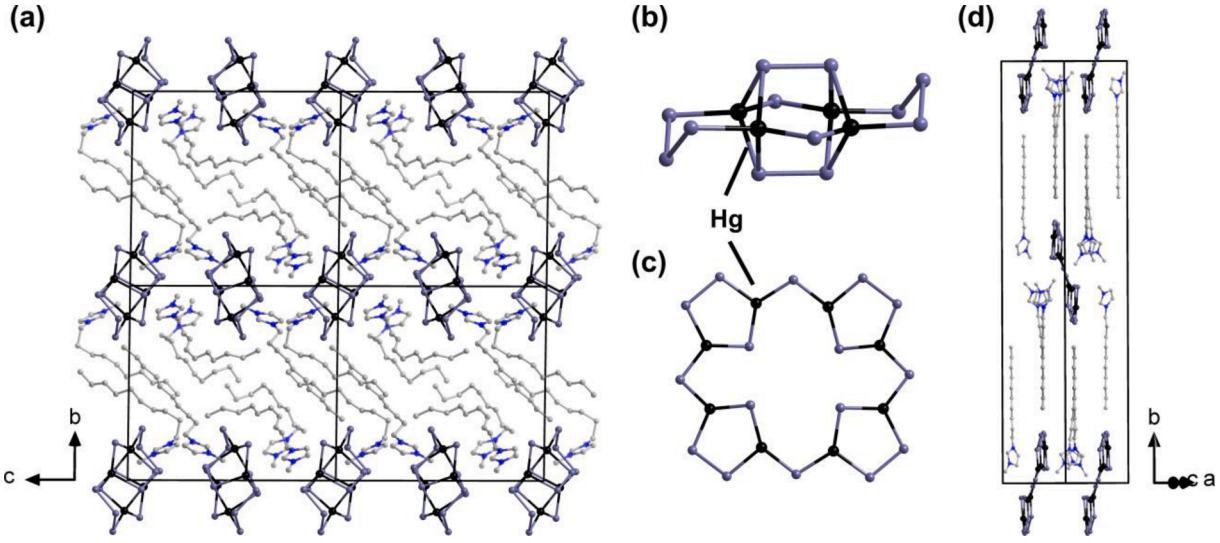

Fig. 17. Crystal structures of organyl-separated tellurido mercurate compounds. (a) 2 × 2 × 2 Supercell of the compound $(C_{10}C_1Im)_4[Hg_4Te_2(Te_2)_2(Te_3)_2]$, viewed along the crystallographic *a*-axis. (b) Anionic substructure of the latter. (c) Anionic substructure of porphyrin-related tellurido mercurate $[Hg_8Te_8(Te_2)_4]^{8-}$. (d) 2 × 2 × 2 Supercell of the latter, viewed along the crystallographic *c*-axis. H atoms are omitted for clarity.

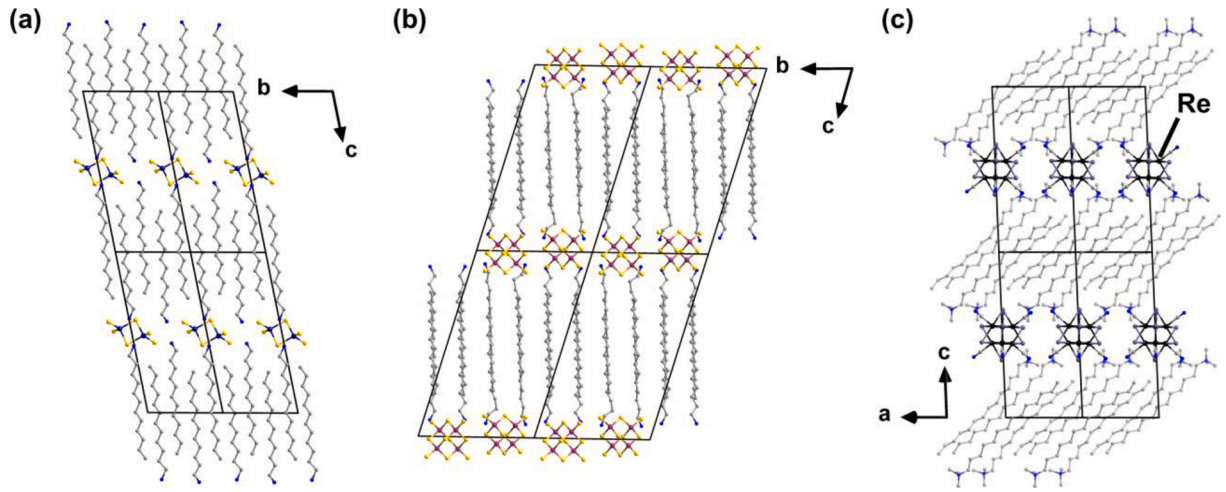

Fig. 18. Surfactant-thermally synthesized compounds with a lamellar crystal structure, all given as their 2 × 2 × 2 supercells viewed along specific crystallographic axes: (a) $[C_{12}H_{25}NH_3]_4[Sn_2S_6]$ (viewed along *a*-axis). (b) $[C_{14}H_{29}NH_3]_4[Ge_4S_{10}]$ (viewed along *a*-axis). (c) $[C_{14}H_{29}N(CH_3)_3]_4[Re_6Te_8(CN)_6]$ (viewed along *b*-axis). H atoms are omitted for clarity.

anion (in **62**; Fig. 18b; $[C_{14}H_{29}NH_3]_4[Ge_4S_{10}]$ shown as an example) [89,90]. Another series of examples is given with $[C_nH_{2n+1}N(CH_3)_3]_4[Re_6Ch_8(CN)_6]$ (**63**, n = 14, 16, 18; Ch = S, Se, Te). The cores of the $[Re_6Ch_8(CN)_6]^{4-}$ cluster anions exhibit a Chevrel phase-like structure, with octahedral Re_6 units face-capped by eight μ_3-Ch ligands, and with additional $(CN)^-$ ligands at the Re atoms. All three congeners of $[Re_6Ch_8(CN)_6]^{4-}$ are embedded in lamellar layers provided by the ammonium surfactant (Fig. 18c) [91]. The syntheses of **63** represents a cation exchange reaction of $K_4[Re_6Ch_8(CN)_6]$ with the surfactants $[C_nH_{2n+1}N(CH_3)_3]Br$.

All ligand-functionalized and organyl-separated discrete chalcogenido metalate cluster-based compounds presented in Section 3.2 are summarized in Table 4.

Table 4
Summary of the ligand-functionalized and organyl-separated discrete chalcogenido metalate-based cluster compounds presented in Section 3.2.

Compound	Reactants	Temperature (°C)	Ref.
$(C_{10}C_1Im)_6[Hg_6Te_6(Te_2)_2(TeMe)(TeDec)]$ (**57**)	$Na_2[Hg_3Te_4]$ in $(C_{10}C_1Im)[BF_4]$ with en or dmmp	80	[85]
$(C_{10}C_1Im)_6[Hg_6Te_6(Te_2)_2(TeDec)_2]$ (**58**)	$Na_2[HgTe_2]$, $ZnCl_2$ in $(C_{10}C_1Im)[BF_4]$	rt	[85]
$(C_{10}C_1Im)_4[Hg_4Te_2(Te_2)_2(Te_3)_2]$ (**59**)	$Na_2[Hg_3Te_4]$ in $(C_{10}C_1Im)[BF_4]$ with en	80	[85]
$(C_{10}C_1Im)_8[Hg_8Te_8(Te_2)_4]$ (**60**)	$Na_2[HgTe_2]$ in $(C_{10}C_1Im)[BF_4]$	80	[86]
$[H^+\text{-}C_{12}H_{25}NH_2]_4[Sn_2S_6]\cdot 2H_2O$ (**61**)	$SnCl_4$, Na_2S, dodecylamine in EtOH/H_2O	rt	[88]
$[C_nH_{2n+1}N(CH_3)_{3-m}H_m]_4[Ge_4S_{10}]$ (**62**)	$Na_4[Ge_4S_{10}]$, $(C_nH_{2n+1}N(CH_3)_{3-m}H_m)X$ in EtOH/H_2O (n = 12, 14, 16, 18, m = 0, 3, X = Cl, Br)	rt – 60	[89,90]
$[C_nH_{2n+1}N(CH_3)_3]_4[Re_6Ch_8(CN)_6]$ (**63**)	$K_4[Re_6Ch_8(CN)_6]$, $C_nH_{2n+1}N(CH_3)_3]Br$ in H_2O (/acetone) (Ch = S, Se, Te, n = 14, 16, 18)	rt	[91]

3.3. Ligand-bridged and ligand-functionalized chalcogenido metalate-based polymers exhibiting other cluster architectures

In this section, we present different ligand-bridged and ligand-functionalized chalcogenido metalate clusters, in particular hydrazine-functionalized clusters, consisting of irregular building blocks, which were obtained from surfactant-thermal and hydrazine-thermal syntheses.

In 2013, a one-dimensional chain containing a hydrazine-bridged ternary anion, 1D-$\{[Mn_2As_2S_8(N_2H_4)_2]^{2-}\}$ (in **64**; Fig. 19a), was obtained by the reaction of Mn, As_2S_3, and PEG-400 as surfactant, from $N_2H_4\cdot H_2O$ at 110 °C. UV–vis investigations of **64** were performed and revealed a band gap of 2.46 eV, which is blue-shifted as compared to the optical band gap of a related compound comprising non-functionalized discrete clusters, $[NH_4]_8[Mn_2As_4S_{16}]$ (2.31 eV) [92]. Using the cationic surfactant [HTBP]Br as the reaction medium, a hydrazine-functionalized chalcogenido metalate, namely 2D-$[(N_2H_4)_2Mn_3Sb_4S_8(\mu_3\text{-}OH)_2]$ (**65**), was observed. The structure of this compound features layers bearing 2D-$[Mn_3(\mu_3\text{-}OH)_2]$ chains. Compound **65** proved to be a stable photocatalyst in photocatalytic studies for continuous H_2 evolution from H_2O under visible-light illumination without any co-catalyst [93]. Another example, 2D-$[Mn_3Ge_2S_7(NH_3)_4]$ (**66**), features NH_3 ligands, which are believed to stem from the decomposition of hydrazine during the reaction. The anionic structure of **66** exhibits $[GeS_4]^{4-}$ tetrahedra and Mn^{2+} ions in an either octahedral $\{MnS_4N_2\}$ or tetrahedral $\{MnS_3N\}$ coordination environment. A quasi-layered anionic substructure containing T2 cluster anions, $[\{Mn(en)_2\}MnGe_3Se_9]^{2-}$ (in **67**), was obtained from Mn, GeSe, Se, and en in PEG-400 as the reaction medium. Compound **67** contains an $[Mn(en)_2]^{2+}$ complex which is attached to the $[MnGe_3Se_9]^{4-}$ cluster core; the overall cluster structure is the same as that of solvothermally synthesized compound $[Mn(en)_2(H_2O)][\{Mn(en)_2\}_2MnGe_3S_9]$ [94]. Also, a 1D chain of $(H^+\text{–}1,2\text{-dap})_2[\{Mn(1,2\text{-dap})_2\}Ge_2Se_7]$ (**68**, 1,2-dap = 1,2-diaminopropane) was observed by the surfactant-thermal reaction of Mn, GeSe, Se, and 1,2-dap in PEG-400. In **68**, two $[Mn(1,2\text{–dap})]^{2+}$ complexes are attached to the cluster core $[Ge_2Se_7]^{6-}$, which exhibits a five membered ring upon corner-sharing of two $[GeSe_4]^{4-}$ tetrahedra and partial oxidation to form a diselenide unit (Fig. 19b) [95]. Two two-dimensional, functionalized chalcogenido antimonate compounds, 2D-$[MnSb_2S_4(N_2H_4)_2]$ (**69**, Fig. 19c) and 2D-$[Mn(TEPA)Sb_6S_{10}]$ (**70**), were synthesized surfactant-thermally using PEG-400 or sodium dodecyl sulfate (SDS) as reaction medium, respectively. While in **69**, 2D-$\{[MnS_2N_4]^{2-}\}$ units connect 1D-$\{[SbS_2]^-\}$ chains *via* corner-sharing of S atoms to form neutral 2D frameworks, in **70**, 8-membered rings of

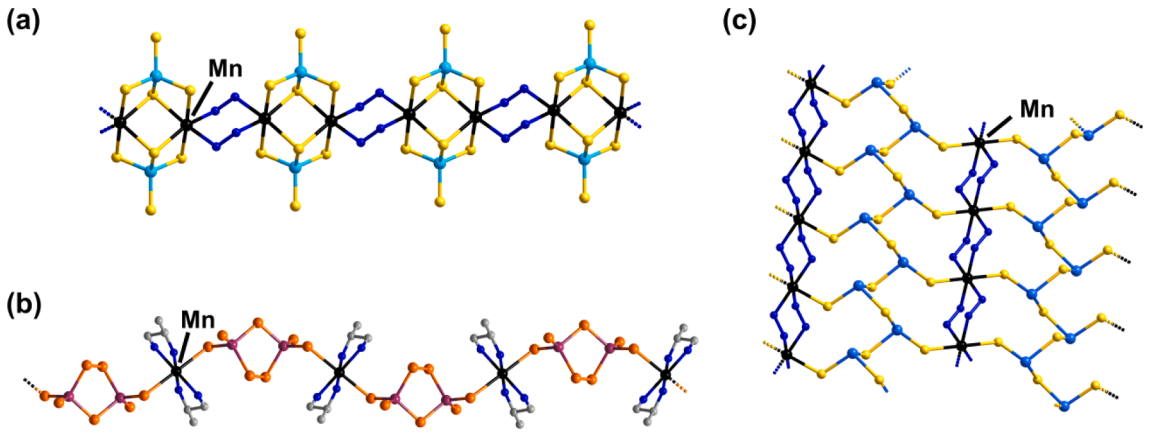

Fig. 19. Examples for compounds observed from surfactant-thermal syntheses. (a) Hydrazine-bridged 1D-{$[Mn_2As_2S_8(N_2H_4)_2]^{2-}$}. (b) Structure of the 1D-{[{Mn(1,2–dap)$_2$}$Ge_2Se_7]^{2-}$} anion. (c) The layered structure of 2D-$[MnSb_2S_4(N_2H_4)_2]$. H atoms are omitted for clarity.

$[Sb_4S_8]^{4-}$, 24-membered rings of $[Sb_{12}S_{24}]^{12-}$, and Mn atoms are tethered together to form a neutral, layered framework of 2D-$[MnSb_6S_{10}]$. UV–vis absorption spectra of the compounds indicate band gaps of 1.96 eV (for **69**) and 2.12 eV (for **70**). Both compounds show active visible light-driven photocatalytic properties for H_2 production from H_2O, with a better performance observed for **69** [96].

The hydrazine-thermal synthesis route is also suitable for the synthesis of crystalline compounds comprising neutral functionalized chalcogenido metalate clusters. The first example prepared this way was 3D-$[Mn_2SnS_4(N_2H_4)_2]$ (**71**). The compound features a 3D framework, in which the hydrazine ligands act as bridges to connect octahedral $[MnL_6]$ (L = S, N) units, thereby forming a three-dimensional structure. Compound **71** also shows strong antiferromagnetic interactions between the Mn^{2+} centers (μ_{eff} = ~5.5–5.6 μ_B, cf., μ_{eff} = 5.92 μ_B for free Mn^{2+}) and order at ~ 41 K [97]. The first two examples in the Mn/pnictide-hydrazine chalcogenide family synthesized *via* the hydrazine-thermal reaction protocol were 3D-$[Mn_2Sb_2S_5(N_2H_4)_3]$ (**72**; Fig. 20a) and 3D-$[Mn_2Sb_4S_8(N_2H_4)_2]$ (**73**). The structures of both compounds are three-dimensional frameworks, bearing neutral hydrazine molecules as bridges that adopt three different roles: (a) intra-layer bridging ligands, (b) inter-layer bridges, and (c) templates for the formation of the 3D frameworks [98,99]. The UV–vis spectrum of compound **72** showed a band gap at around 2.09 eV, while compound **73** revealed an absorption edge at around 1.59 eV. In **72**, magnetic measurements (Fig. 20b) revealed a significant antiferromagnetic interaction (θ = –177.57 K) between the Mn^{2+} ions with μ_{eff} = 5.76 μ_B (cf., μ_{eff} = 5.92 μ_B for free Mn^{2+}) [93]. Magnetic susceptibility measurements of **73** showed that at high temperatures, the Mn^{2+} ions adopt a high spin configuration (μ_{eff} = 4.24 μ_B, cf., μ_{eff} = 4.3 μ_B for known high spin Mn^{2+}), while at around 40 K, a transition from paramagnetic behavior to antiferromagnetic coupling occurred. In addition, compound **72** also shows photocatalytic properties for the generation of H_2 from H_2O under visible-light illumination at about 4.64 μmol/h·g (Fig. 20c) [99].

In 2016, salts of 3D-{$[Mn_6(\mu_6\text{-}S)(\mu\text{-}N_2H_4)_3(\mu_3\text{-}AsS_3)_4]^{2-}$} (**74**) and 2D-{$[Mn_6(\mu_6\text{-}S)(N_2H_4)_2(\mu\text{-}N_2H_4)_2(\mu_3\text{-}AsS_3)_4]^{2-}$} (**75**; Fig. 20d), were synthesized hydrazine-thermally from the corresponding elements in different hydrazine/amine mixtures. The anionic substructures of both compounds are based on $[Mn_6(\mu_6\text{-}S)(\mu_3\text{-}AsS_3)_4]^{2-}$ clusters and covalently

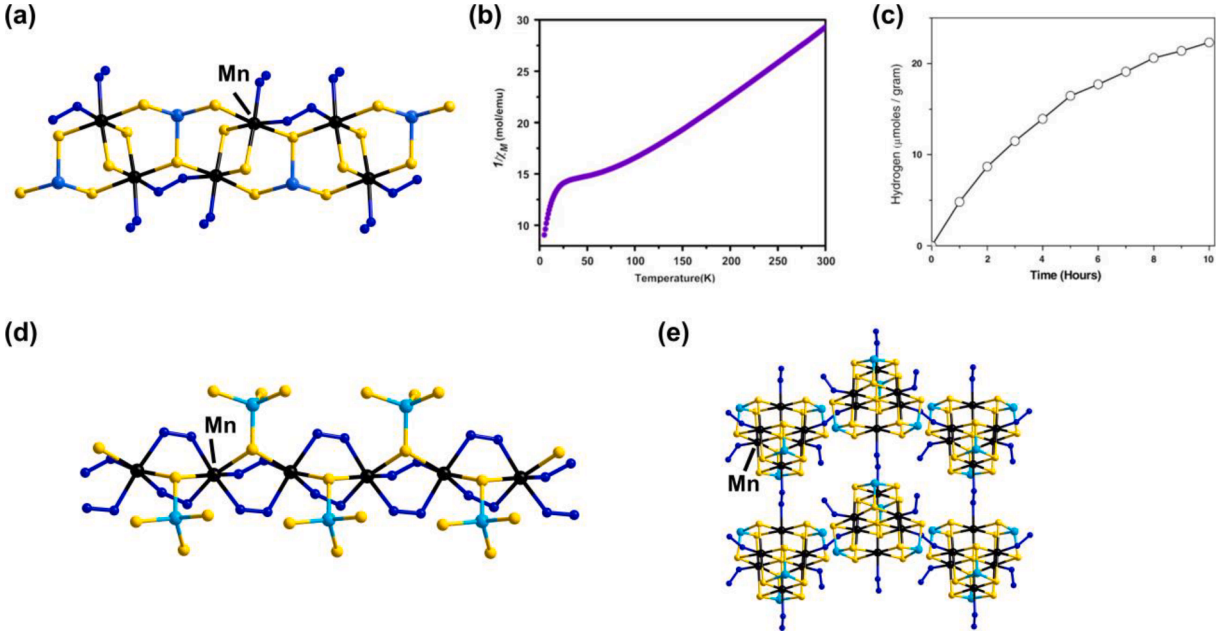

Fig. 20. Hydrazine-thermally synthesized compounds with N_2H_4-bridges. (a) 1D-$[Mn_2Sb_2S_5(N_2H_4)_3]$. (b) Magnetic properties of the latter plotted as $1/\chi$ *vs.* T. (c) Photocatalytic hydrogen evolution from H_2O over this compound as catalyst. (d) 1D-{$[Mn(\mu\text{-}N_2H_4)_2(\mu\text{-}AsS_4)]^-$} anion. (e) 2D-{$[Mn_6(\mu_6\text{-}S)(\mu\text{-}N_2H_4)_2(N_2H_4)_2(\mu_3\text{-}AsS_3)_4]^{2-}$} anion. Reproduced from Ref. [98] with permission from Elsevier. H atoms are omitted for clarity.

bound N_2H_4 bridges. In the $[Mn_6(\mu_6\text{-}S)(\mu_3\text{-}AsS_3)_4]^{2-}$ clusters, six Mn^{2+} cations are arranged in an octahedral fashion and linked through the central $\mu_6\text{-}S^{2-}$ ligand. Each $\{Mn_3\}$ face of the octahedron is capped by an $\{AsS_3\}$. Together with the central $\mu_6\text{-}S^{2-}$, these atoms form four heteratomic cubes that meet at the central sulfide ligand, and share a μ_6-S–Mn edge per neighboring pair. While in **75**, each cluster exhibits two N_2H_4 bridges and two terminal N_2H_4 ligands to form a 2D layer, compound **74** features three N_2H_4 bridging ligands per cluster unit which are connected in a three-dimensional fashion. Investigation by UV–vis spectroscopy showed a larger band gap for the material based on the 2D anion (2.34 eV), and a larger one (2.21 eV) for the compounds comprising the 3D substructure. In both cases, the band gap is slightly wider than reported for the related, yet purely inorganic, cluster compound $[NH_4][MnAs_3S_6]$ (2.08 eV) [100].

Another series of new polymeric Mn-based sulfido arsenates were also obtained using the hydrazine-thermal method, $[Mn(en)_3][(N_2H_4)_2Mn_6(\mu_6\text{-}S)(\mu\text{-}N_2H_4)_2(\mu_3\text{-}AsS_3)_4]$ (**76**), $(H^+\text{–}N_2H_4)[Mn(\mu\text{-}N_2H_4)_2(\mu\text{-}AsS_4)]\cdot 0.5en$ (**77**, Fig. 20e), 3D-$[Mn(\mu\text{-trien})\{Mn(\mu\text{-}N_2H_4)(\mu\text{-}AsS_3)\}_2]$ (**78**), 1D-[{Mn

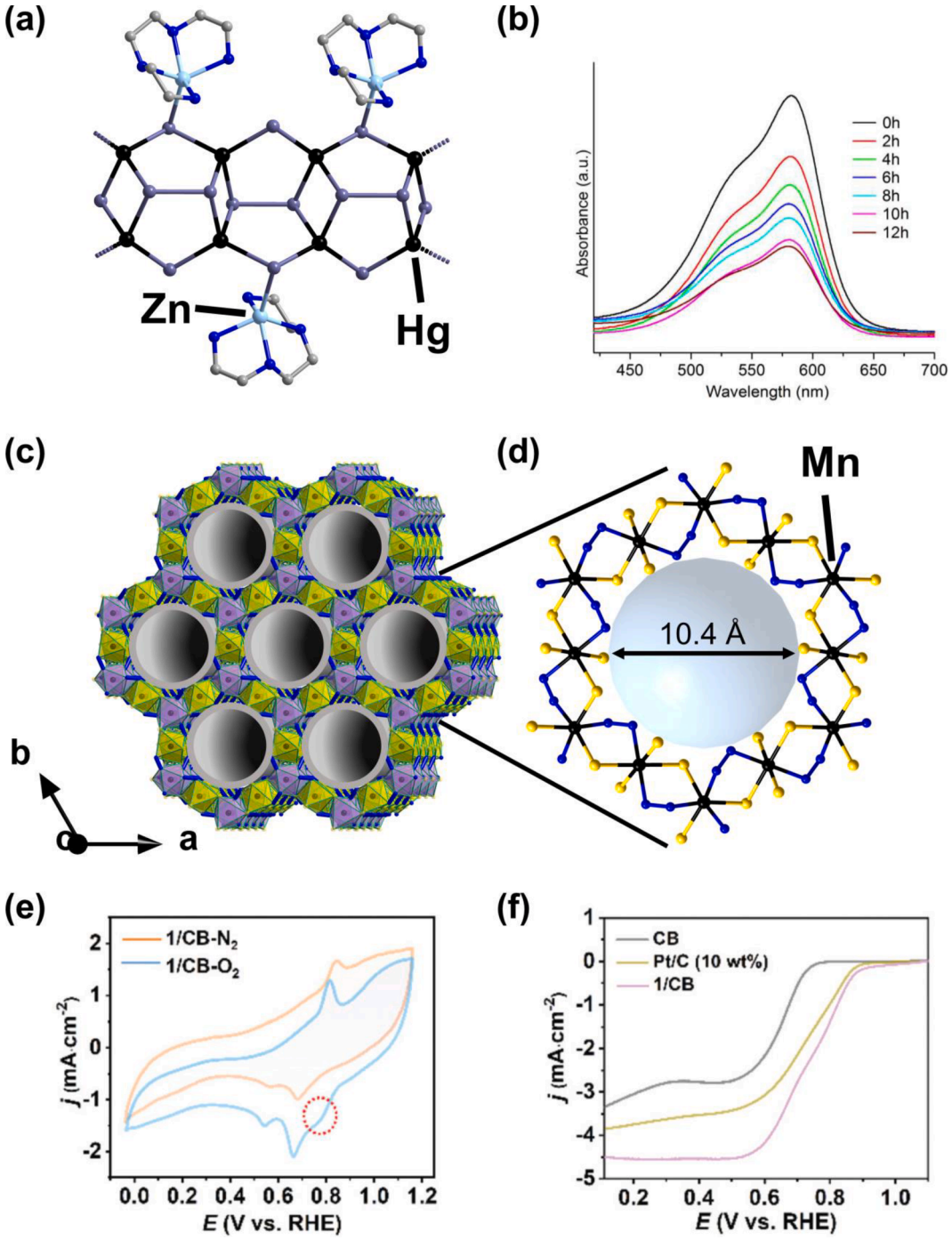

Fig. 21. (a) Molecular structure of 1D-[Zn(trien){Hg_2Te_4}]. (b) Time-dependent absorption spectra of the cv degradation by using tha latter as a photocatalyst; reproduced from Ref. [102] with permission from American Chemical Society. (c) Representation of the crystal structure of the 3D-$\{[Mn_5Sb_6S_{15}(N_2H_4)_6]^{2-}\}$ anion in the latter with 1D channels running along the crystallographic c-axis. (d) Representation of one of the dodecanuclear rings in the 2D-$[Mn_5S_{12}(N_2H_4)_6]$ substructure of $(H_2^+\text{–en})[Mn_5Sb_6S_{15}(N_2H_4)_6]\cdot DMF\cdot 0.5N_2H_4$. (e) CV curves of an electrode containing this compound and carbon black (CB). (f) Linear sweep voltammograms (LSV) curves with CB, Pt/C (10 wt%) and a mixture of the compound with CB; reproduced from Ref. [103] with permission from Royal Society of Chemistry.

$(N_2H_4)\}_2(\mu\text{-}N_2H_4)_2\{Mn(\mu\text{-}N_2H_4)_2\text{-}(\mu\text{-}AsS_3)_2\}]$ (**79**), 2D-$[Mn_3(\mu\text{-}N_2H_4)_6(\mu_3\text{-}AsS_4)(\mu_2\text{-}AsS_4)]$ (**80**), and $[Mn(NH_3)_6][\{Mn(NH_3)(\mu\text{-}AsS_4)\}_2]$ (**81**). The sulfido arsenate units found here, $\{AsS_3\}$ and $\{AsS_4\}$, coordinate to Mn^{2+} ions in different coordination modes to form Mn–As–S ternary clusters, chains, and layers, respectively. The hydrazine molecules act as bridging ligands between Mn^{2+} ions in the clusters, the chains, and the layers. This allows to tune the semiconducting band gaps in these compounds, which are in the range of 2.19–2.47 eV. Moreover, **74** exhibits stronger antiferromagnetic coupling interactions between the magnetic Mn^{2+} ions than **77** ($\theta = -126.45$ K *vs.* –19.85 K) [101].

An organic–inorganic hybrid tellurido mercurate cluster containing a covalently bound $[TM(trien)]^{2+}$ complex, 1D-$[TM(trien)\{Hg_2Te_4\}]$ with TM = Zn (**82a**; Fig. 21a) or Mn (**82b**), was synthesized in a hydrazine-assisted solvothermal reaction of $TMCl_2$, $HgCl_2$, and Te in a mixture of N_2H_4/trien. The compounds feature one-dimensional strands based on bowl-type $\{Hg_4(Te)_4(Te_2)\}$ units that are linked into the chains by sharing $\{Hg_2Te_2\}$ faces with neighboring units. The $[TM(trien)]^{2+}$ complex fragments are connected to every second Te atom in the strands. The UV–vis spectra of the two semiconducting compounds indicate a slight red-shift of the band gap of the Mn-based compound (0.96 eV) as compared to that of the Zn-based compound (0.98 eV). The photocatalytic properties of the Mn-based cluster were investigated by the degradation of cv in aqueous solution (Fig. 21b). After 12 h, it was found that 62% of cv had been degraded, indicating an only moderate photocatalytic activity—in contrast to $[Mn(TEPA)(N_2H_4)]_2[Hg_4Te_{12}]$, featuring discrete $[Hg_4Te_{12}]^{4-}$ anions, which showed 92% cv degradation after 12 h [102].

The Mn-based sulfido antimonate $(H_2^+\text{–en})[Mn_5Sb_6S_{15}(N_2H_4)_6]\cdot DMF\cdot 0.5N_2H_4$ (**83**) was synthesized from Mn, Sb_2S_3, and S with DMF and en in $N_2H_4\cdot H_2O$ at 75 °C. The anion 3D-$\{[Mn_5Sb_6S_{15}(N_2H_4)_6]^{2-}\}$ consists of a three-dimensional metal chalcogenide open framework (MCOF) in which $\{Sb_2S_5\}$ building units act as pillars between 2D-$[Mn_5S_{12}(N_2H_4)_6]$ layers with N_2H_4 ligands acting as bridges besides $\mu\text{-}S^{2-}$ ligands (Fig. 21c). In the Mn/S substructure, the Mn^{2+} ions adopt two different coordination environments: one is octahedrally coordinated by three S atoms and three hydrazine molecules, and the other one is octahedrally coordinated by four S atoms and two hydrazine molecules. The octahedra are edge-linked into dodecanuclear rings that are stacked to form the walls of straight hexagonal channels (Fig. 21d) with a diameter of ~ 10 Å (disregarding van der Waals radii), in which the $(H_2^+\text{–en})^{2+}$ counterions are located. The channels are linked into a honeycomb pattern, as the $\{MnS_4N_2\}$ octahedra belong to two channel walls each, and the $\{MnS_3N_3\}$ octahedra are part of the walls of three adjacent channels. Compound **83** is well suited for electrocatalytic oxygen reduction reactions (ORR) as displayed in Fig. 21e–f [103].

All ligand-bridged and ligand-functionalized chalcogenido metalate cluster-based polymeric compounds presented in Section 3.3 are summarized in Table 5.

4. Ligand-functionalized silver chalcogenide cluster-based compounds

4.1. Ligand-functionalized silver chalcogenide/chalcogenolate clusters

In this section, we review the syntheses and structures of silver chalcogenide/chalcogenolate cluster-based molecules with a special emphasis on the comparison of different types of protecting ligands. Similar copper and gold chalcogenide/chalcogenolate compounds were also reported, which can be completely analogous or differ to certain extents from the species comprising silver atoms (which in part is owing to relativistic effects present in the gold compounds). However, as the number of compounds that were published in this area is huge, we chose to focus on the clusters including silver atoms here, and refer the reader to other recently published review articles for the corresponding copper and gold compounds [104–106].

Ligand-functionalized silver nanoclusters consist of an inorganic silver-chalcogenide cluster core and chalcogenolate protecting ligands on the surface. Normally, the description in terms of such compounds is always challenging due to their structural complexity, especially for the ones containing larger cluster cores [15]. However, the positions of the ligands on the cluster surface can be well distinguished and therefore can help to elucidate the structures at the interface between ligand shell and cluster core. Furthermore, the surface ligands play a role as stabilizing agents to protect the cluster cores and have thus a significant influence on the overall molecular structures. Herein, we summarize the use of chalcogenide Ch^{2-} (Ch = S, Se, and Te), chalcogenolate (RCh) (Ch = S, Se, and Te), dichalcogenidophosphate $[R_2PCh_2]^-$ (Ch = S, Se), and a few examples of multichalcogenolate $(RCh_x)^{q-}$ (Ch = S, x > 2) anions as bridging ligands between the noble metal atoms of the cluster cores. Additionally, (RCh), $[R_2PCh_2]^-$, and $(RCh_x)^{q-}$ can also act as ligands on the cluster surface.

Silver clusters in which the silver atoms are only linked by naked Ch^{2-} anions have to be stabilized by, for example, phosphine groups at the surface silver atoms. However, these compounds are rare due to a lack of suitable Ch^{2-} precursors. The most suitable ones in this context for introducing Ch^{2-} are bis(trimethylsilyl) chalcogenides. For instance, the

Table 5
Summary of the ligand-bridged and ligand-functionalized chalcogenido metalate-based polymers compounds presented in Section 3.3.

Compound	Dimensionality	Reactants	Temperature (°C)	Ref.
$[Mn(NH_3)_6][Mn_2As_2S_8(N_2H_4)_2]$ (**64**)	1D	Mn, As_2S_3, PEG-400 in $N_2H_4\cdot H_2O$	110	[92]
$[(N_2H_4)_2Mn_3Sb_4S_8(\mu_3\text{-}OH)_2]_n$ (**65**)	2D	Mn, Sb_2S_5, S, in [HTBP]Br with $N_2H_4\cdot H_2O$	175	[93]
$[Mn_3Ge_2S_7(NH_3)_4]_n$ (**66**)	2D	Mn, S, GeS_2 in PEG-400 with $N_2H_4\cdot H_2O$	160	[95]
$[Mn(en)_2(H_2O)][\{Mn(en)_2\}MnGe_3Se_9]$ (**67**)	2D	Mn, Se, GeSe in PEG–400 with en	160	[95]
$(H^+\text{–}1,2\text{-dap})_2[\{Mn(1,2\text{-dap})_2\}Ge_2Se_7]$ (**68**)	1D	Mn, Se, GeSe in PEG–400 with 1,2-dap	160	[95]
$[MnSb_2S_4(N_2H_4)_2]_n$ (**69**)	2D	Mn, Sb_2S_3, S in PEG–400 with $N_2H_4\cdot H_2O$	120	[96]
$[Mn(TEPA)Sb_6S_{10}]_n$ (**70**)	2D	Mn, Sb_2S_5, S in SDS with TEPA and H_2O	160	[96]
$[Mn_2SnS_4(N_2H_4)_2]_n$ (**71**)	3D	Sn, Mn, S in $N_2H_4\cdot H_2O$ and H_2O	150	[97]
$[Mn_2Sb_2S_5(N_2H_4)_3]_n$ (**72**)	3D	Mn, Sb_2S_3, S in $N_2H_4\cdot H_2O$ and H_2O	140	[98]
$[Mn_2Sb_4S_8(N_2H_4)_2]_n$ (**73**)	3D	Mn, Sb_2S_3, S in $N_2H_4\cdot H_2O$ and H_2O	160	[99]
$[Mn(dien)_2][Mn_6(\mu_6\text{-}S)(\mu\text{-}N_2H_4)_3(\mu_3\text{-}AsS_3)_4]\cdot H_2O$ (**74**)	3D	Mn, As, S in N_2H_4/dien	120	[100]
$[Mn(1,2\text{-dap})_2][Mn_6(\mu_6\text{-}S)(\mu\text{-}N_2H_4)_2(N_2H_4)_2(\mu_3\text{-}AsS_3)_4]\cdot H_2O$ (**75**)	2D	Mn, As, S in N_2H_4/1,2–dap	120	[100]
$[Mn(en)_3][(N_2H_4)_2Mn_6(\mu_6\text{-}S)(\mu\text{-}N_2H_4)_2(\mu_3\text{-}AsS_3)_4]$ (**76**)	2D	Mn, As, S in $N_2H_4\cdot H_2O$/en	110	[101]
$(H^+\text{–}N_2H_4)[\{Mn(\mu\text{-}N_2H_4)_2(\mu\text{-}AsS_4)\}\cdot 0.5en]$ (**77**)	1D	Mn, As, S in $N_2H_4\cdot H_2O$/en	90	[101]
$[Mn(\mu\text{-trien})\{Mn(\mu\text{-}N_2H_4)(\mu\text{-}AsS_3)\}_2]$ (**78**)	3D	Mn, As, S in $N_2H_4\cdot H_2O$/trien	110	[101]
$[\{Mn(N_2H_4)\}_2(\mu\text{-}N_2H_4)_2\{Mn(\mu\text{-}N_2H_4)_2(\mu\text{-}AsS_3)_2\}]_n$ (**79**)	1D	Mn, As, S in $N_2H_4\cdot H_2O$/trien	90	[101]
$[Mn_3(\mu\text{-}N_2H_4)_6(\mu_3\text{-}AsS_4)(\mu_2\text{-}AsS_4)]_n$ (**80**)	2D	Mn, As, S in $N_2H_4\cdot H_2O$/DMF	90	[101]
$[Mn(NH_3)_6][\{Mn(NH_3)(\mu\text{-}AsS_4)\}_2]$ (**81**)	1D	Mn, As, S in $N_2H_4\cdot H_2O/NH_{3(l)}$	90	[101]
[TM(trien){Hg_2Te_4}] (**82**)	1D	$TMCl_2\cdot xH_2O$ (TM = Mn, Zn, x = 4, 0), $HgCl_2$, Te, N_2H_4 in trien	120	[102]
$(H_2^+\text{–en})[Mn_5Sb_6S_{15}(N_2H_4)_6]\cdot DMF\cdot 0.5N_2H_4$ (**83**)	3D	Mn, Sb_2S_3, S in DMF, en and $N_2H_4\cdot H_2O$	75	[103]

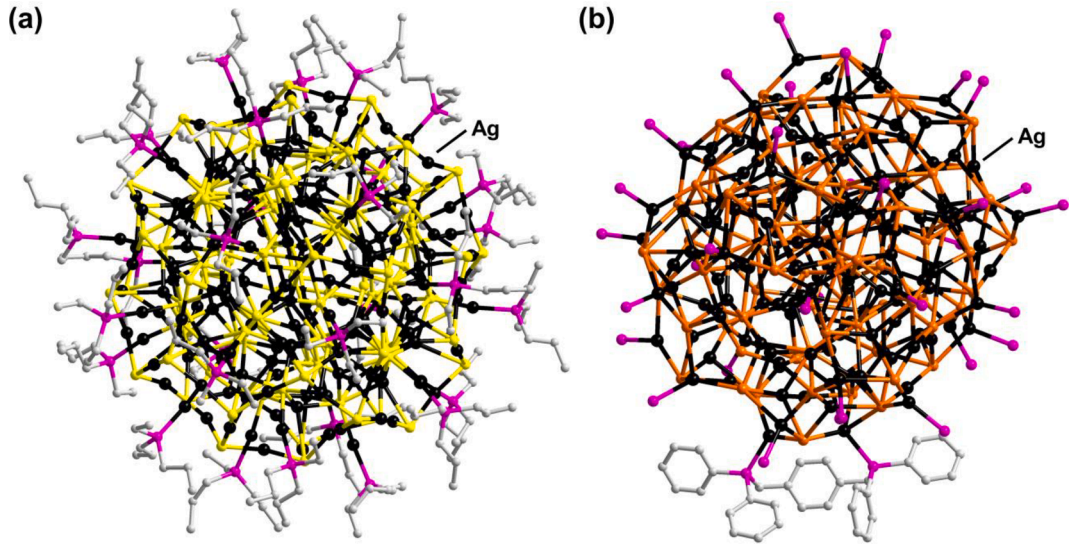

Fig. 22. Molecular structures of huge phosphine-protected silver chalcogenolate clusters. (a) $[Ag_{188}S_{94}(P^nPr_3)_{30}]$. (b) $[Ag_{154}Se_{77}(dppxy)_{18}]$. Most Ph groups and all H atoms are omitted for clarity.

reaction of silver trifluoracetate, Ag(TFA) with $S(SiMe_3)_2$ and P^nPr_3 in diglyme allowed for the formation of $[Ag_{188}S_{94}(P^nPr_3)_{30}]$ (**84**, Fig. 22a), which contains an Ag:S ratio of 2:1, and has a diameter of ~ 2.0 nm [107]. The P^nPr_3 ligands are connected by thirty silver atoms from the outer shell of the cluster and distributed on the surface as protecting agents, while the remaining Ag^+ cations at the inner cluster core are bridged by S^2 ligands. By changing the phosphine from P^nPr_3 to P^nBu_3, one obtains the isostructural cluster $[Ag_{188}S_{94}(P^nBu_3)_{30}]$ (**85**) [107]. Both cluster cores are disordered, thus referring to the inherent property of Ag_2S to be a cation conductor with notable Ag^+ mobility. However, this also indicates that a variation of the different phosphine groups does not affect the disorder - within the clusters. Even though this route has been proven to be effective, it is still possible to form compounds that only contain Ch^2 anions as bridges between silver atoms in the presence of chalcogenolates. $[Ag_{154}Se_{77}(dppxy)_{18}]$ (**86**, Fig. 22b, dppxy = 1,4-bis(diphenylphosphanylmethyl)benzene) can be isolated upon addition of $Se(SiMe_3)_2$ to a suspension of AgS^tBu and dppxy in DCM and toluene at 55 °C [108]. Here, only Se^2 bridges form, despite the presence of thiolates. The reason being that $Se(SiMe_3)_2$ is more reactive than AgS^tBu under such reaction conditions, and also dppxy exhibits better coordination abilities than the (S^tBu) group; therefore, dppxy is preferred as a bidentate ligand to cover the cluster surface.

A greater variety of structural motifs can be achieved by using different chalcogenolate ligands. Two examples are given in Fig. 23. Adding $(Et_4N)Br$ to a mixture of Ag_2SO_4 and 2-TBI (2-thiobenzimidazol) in DMF and MeCN allowed for the formation of $[Et_4N][Ag_4(2\text{-TBI})_6(SO_4)_3]_2[Br@Ag_8(2\text{-TBI})_{12}(SO_4)_2]\bullet 4MeCN\bullet 3DMF$ (**87**, Fig. 23a), which represents a rare co-crystallization product of two different—a cationic and an anionic—silver thiolate clusters [109]. Without the addition of $[Et_4N]Br$, and by changing Ag_2SO_4 to AgX (X = Cl, Br) and MeCN to H_2O, two silver-thiolate coordination polymers, 2D-$[Ag_{14}(2\text{-TBI})_{12}X_2]$ (**88a**, X = Cl; **88b**, X = Br; Fig. 23b), were isolated [110]. Owing to the hydrophobic nature of the ligand shell, as well as the *in situ* formation of a dynamic proton layer while treating with acid, both compounds are stable in concentrated acidic or basic solutions, and also in various common solvents.

With the use of 4-cyanobenzenethiol or 4-nitrobenzenethiol as chalcogenolate ligands, the isostructural compounds $[Ag_6(S\text{-}C_6H_4\text{-}CN)_6(PPh_3)_6]$ (**89**, Fig. 24a) and $[Ag_6(S\text{-}C_6H_4\text{-}NO_2)_6(PPh_3)_6]$ (**90**, Fig. 24b) were obtained following the same synthetic approach as described before [111]. Here, the chalcogenolate ligands not only serve as a ligand shell, but also act as bridges to link the silver atoms. Upon reacting the former product **89** with $FeCl_2$ in THF and pentane at room temperature, a larger neutral complex $[Ag_{14}S(S\text{-}C_6H_4\text{-}CN)_{12}(PPh_3)_8][FeCl_2(THF)_4]_3$ (**91**, Fig. 24c) was isolated with an interstitial sulfide anion in the center of the $\{Ag_{14}\}$ cluster core [111]. The central S^{2-} has apparently been released from the 4-cyanobenzenethiol ligand despite its stability, since no other sulfur sources were present in the reaction mixture. A similar cluster framework, $[Ag_{14}S(S\text{-}C_6H_4\text{-}NCS)_{12}(PPh_3)_8]$ (**92**, Fig. 24d), was obtained from the treatment of Ag(OAc), $SCN\text{-}C_6H_4\text{-}SH$ and PPh_3 in THF and Et_2O [111]. With the reaction of $AgNO_3$ and $4\text{-}^tBu\text{-}C_6H_4\text{-}SH$ in NEt_3, EtOH, and MeCN at room temperature, a polymeric strand of 1D-$\{[Ag_8Ag_{4/2}(S\text{-}C_6H_4\text{-}4\text{-}^tBu)_{12}]^2\}$ (in **93**) was formed with $[H^+\text{–}NEt_3]$ cations as structure directing agents and counterions [112]. Moreover, the product can be used as a precursor for further transformation, since it reacts readily with CS_2 in solution. Addition of pure MeCN to the above solution enabled the formation of a larger molecular cluster anion, $[Ag_{50}S_7(S\text{-}C_6H_4\text{-}4\text{-}^tBu)_{40}]^4$ (in **94**) [112]. These cases demonstrate that the modulation of the

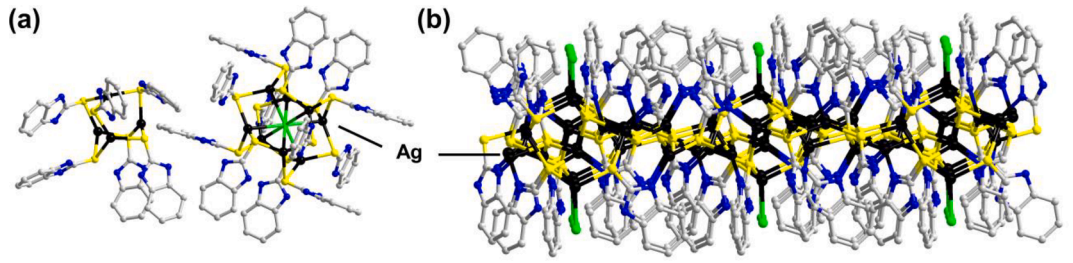

Fig. 23. TBI-stabilized silver sulfide clusters. (a) Co-crystallizing $[Ag_4(2\text{-TBI})_6(SO_4)_3]^{2-}$ anions and $[Br@Ag_8(2\text{-TBI})_{12}(SO_4)_2]^{3+}$ cations. (b) Silver thiolate-based coordination polymer of 2D-$[Ag_{14}(2\text{-TBI})_{12}X_2]$ (X Cl, Br). H atoms and template cations of the first compound are omitted for clarity.

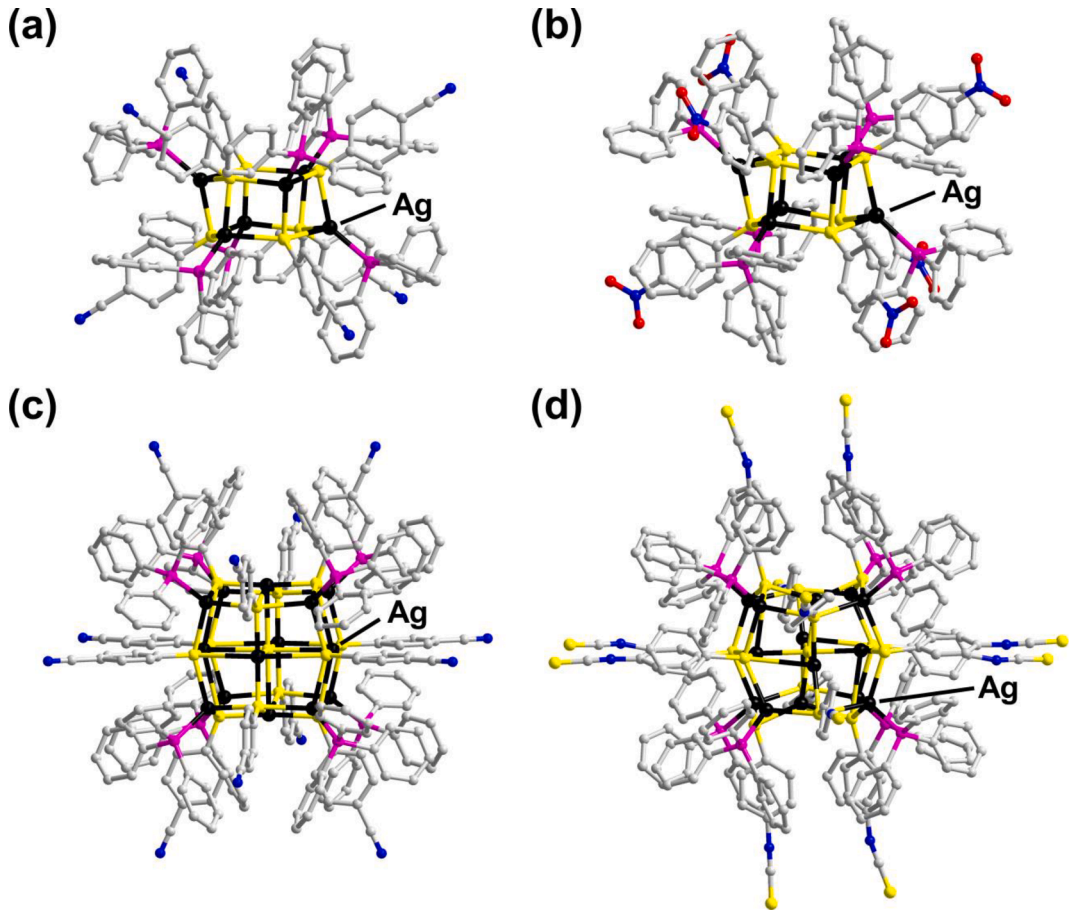

Fig. 24. Molecular structures of thiolate and phosphine co-functionalized silver sulfide clusters. (a) $[Ag_6(S\text{-}C_6H_4\text{-}CN)_6(PPh_3)_6]$. (b) $[Ag_6(S\text{-}C_6H_4\text{-}NO_2)_6(PPh_3)_6]$. (c) $[Ag_{14}S(S\text{-}C_6H_4\text{-}CN)_{12}(PPh_3)_8]$. (d) $[Ag_{14}S(S\text{-}C_6H_4\text{-}NCS)_{12}(PPh_3)_8]$. H atoms are omitted for clarity.

chalcogenolate ligands is important but not the only parameter for modifying the molecular structures. Other parameters, such as the solvent, the reaction temperature, or the silver and chalcogen sources, need be taken into account, too.

In order to obtain larger silver chalcogenide nanoclusters, the charge distribution and electronic charge compensation within the cluster compound is an important factor. To do so, highly reactive $Ch(SiMe_3)_2$ can be introduced as chalcogenide sources to balance the positive charge of the inorganic cluster core. Another way is to generate chalcogenolate ligands *in situ* from $RChSiMe_3$ to compensate corresponding charge on the surface. Following these routes, a combined use of $Ch(SiMe_3)_2$ and $RChSiMe_3$ with different silver salts in various solvents has led to a wide spectrum of molecular clusters. In the presence of bis (diphenylphosphanyl)methane (dppm) as stabilizer, the reaction of $(Me_2N)C_6H_4S(SiMe_3)_2$ and $S(SiMe_3)_2$ with $Ag(O_2CPh)$ in THF and Et_2O afforded $[Ag_{65}S_{13}(S\text{-}C_6H_4\text{-}NMe_2)_{39}(dppm)_5]$ (**95**, Fig. 25a), which consists of 65 silver and 13 chalcogenide atoms in the cluster core with a diameter approximately up to 1.7 nm [113].

By replacing $S(SiMe_3)_2$ with $Se(SiMe_3)_2$, and dppm with PPh_3, even larger clusters such as $[Ag_{76}Se_{13}(S\text{-}C_6H_4\text{-}NMe_2)_{50}(PPh_3)_{6.5}]$ (**96**, Fig. 25b) and $[Ag_{88}Se_{12}(S\text{-}C_6H_4\text{-}NMe_2)_{63}(PPh_3)_6]$ (**97**, Fig. 25c) were obtained [113]. The positive charges of the Ag^+ cations of **96** are compensated by the negative charges of the Se^{2-} anions and the $(S\text{-}C_6H_4\text{-}NMe_2)^-$ ligands. The situation within the cluster, shown in Fig. 25c, seems to be more complicated, since the 88 Ag^+ cations should provide 88 positive charges. However, the 12 Se^{2-} anions and the 63 (S-

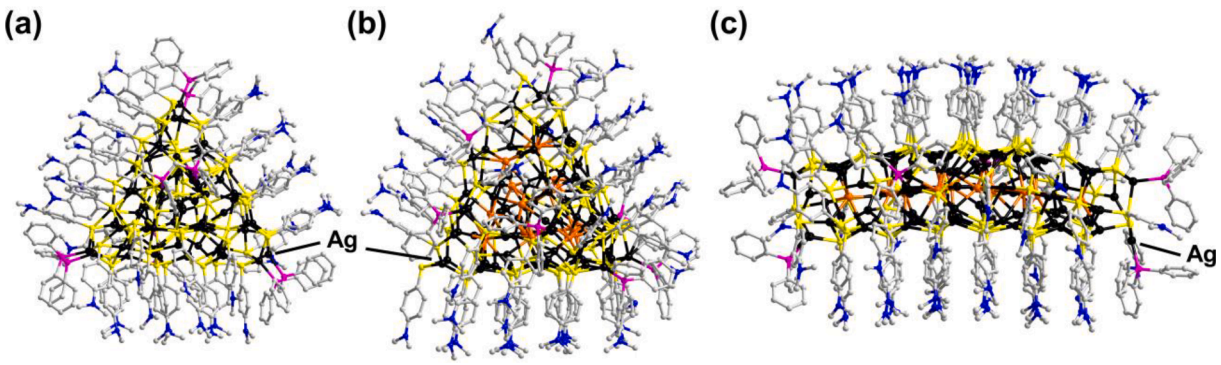

Fig. 25. Molecular structures of thiolate and phosphine co-functionalized silver chalcogenide nanoclusters. (a) $[Ag_{65}S_{13}(S\text{-}C_6H_4\text{-}NMe_2)_{39}(dppm)_5]$. (b) $[Ag_{76}Se_{13}(S\text{-}C_6H_4\text{-}NMe_2)_{50}(PPh_3)_{6.5}]$. (c) $[Ag_{88}Se_{12}(S\text{-}C_6H_4\text{-}NMe_2)_{63}(PPh_3)_6]$. H atoms are omitted for clarity.

C_6H_4-NMe_2) ligands can only contribute 87 electrons. Therefore, one of the silver atoms must be formally uncharged. Since no neutral Ag atom could be observed by inspection of the respective coordination environments, the authors thus assumed that the 87 positive charges are equally distributed over all Ag atoms [113].

By introducing a ferrocene (Fc) group through the addition of $FcCH_2SSiMe_3$, silver-chalcogenide clusters with potentially interesting electrocatalytic properties become accessible. For example, $[Ag_{10}(SCH_2Fc)_{10}(PPh_3)_4]$ (**98**, Fig. 26a), and the larger clusters $[Ag_{48}S_6(SCH_2Fc)_{36}]$ (**99**, Fig. 26b) have been prepared [114]. The latter can be reversibly oxidized, as confirmed by CV.

Reacting $Ph(SSiMe_3)$, $Ag(O_2CPh)$, and $S(SiMe_3)_2$ in the presence of tridentate 1,1,1-trsi(diphenylphosphinomethyl)ethane (triphos) as a stabilizer in diglyme allowed for the formation of a neutral $[Ag_{70}S_{16}(SPh)_{34}(PhCO_2)_4(triphos)_4]$ cluster (**100**, Fig. 27a). In this case, the Ag atoms adopt a d^{10} configuration with no detectable Ag•••Ag interactions. Upon replacing triphos with bidentate dppm ligands, and diglyme with DME, $[Ag_{70}S_{20}(SPh)_{28}(dppm)_{10}](TFA)_2$ (**101**) could be isolated (Fig. 27b) [107]. Even though **100** and **101** contain the same number of silver atoms in the inner cores, the amount of sulfide atoms as well as the number of thiolate groups differ [115]. This shows that going from a tridentate P-donor ligand to a bidentate one has a significant effect on the cluster composition and size. For example, in the presence of bis(diphenylphosphino)butane (dppb), reactions of Ag(TFA), ^{t}BuS-$SiMe_3$, and $S(SiMe_3)_2$ in THF yield the high-nuclearity cluster $[Ag_{262}S_{100}(S^tBu)_{62}(dppb)_6]$ (**102**, Fig. 27c) [115]. In addition, by reaction of $Ag(S^tBu)$ and $S(SiMe_3)_2$ in toluene and chloroform, a compound comprising the larger cluster molecules $[Ag_{320}S_{130}(S^tBu)_{60}(dppp)_{12}]$ (**103**) was isolated using 1,3-bis(diphenylphosphanyl)propane (dppp) as stabilizer, which further emphasized the structure-regulating role of phosphine ligands [108].

The spatial expansion of the cluster is influenced by the distance between two P donor atoms of the bidentate phosphine, though it is not the only decisive parameter. Replacing the dppb stabilizer with a larger dppxy ligand resulted in the crystallization of smaller $[Ag_{123}S_{35}(S^tBu)_{50}]$ (**104**) and, also, larger $[Ag_{344}S_{124}(S^tBu)_{96}]$ clusters (**105**, Fig. 28a) [116]. However, it is hard to correlate the influence of different types of phosphines with the final cluster structures, since the phosphines are not incorporated into the molecular structures in these two cases. Certainly, to achieve high-nuclearity clusters, it is usually necessary to combine Ch $(SiMe_3)_2$ and $RChSiMe_3$ in these reactions (with very few exceptions) to balance the excess positive charges of the inner cluster cores as needed.

Another possibility for an effective synthetic approach to silver chalcogenide nanoclusters is the use of a silver chalcogenate, Ag(ChR), with $Ch(SiMe_3)_2$ directly under the same reaction conditions. Following this method, the reaction of $Ag(S^tC_5H_{11})$ with $S(SiMe_3)_2$ in the presence of 4,4′-bis(diphenylphosphanyl)biphenyl (dppbp) in THF and *p*-xylene afforded the largest coinage metal cluster that was structurally characterized to date, $[Ag_{490}S_{188}(S^tC_5H_{11})_{114}]$ (**106**) [108]. However, in this case, only 108 chalcogenolate groups could be fully identified by single crystal X-ray diffraction (SC-XRD). Without the addition of *p*-xylene, $[Ag_{352}S_{128}(S^tC_5H_{11})_{96}]$ (**107**, Fig. 28b) was isolated instead, albeit in very low yield. The latter is likely an intermediate of the formation of **106** (Fig. 28c), since **106** could be obtained after 3–4 weeks alongside 10–20% of **107**. Notably, the measured MALDI-TOF spectrum of **106** corresponds within a reasonable range with the simulated one. That is despite the fact, that the chalcogenolate groups are easily lost under the given conditions [108].

The discussion presented herein shows that (a) employing Ch $(SiMe_3)_2$ together with $RChSiMe_3$, or combining M(ChR) (M = Ag, Cu, Au; Ch = S, Se, Te) with $Ch(SiMe_3)_2$, and (b) addition of a bidentate phosphine as stabilizer is helpful in the generation of huge silver chalcogenide-based nanoclusters, although in some cases, the phosphines are not incorporated into the clusters themselves, is necessary to form these high-nuclearity clusters.

In the recent past, a steadily increasing number of novel coinage metal (nano)clusters have been synthesized *via* solvothermal approaches [117] and *via* an *in situ* reduction method [118,119], without the need for silylated chalcogenide as reagents. For instance, the solvothermal reaction of $Ag(S^tBu)$ with $AgNO_3$ in MeOH, EtOH, and DMF led to the crystallization of $[CO_3@Ag_{20}(S^tBu)_{10}(DMF)_6(NO_3)_8]$ (**108**, Fig. 29a) in high yield [120]. The thiolates serve as both bridging and surface ligands to stabilize this drum-like nanocluster. The unexpected inner templating anion, CO_3^{2-}, is presumed to be generated *in situ* from atmospheric CO_2. Replacing the nitrate anion and DMF with 1,3-dioxo-1*H*-benzo[*de*]isoquinolin-2(3*H*)-yl)acetic acid (DOBzQA) ligands and MeCN, respectively, allowed for the formation of $[CO_3@Ag_{20}(S^tBu)_{10}(DOBzQA)_8(MeCN)_4]$ (**109**), a fluorescent compound. Its decoration with ferrocenecarboxylic functional groups resulted in the formation of a corresponding compound exhibiting electrochemical activity, $[CO_3@Ag_{20}(S^tBu)_{10}(FcC_5H_4CO_2)_8(MeCN)_4]$ (**110**, Fig. 29b) [121]. The introduction of chiral amino ligands furthermore allowed for the

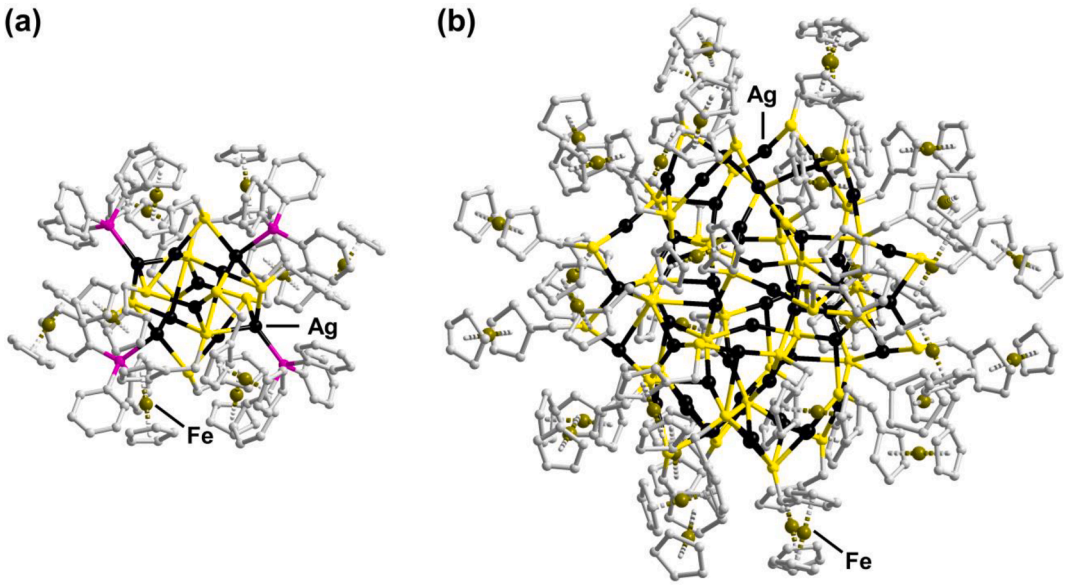

Fig. 26. Molecular structures of ferrocenyl-functionalized silver sulfide clusters (a) $[Ag_{10}(SCH_2Fc)_{10}(PPh_3)_4]$, and (b) $[Ag_{48}S_6(SCH_2Fc)_{36}]$ molecules. H atoms are omitted for clarity.

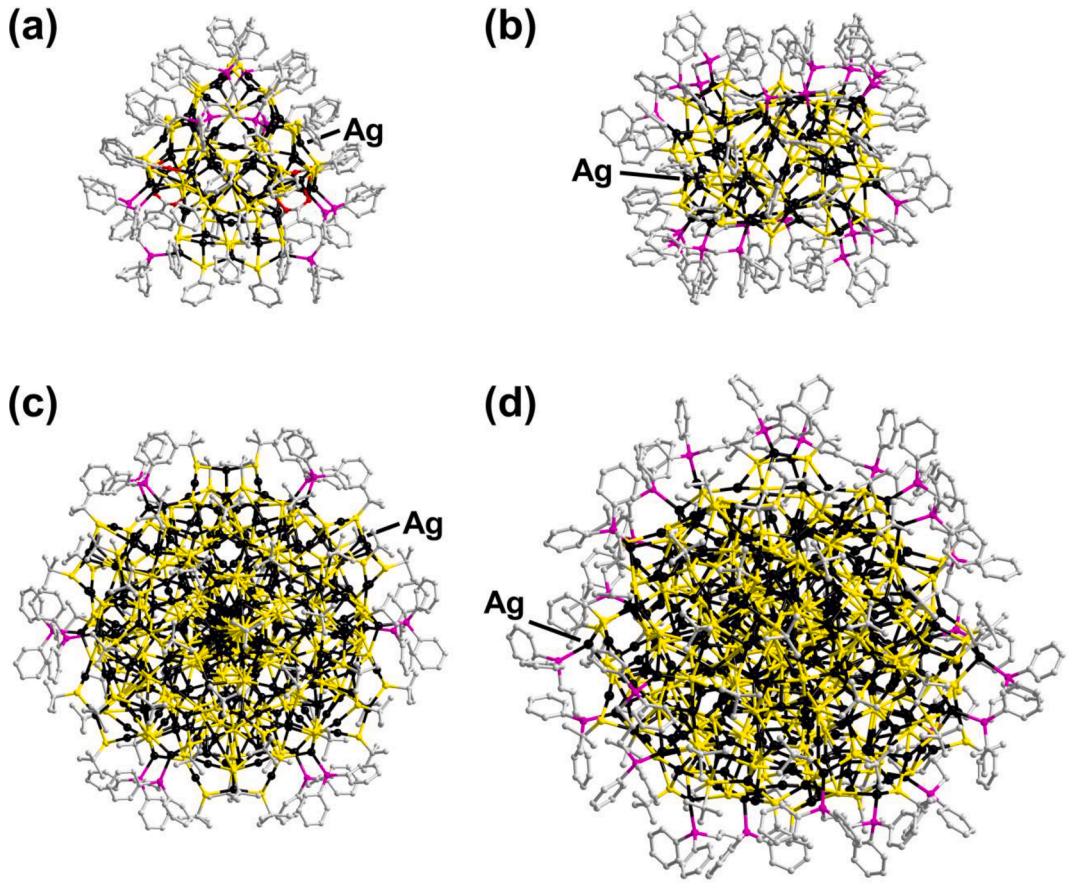

Fig. 27. Molecular structures of silver sulfide nanoclusters stabilized by bidentate or tridentate phosphine ligands. (a) $[Ag_{70}S_{16}(SPh)_{34}(PhCO_2)_4(triphos)_4]$. (b) $[Ag_{70}S_{20}(SPh)_{28}(dppm)_{10}](TFA)_2$. (c) $[Ag_{262}S_{100}(S^tBu)_{62}(dppb)_6]$. (d) $[Ag_{320}S_{130}(S^tBu)_{60}(dppp)_6]$. H atoms are omitted for clarity.

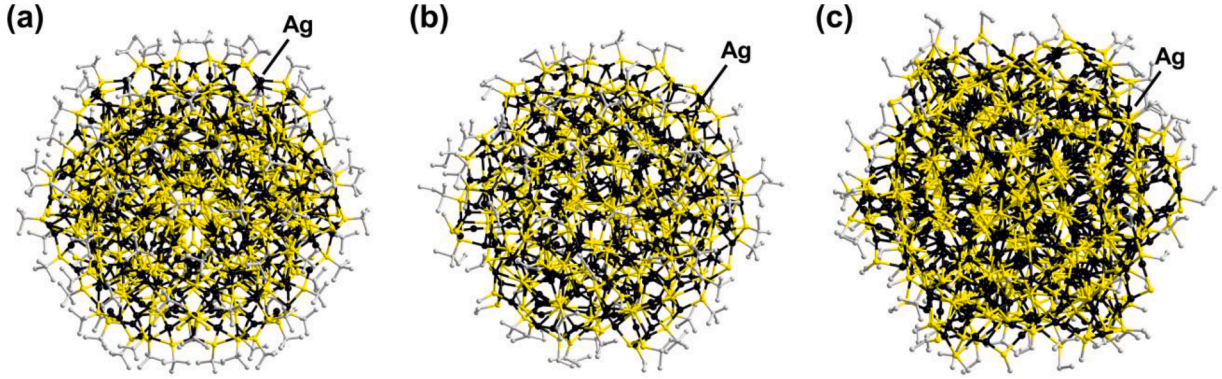

Fig. 28. Molecular structures of thiolate-protected silver sulfide nanoclusters (a) $[Ag_{344}S_{124}(S^tBu)_{96}]$, (b) $[Ag_{352}S_{128}(S^tC_5H_{11})_{96}]$, and (c) $[Ag_{490}S_{188}(S^tC_5H_{11})_{114}]$. H atoms are omitted for clarity.

formation of chiral silver sulfide nanoclusters. However, other species, such as the benzoate-substituted cluster $[CO_3@Ag_{20}(S^tBu)_{10}(BzO_2)_8(DMA)_2(MeCN)_2]$ cluster (**111**; Fig. 29c; DMA = dimethylacetamide), show neither fluorescent potential or electrochemical performance nor chirality [121]. These results and comparisons provide a deeper understanding of the selective functionalization of coinage metal nanoclusters as an elegant means of influencing their properties.

The *in situ* reduction method mentioned above has seen a great amount of success [122]. Most commonly, $Na[BH_4]$ and $Na[BH_3CN]$ were used to reduce Ag^+ to Ag in this context. By this, the coinage metal cluster cores can be stabilized without the insertion of any bridging chalcogenide ligands. For instance, in the presence of $Na[BH_4]$, the reaction of $AgNO_3$, pentafluorobenzenethiol (PFBT), and PPh_3 in MeOH and DCM afforded the formation of $Na_2[Ag_{39}(PFBT)_{24}(PPh_3)_8]$ (**112**). Herein, it was found that 17 of the 39 silver atoms were formally uncharged, and thus the cluster is isolable without further sulfide ligands. Further experiments led to the synthesis of a mixed-metallic analogue with Ag and Cu atoms in $Na_2[Ag_{37}Cu_2(PFBT)_{24}(PPh_3)_8]$ (**113**), and also to the formation of a heteronuclear cousin in $Na_2[Ag_{37}Cu_2(PFBT)_{24}(PPh_3)_8][Ag_{14}(PFBT)_6(PPh_3)_8]$ (**114**) [118]. By decreasing the number of C–F bonds in the thiolate reagents, using 3,4-difluorobenzenethiol or 4-fluorobenzenethiol, in reactions with $AgNO_3$ under the same conditions enabled the crystallization of two isostructural clusters, $[Ag_{44}(S\text{-}C_6H_3\text{-}F_2)_{30}]^4$ (in **115**)

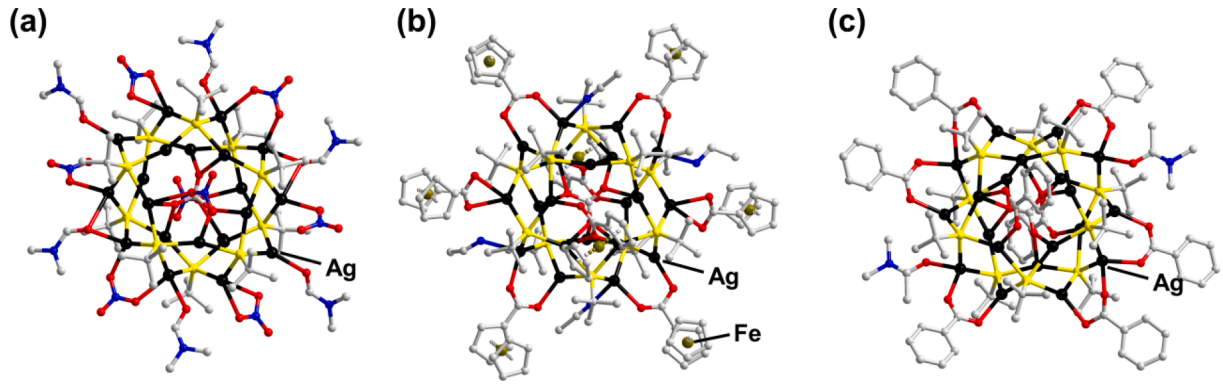

Fig. 29. Molecular structures of related silver sulfide nanoclusters decorated with different ligand groups. (a) $[CO_3@Ag_{20}(S^tBu)_{10}(DMF)_6(NO_3)_8]$. (b) $[CO_3@Ag_{20}(S^tBu)_{10}(FcC_5H_4CO_2)_8(MeCN)_4]$. (c) $[CO_3@Ag_{20}(S^tBu)_{10}(BzO_2)_8(DMA)_2(MeCN)_2]$. H atoms are omitted for clarity.

and $[Ag_{44}(S\text{-}C_6H_4\text{-}F)_{30}]^4$ (in **116**). Further substitution of F by CF_3 in the thiolate led to the formation of $[Ag_{44}(S\text{-}C_6H_4\text{-}CF_3)_{30}]^4$ (in **117**). Each of the three cluster anions comprise ten formally uncharged Ag atoms [124].

Varying the chalcogenolate ligands provides a method for tuning optical properties. The reaction of Ag(Tos) (Tos = tosyl) with 2,4-dimethylbenzenethiolate (2,4-DMBT) and PPh_3 in the presence of Na$[BH_3CN]$ and EtOH, for example, led to the formation of $[Ag_{40}(2,4\text{-}DMBT)_{24}(PPh_3)_8]$ (**118**; Fig. 30a). However, the use of 2,5-dimethylbenzenethiolate (2,5-DMBT) afforded the larger cluster $[Ag_{46}(2,5\text{-}DMBT)_{24}(PPh_3)_8](Tos)_2$ (**119**; Fig. 30b). Given the correlation between the structures and optical properties, the authors noted that the crystal packing is essential to tune the optical features of coinage metal nanoclusters. Alternatively, the treatment of **118** in DCM and MeOH with small amounts of 2,5-DMBT afforded mixed single crystals of **119** and $[Ag_{43}(2,5\text{-}DMBT)_{25}(PPh_3)_4]$ (**120**; Fig. 30c) [125].

The reaction of Ag$[SbF_6]$ with HSCy, $[PPh_4]$Br and Na$[BH_4]$ in the solvent mixture DCM, MeOH, triethylamine (TEA) and hexane yielded $[Ag_{206}(SCy)_{70-x}F_xCl_2]^{q+}$ (x = 0–4; q = 2–5; in **121**; Fig. 31a) [126]. The presence of differently charged isomers has been shown by means of ESI-MS analyses. Considering the charge balance, a considerable number of the silver atoms in the cluster core are formally uncharged. An overall metalloid nature of the cluster core was confirmed indeed by electrochemistry, plasmonic absorption, and density functional theory calculations (DFT). Furthermore, the treatment of **93** with $[PPh_4]$Br under the same reaction conditions led to the formation of $[PPh_4]_4[Ag_{136}(S\text{-}4\text{-}^tBuPh)_{64}Cl_3Ag_{0.45}]$ (**122**; Fig. 31b). The addition of Ag$[BF_4]$ afforded $[Ag_{374}(S\text{-}4\text{-}^tBuPh)_{113}Br_2Cl_2]$ (**123**; Fig. 31c), containing a metallic core with 257 uncharged silver atoms, which represents the largest reported coinage metal cluster when also taking the ligands into account [127].

In this section, we have illustrated the wide spectrum of silver chalcogenide cluster-based compounds, where the cluster cores are either (a) terminated and bridged by chalcogenolate (RCh) moieties, or (b) linked by chalcogenide anions and shielded by (RCh) groups with or without further functionality. In the first case, smaller coinage metal chalcogenide clusters are obtained. Upon introduction of chalcogenide atoms, as in the second case, larger clusters are formed for reasons of charge balance. Larger clusters can alternatively be approached by (c) the reduction of Ag^+ cations.

Besides the use of chalcogenide Ch^2 and chalcogenolate (RCh) anions as either bridging or surface-decorating ligands, there are also some works reporting the functionalization of such high-nuclearity clusters with dichalcogenolate $[(R)_2PCh_2]$ anions (Ch = S, Se), and even with multichalcogenolate $(RCh_x)^q$ anions (Ch = S, x > 2) as ligands. Some examples are given in Scheme 2.

The treatment of $[Ag(MeCN)_4][PF_6]$ salts with $[NH_4][Ch_2P(R)_2]$ under the given reaction conditions allowed for the formation of a series of relatively smaller silver dichalcogenolate clusters. The variation of solvents and auxiliaries is regarded the most important factor in these reactions. For instance, the reaction of $[Ag(MeCN)_4][PF_6]$ and $[NH_4][S_2P(O^iPr)_2]$ in DCM and H_2O afforded $[Ag_6(S_2P(O^iPr)_2)_6]$ (**124a**) [128]. Replacing $[NH_4][S_2P(O^iPr)_2]$ with $[NH_4][Se_2P(O^iPr)_2]$ yielded the analogous $[Ag_6(Se_2P(O^iPr)_2)_6]$ clusters (**124b**) [129]. Interestingly, the neutral $[Ag_6(Se_2P(O^iPr)_2)_6]$ cluster co-crystallized with the larger $[Ag_8(Se)\{Se_2P(O^iPr)_2\}_6]$ (**125a**), which shows an additional Se atom embedded in a cubic $\{Ag_8\}$ core as elucidated by SC-XRD. This showcased that the formation of a heteronuclear silver selenolate cluster is also possible. Using THF as a solvent and Na_2S as an additional sulfide source, the sulfur analogue, $[Ag_8(S)\{S_2P(O^iPr)_2\}_6]$ (**125b**), was formed [130]. Further varying the chalcogenolate source as well as the solvent allowed for the isolation of the even larger clusters $[Ag_{10}(Se)\{Se_2P(OEt)_2\}_6]$ (**126**; Fig. 32a) and $[Ag_{10}(Se)(Se_2P(O^iPr)_2)_6]$ (**127**) [130]. In

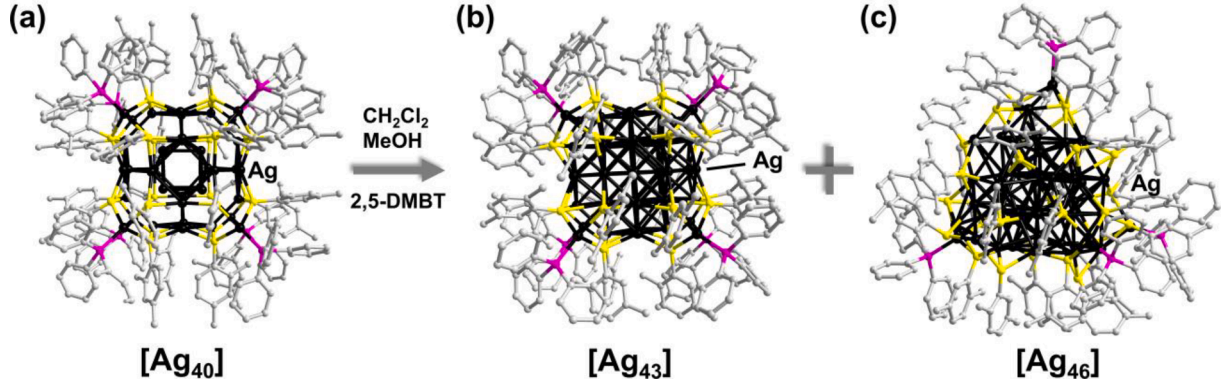

Fig. 30. Transformation of silver sulfide nanoclusters. (a) $[Ag_{40}(2,4\text{-}DMBT)_{24}(PPh_3)_8]$. (b) $[Ag_{46}(2,5\text{-}DMBT)_{24}(PPh_3)_8](Tos)_2$. (c) $[Ag_{43}(2,5\text{-}DMBT)_{25}(PPh_3)_4]$. H atoms are omitted for clarity.

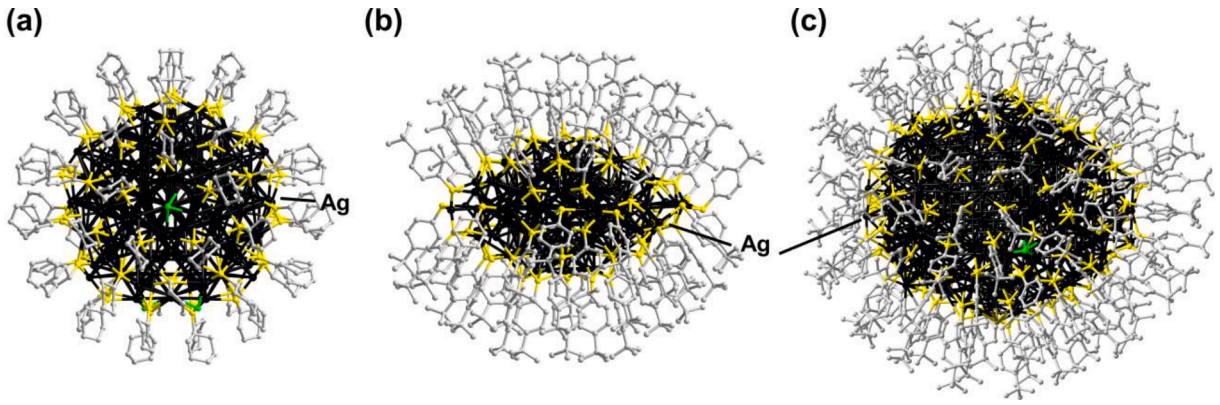

Fig. 31. Molecular structures of huge metalloid silver sulfide nanoclusters. (a) $[Ag_{206}(SCy)_{68}F_2Cl_2]^{q+}$ (q 2, 3, 4, 5). (b) $[PPh_4][Ag_{136}(S\text{-}4\text{-}^tBuPh)_{64}Cl_3Ag_{0.45}]$. (c) $[Ag_{374}(S\text{-}4\text{-}^tBuPh)_{113}Br_2Cl_2]$. H atoms are omitted for clarity.

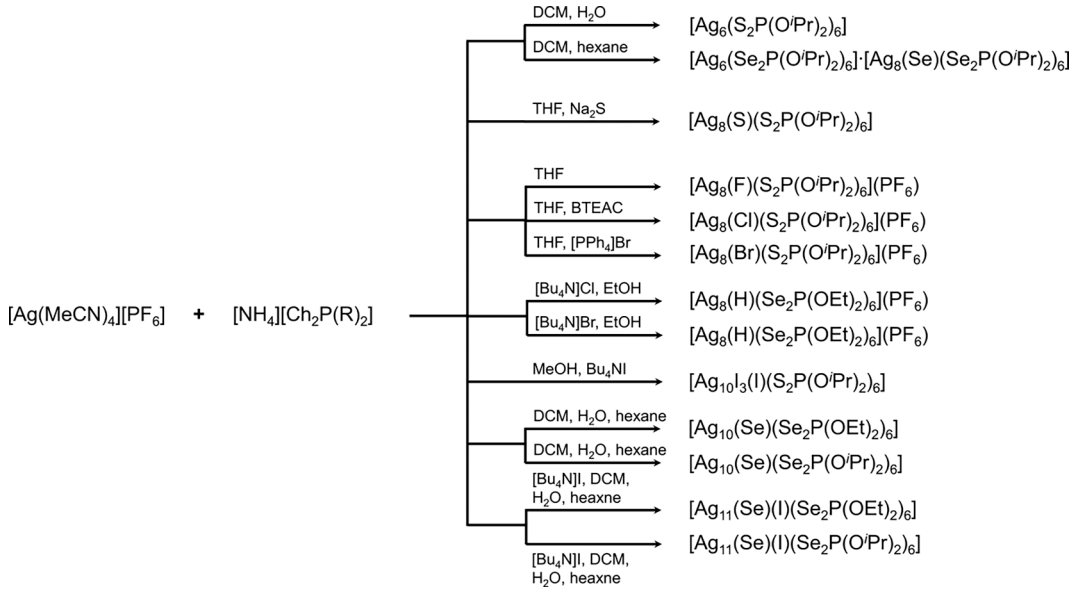

Scheme 2. Illustration of the syntheses of smaller silver dichalcogenolate clusters exhibiting dichalcogenolate groups by the use of salts of dichalcogenolate $[(R)_2PCh_2]^-$ anions as reactants.

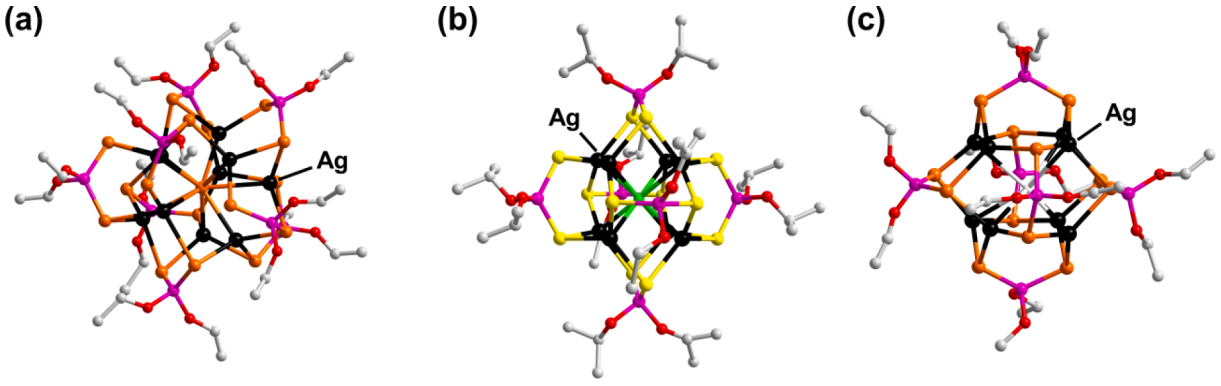

Fig. 32. Molecular structure of chalcogenide-centered or halide-centered silver chalcogenide clusters comprising dichalcogenolate ligands. (a) $[Ag_{10}(Se)(Se_2P(OEt)_2)_6]$. (b) $[Ag_8(F)\{S_2P(O^iPr)_2\}_6](PF_6)$. (c) $[Ag_8(H)(Se_2P(OEt)_2)_6][PF_6]$. H atoms are omitted for clarity.

these cases, the selenide ligand is encapsulated in a distorted trapezoidal-prismatic configuration, and the cluster cores are further surrounded by six selenolate ligands.

Given the crystallization of coinage metal clusters with interstitial chalcogenide anions, similar coinage metal clusters have also been realized with interstitial halide anions. For this, the use of halogenated solvents or halide salts has been proven useful. For example, the reaction of $[Ag(MeCN)_4][PF_6]$ and $[NH_4][S_2P(O^iPr)_2]$ in THF led to the

formation of the fluoride-centered species $[Ag_8(F)(S_2P(O^iPr)_2)_6][PF_6]$ (**128a**; Fig. 32b) [130]. Addition of benzyltriethylammonium chloride (BTEAC) or $[PPh_4]Br$ to the aforementioned reaction solution resulted in a replacement of the central fluoride anions with chloride or bromide, and led to the formation of chloride-centered $[Ag_8(Cl)(S_2P(O^iPr)_2)_6][PF_6]$ (**128b**) or bromide-centered $[Ag_8(Br)(S_2P(O^iPr)_2)_6][PF_6]$ clusters (**128c**), respectively [130]. All of these structures are identical and crystallize with cubic inorganic cores, which are further surrounded by six dichalcogenolate units at each face of the cubic core. The next logical step was to synthesize iodide-centered clusters. This could be achieved by adding $[Bu_4N]I$, which afforded the larger neutral clusters $[Ag_{10}I_3(I)(S_2P(O^iPr)_2)_6]$ (**129**), $[Ag_{11}(Se)(I)(Se_2P(OEt)_2)_6]$ (**130**), and $[Ag_{11}(Se)(I)(Se_2P(O^iPr)_2)_6]$ (**131**). [130,131] Their different structures, as compared to the F^-, Cl^-, and Br^- containing cousins, might be caused by the template effect of the larger I^- anions.

With the addition of $Na[BH_4]$ as a reducing agent, hydride-centered molecules are obtained under different reaction conditions. For instance, in the presence of $Na[BH_4]$, the reaction of $[Ag(MeCN)_4][PF_6]$ and $[NH_4][Ch_2P(OR)_2]$ (Ch = S, Se; R = Et, ^{i}Pr) in DCM enabled the crystallization of the hydride-centered heptanuclear clusters of $[Ag_7(H)(Se_2P(O^iPr)_2)_6]$ (**132**) and $[Ag_7(H)(S_2P(O^iEt)_2)_6]$ (**133**) [132]. The presence of the hydride was fully confirmed by means of NMR, ESI-MS, and DFT calculations. Additionally, these clusters can also be generated from larger clusters through stepwise fragmentation. The reaction of $[Ag_{10}(Ch)(Ch_2P(OR)_2)_6]$ with $Na[BH_4]$ in DCM lead to an exchange of the Ch^{2-} anion with an H^- anion, which allowed for the formation of the hydride-centered, cationic species $[Ag_8(H)(Ch_2P(OR)_2)_6][PF_6]$ (**134**, R = ^{i}Pr; **135**, R = Et; Fig. 32c) as an intermediate. Upon further addition of $Na[BH_4]$, the latter transform into the smaller clusters **132** and **133**, respectively [133].

Besides the use of dichalcogenidophosphonates as bidentate ligands, dithiolatecarborane has recently been established as another significant type of surface-capping agents for the functionalization of coinage metal clusters. [134,135] For example, the reaction of 1-thiol-*o*-carborane with Ag(TFA) in MeCN afforded $[Ag_{14}(S_2C_2B_{10}H_{10})_6(MeCN)_4]\bullet 4MeCN$ (**136**, Fig. 33a), which contains a metallic core where a partial reduction of Ag^+ to Ag^0 is observed [134]. Because of the coordination of labile MeCN moieties, this compound is not stable. For the same reason, however, it can be functionalized with other coordinating molecules. For example, through immersing the compound **136** in a solution of DCM and pyridine or 4-methylpyridine, the pyridine and 4-methylpyridine molecules substitute all MeCN molecules, thereby affording the analogous species $[Ag_{14}(S_2C_2B_{10}H_{10})_6(py)_4]$ (**137**; Fig. 33b) and $[Ag_{14}(S_2C_2B_{10}H_{10})_6(4\text{-}CH_3\text{-}py)_4]$ (**138**). A linkage of this type of clusters into polymers with multidentate ligands has also proven successful (Section 4.2). Apart from the isolation of smaller clusters, the use of dimercaptocarborane also contributes to the formation of relatively larger clusters. By reacting achiral 9,12-dimercapto-1,2-*closo*-carborane with Ag(TFA) in MeCN and after addition of PPh_3 and $Na[BH_4]$, the neutral cluster $[Ag_{33}(S_2C_2B_{10}H_{10})_{12}]$ formed (**139**; Fig. 33c). A partial replacement of Ag^+ with Cu^+ in the cluster core breaks the symmetry and results in the formation of chiral compounds [135]. This serves as an efficient method to manipulate the chiroptical properties of specific coinage metal clusters.

Multidentate chalcogenolates have also been employed for inducing chirality in such clusters. In the presence of dppm, the reaction of 8,9,12-trimercapto-1,2-*closo*-carborane with Ag(TFA) in MeCN and N_2H_4 led to a racemic mixture of clusters $(R/L\text{-})[Ag_{30}(S_3C_2B_{10}H_9)_8(dppm)_6]$ (**140**; Fig. 34a) [136]. The chirality of the cluster is attributed to the chiral arrangement of the trimercaptocarborane ligands. The ligands thus not only serve as protective agents, but also act as a chirality inducer in some specific cases.

Most recently, even thiacalix[4]arene groups, which contain multiple sulfide and oxide coordination sites, have been utilized to stabilize coinage metal clusters. Reactions of $[^nBu_4N]_4(\alpha\text{-}Mo_8O_{26})$, $(AgSEt)_n$, and Ag(Tos) with *p*-phenyl-thiacalix[4]arene (H_4PTC4A) in MeCN, TCM, and DMF enabled the crystallization of $[Ag_{18}(Mo_2O_5PTC4A)_6(EtS)_6(Tos)]\bullet 2Ag(MeCN)_3\bullet 4TCM$ (**141**, Fig. 34b) [137]. The formation of the anionic $[(Mo_2O_5PTC4A)]^{12-}$ metallamacrocycle is instrumental for stabilizing the inner inorganic cluster core, and was confirmed by mass spectrometry. Crystals of the compound are soluble in DCM/MeOH, and the cluster remains intact as evidenced by ESI-MS measurements. Under the given reaction conditions, the replacement of *p*-phenyl-thiacalix[4]arene with p-tert-butylthiacalix[4]arene allowed for the isolation of $[Ag_{155}(SCy)_{40}(T\text{-}C4A)_5Cl_2]$ (**142**; Fig. 34c) [138]. The arrangement of the silver atoms in the inorganic core leads to an uncommon *pseudo*-5-fold symmetry.

Although it has been a challenge to synthesize soluble coinage metal clusters for a long time, the silver clusters functionalized with thiacalix[4]arenes are well soluble in common solvents. Because of the good solubility of both starting materials and thiacalix[4]arene-stabilized coinage metal chalcogenide clusters, future work might contribute to the understanding of cluster growth mechanisms by *in situ* studies in solution.

All ligand-functionalized silver cluster-based compounds presented in Section 4.1 are summarized in Table 6.

4.2. Ligand-bridged silver cluster-based polymers

Polymeric networks can be synthesized by reactions of silver chalcogenides or silver chalcogenolates with pyridinium-based compounds. Inserting these ligands as bridges between the respective silver clusters yields large porous networks.

For example, a step-wise ligand-substitution reaction of $[Ag_{12}(S^tBu)_6(TFA)_6(MeCN)_6]$ with bpy led to the formation of the highly stable silver chalcogenolate polymer 2D-$[Ag_{12}(S^tBu)_8(TFA)_4(bpy)_4]$ (**143a**; Fig. 35a) [139]. The crystals of $[Ag_{12}(S^tBu)_6(TFA)_6(MeCN)_6]$ decomposed completely within 30 min after exposure to air. By contrast, the polymeric compound **143a** is air-stable for over one year, as confirmed

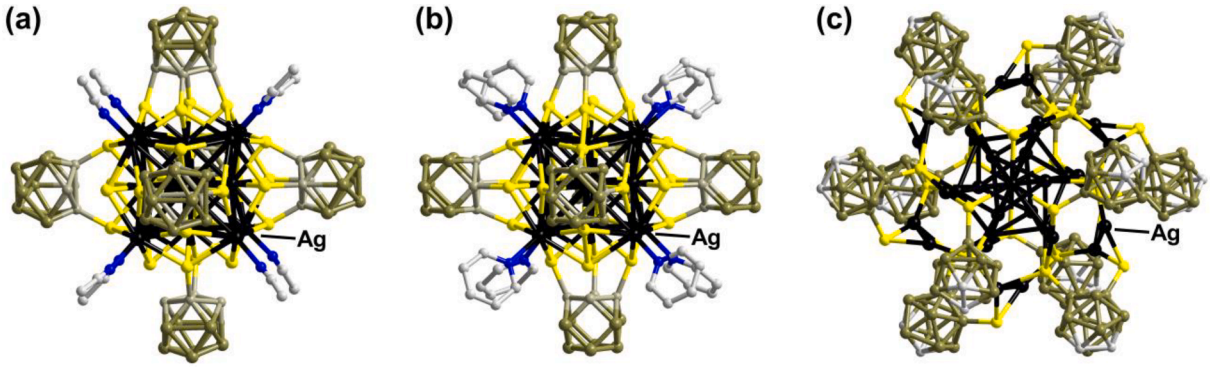

Fig. 33. Molecular structures of silver sulfide nanoclusters with dithiolatecarborane-derived ligands. (a) $[Ag_{14}(S_2C_2B_{10}H_{10})_6(MeCN)_4]$. (b) $[Ag_{14}(S_2C_2B_{10}H_{10})_6(py)_4]$. (c) $[Ag_{33}(S_2C_2B_{10}H_{10})_{12}]$. H atoms are omitted for clarity.

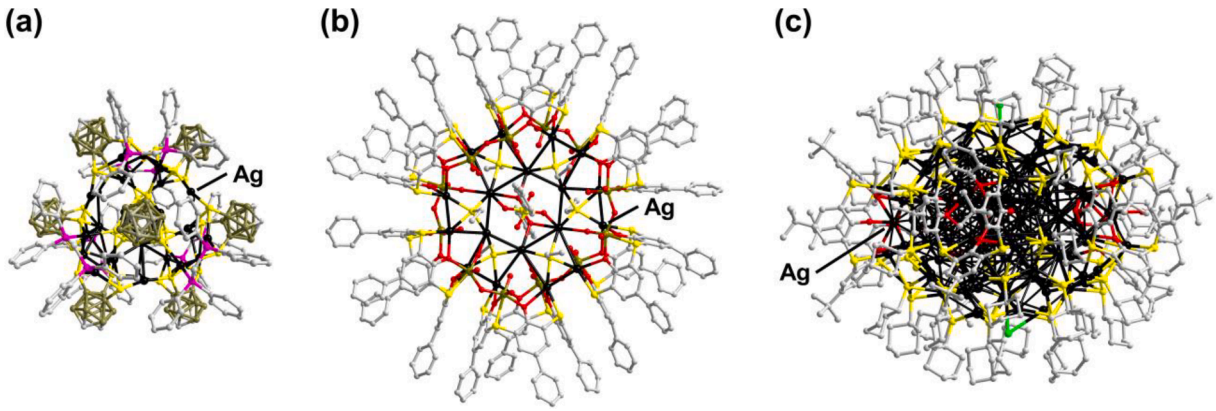

Fig. 34. Molecular structures of chiral or thiacalix[4]arene-functionalized silver sulfide nanoclusters. (a) $[Ag_{30}(S_3C_2B_{10}H_9)_8(dppm)_6]$. (b) $[Ag_{18}(Mo_2O_5PT\text{-}C4A)_6(EtS)_6(Tos)]$. (c) $[Ag_{155}(SCy)_{40}(TC4A)_5Cl_2]$. H atoms are omitted for clarity.

by powder X-ray diffraction (PXRD). The polymeric 2D-$[Ag_{12}(S^tBu)_8(TFA)_4(bpy)_4]$ shows ultrafast reversible fluorescence properties in vacuum/air, and the switching mechanism has been further elucidated by studying single-crystal structures. It is assumed that molecular O_2 transfers the triplet energy of the bpy ligands and thus quenches its photoluminescence emission. The luminescence property can be restored upon exposure to volatile organic compounds (VOCs) under air. Introducing additional NH_2, CH_3, or F substituents at the third position of the bpy molecules led to the formation of a series of clusters of the formula 2D-$[(Ag_{12}(S^tBu)_8(TFA)_4(bpy\text{-}X)_4]$ (**143b**, X = NH_2; **143c**, X = CH_3; **143d**, X = F) (Fig. 35b, 35c) [140]. It was shown that the use of substituents with lone pairs (here: NH_2) results an increase of the phosphorescence lifetime from microseconds to milliseconds. In contrast, the electron-donating CH_3 group afforded a decrease of the lifetime. These findings underscore the significant role of ligands as bridges for stabilizing silver-chalcogenolate clusters on the one hand, and for engineering their luminescent properties on the other hand.

Novel polymers are accessible *via* fine-tuning of the reaction conditions. For example, replacement of MeCN and EtOH with an excess of dimethylformamide (DMA) and toluene in the reaction described above, led to the formation of 2D-$[(Ag_{12}(S^tBu)_6(TFA)_6(bpy)_4\bullet(DMA_x\bullet tol_y)]$ (**144**; Fig. 36) [141]. Here, the inorganic cluster moieties are compressed to form a cubooctahedron-like topology with bpy as bridging ligands. The compound shows thermochromic photoluminescence properties with dual-emission bands centered at around 463 and 630 nm, respectively. Both emission intensities are highly dependent on the excitation energy, and the differences regarding the emission intensities are remarkable as revealed by photoluminescence spectroscopy. Partial replacement of the bpy bridges with bpy-NH_2 afforded comparable intensities of these two emission peaks at low temperature, which was attributed to the lower temperature-dependence of the photoluminescence emission of bpy-NH_2 than that of the cluster itself.

In the presence of the coordination agent $PhPO(OH)_2$, the reaction of AgS^tBu, Ag(TFA) and bpy in MeCN and EtOH yielded a "breathing" two-dimensional polymer, 2D-$[Ag_{10}(S^tBu)_6(TFA)_2(PhPO_2(OH))_2(bpy)_2]$ (**145**; Fig. 37a) [142]. As elucidated by SC-XRD, the $PhPO(OH)_2$ molecules act as functional hydrogen bond donors to terminate the growth of the inorganic cluster cores. Thus, the clusters are relatively small with only ten silver atoms. Since the introduction of $[PhPO_2(OH)]$ solvent units, the framework is less rigid and can "breath" upon treatment with CH_2Cl_2, $CHCl_3$, and CCl_4, as revealed by SC-XRD. Therefore, the use of coordinating solvents or molecules is believed to be important towards the structure expansion of such cluster-based polymers.

Upon addition of $[PPh_4]Cl$ as an auxiliary instead of $PhPO(OH)_2$, the larger clusters assemble into a one-dimensional strand in 1D-{$[Ag_{15}Cl(S^tBu)_8(TFA)_{5.67}(NO_3)_{0.33}(bpy)_2(DMF)_2]\bullet 4.3DMF\cdot H_2O$} (**146**) or a two-dimensional layer in 2D-{$[Ag_{14}Cl(S^tBu)_8(TFA)_5(DMF)]\bullet 2DMF$} (**147**; Fig. 37b) [143]. Both were crystallized from the same reaction solution. The absence of bpy bridges led to the formation of a discrete cluster molecule in $[Ag_{16}Cl(S^tBu)_8(TFA)(DMF)_4(H_2O)]\bullet 1.5DMF$ (**148**). Upon a comprehensive investigation, it was suggested that the thermal stability, the optical, and the photoluminescence properties correlate with the dimensionality of the formed products, since the charge-transfer from the bridge to the cluster could be effectively modified this way. This has been further studied and confirmed by DFT calculations.

Besides ligands and auxiliaries, the selection of silver salts is regarded as another important parameter to influence the crystallization of the final products. With the reaction of $[Ag(tbt)]_n$ (tbt = tertiarybutylthiol); Ag (TFA), and bpy in MeCN and MeOH, a three-dimensional silver cluster-based framework is formed [144]. However, the coordination environment and composition of the cluster nodes differ from the ones discussed above. This might be caused by their distinct reactivity and steric effect. In addition, the replacement of bpy ligands with smaller pyrazine (pyz) ligands yielded a stable two-dimensional, sheet-like hexagonal structure in 2D-{$[Ag_{12}(tbt)_6(TFA)_6(pyz)_6]\bullet 2MeCN$}(**149**; Fig. 38a) [144]. The neighboring layers are stabilized by van-der-Waals interactions and H•••F hydrogen bonding. Therefore, the bulk crystals can be easily exfoliated to hexagonal nanosheets.

Further investigations using larger pyridyl-based ligands, such as tppe (1,1,2,2-tetrakis(4-(pyridine-4-yl)phenyl)-ethene) and TPyP (5,10,15,20-tetra(4-pyridyl)porphyrin), yielded 3D-{$[Ag_{12}(S^tBu)_6(TFA)][Ag_8(S^tBu)_4(TFA)_4](tppe)_2\bullet 10DMA$} (**150**; Fig. 38b) [145], 3D-{$[Ag_{12}(S^tBu)_6(TFA)_6(tppe)_{1.5}]\bullet 39DMA$} (**151**; Fig. 38c) [146], and 2D-$[Ag_{12}(S^tBu)_6(TFA)_3(TPyP)]$ (**152**; Fig. 38d) [147]. The tppe molecule, which is regarded as an aggregation-induced emission luminogen, endowed the framework compounds with usable luminescent properties. Furthermore, upon exposing the blue-emitting **150** and **151** to air, the guest DMA (Dimethylacetamide) molecules are lost, and the resulting guest-free solids show green emission. By then treating the DMA-free products with DMA again, the fluorescence can be switched back from green to blue. These two works emphasize the utilization of tppe bridges for tailoring the photoluminescence properties of silver cluster-based polymers. Future investigations will help to understand the underlying excitation and de-excitation mechanisms.

The use of catalytically active porphyrin ligands has been proven useful to improve both the photocatalytic and the electrocatalytic activities of silver cluster-based frameworks. For instance, with the addition of TPyP, the reaction of $Ag(S^tBu)$ and Ag(TFA) in CF_3CO_2H, 1,4-dioxane, and TCM afforded **152**, which not only selectively oxidizes 2-chloroethyl ethyl sulfide, but also provides a platform for screening silver cluster-based photocatalysts [147]. By changing the solvent to MeCN and EtOH, a two-dimensional polymer, 2D-{$[Ag_{27}S_2(S^tBu)_{14}(TFA)_8(TPyP)](TFA)$} (**153**; Fig. 39a) with larger cluster nodes formed [148]. This compound possesses highly exposed catalytic sites and shows efficient CO_2 fixation in carboxylative cyclization.

Besides the utilization of N-containing porphyrin ligands, it has

Table 6
Summary of the ligand-functionalized silver cluster-based compounds presented in Section 4.1.

Compound	Dimensionality	Reactants	Temperature (°C)	Ref.
Silver Chalcogenide (Ag^{+}/Ch^{2-})				
$[Ag_{188}S_{94}(P^{n}Pr_3)_{30}]$ (**84**)	0D	Ag(TFA), $P^{n}Pr_3$, $S(SiMe_3)_2$, diglyme	20 °C to rt	[107]
$[Ag_{188}S_{94}(P^{n}Bu_3)_{30}]$ (**85**)	0D	Ag(TFA), $P^{n}Bu_3$, $S(SiMe_3)_2$, diglyme	40 °C to 20 °C to rt	[107]
$[Ag_{154}Se_{77}(dppxy)_{18}]$ (**86**)	0D	$AgS^{t}Bu$, $Se(SiMe_3)_2$, DCM, dppxy, toluene	25 °C to 0 to rt	[108]
Silver-Chalcogenide/Chalcogenolate $\{Ag^{+}/Ch^{2-}/(ChR^{\cdot})\}$				
$[Et_4N][Ag_4(2\text{-TBI})_6(SO_4)_3]_2[Br@Ag_8(2\text{-TBI})_{12}(SO_4)_2]\bullet$ 4MeCN•3DMF (**87**)	0D	Ag_2SO_4, 2-TBI, NEt_4Br, MeCN, DMF	120	[109]
$[Ag_{14}(2\text{-TBI})_{12}X_2]$ (**88**)	2D	AgX, 2-TBI, DMF, H_2O (X = Cl, Br)	125	[110]
$[Ag_6(S\text{-}C_6H_4\text{-}CN)_6(PPh_3)_6]$ (**89**)	0D	Ag(OAc), 4-Cyanothiophenol, PPh_3, THF, hexane	rt	[111]
$[Ag_6(S\text{-}C_6H_4\text{-}NO_2)_6(PPh_3)_6]$ (**90**)	0D	Ag(OAc), 4-Nitrothiophenol, PPh_3, THF	rt	[111]
$[Ag_{14}S(S\text{-}C_6H_4\text{-}CN)_{12}(PPh_3)_8][FeCl_2(THF)_4]_3$ (**91**)	0D	$[Ag_6(S\text{-}C_6H_4\text{-}CN)_6(PPh_3)_6]$, $FeCl_2$, THF, pentane	rt	[111]
$[Ag_{14}S(S\text{-}C_6H_4\text{-}NCS)_{12}(PPh_3)_8]$ (**92**)	0D	Ag(OAc), SCN-C_6H_4-SH, PPh_3, THF, Et_2O	rt	[111]
$[H^{+}\text{–}NEt_3]_2[Ag_8Ag_{4/2}(S\text{-}C_6H_4\text{-}4\text{-}^{t}Bu)_{12}]\bullet n$EtOH (**93**)	1D	$AgNO_3$, 4-^{t}Bu-C_6H_2-SH, NEt_3, EtOH, MeCN	rt	[112]
$[H^{+}\text{–}NEt_3]_4[Ag_{50}S_7(S\text{-}C_6H_4\text{-}^{t}Bu\text{-}4)_{40}]\bullet 2CS_2\bullet 6$EtOH (**94**)	0D	$[H^{+}\text{-}NEt_3]_2[Ag_8Ag_{4/2}(S\text{-}C_6H_4\text{-}^{t}Bu\text{-}4)_{12}]\bullet n$EtOH, CS_2, MeCN	rt	[112]
$[Ag_{65}S_{13}(S\text{-}C_6H_4\text{-}NMe_2)_{39}(dppm)_5]$ (**95**)	0D	$Ag(O_2CPh)$, $(Me_2N)C_6H_4(SSiMe_3)_2$, $S(SiMe_3)_2$, dppm, THF, Et_2O	60 °C to rt	[113]
$[Ag_{76}Se_{13}(S\text{-}C_6H_4\text{-}NMe_2)_{50}(PPh_3)_{6.5}]$ (**96**)	0D	$Ag(O_2CPh)$, $Se(SiMe_3)_2$, PPh_3, $(Me_2N)C_6H_4(SSiMe_3)$, THF, Et_2O	60 °C to rt	[113]
$[Ag_{88}Se_{12}(S\text{-}C_6H_4\text{-}NMe_2)_{63}(PPh_3)_6]$ (**97**)	0D	$Ag(O_2CPh)$, $Se(SiMe_3)_2$, PPh_3, $(Me_2N)C_6H_4(SSiMe_3)$, THF, Et_2O	60 °C to rt	[113]
$[Ag_{10}(SCH_2Fc)_{10}(PPh_3)_4]$ (**98**)	0D	Ag(OAc), PPh_3, TCM, $[CpFe(\eta^5\text{-}C_5H_4CH_2SSiMe_3)]$; pentane	0 °C to rt	[114]
$[Ag_{48}S_6(SCH_2Fc)_{36}]$ (**99**)	0D	Ag(OAc), PPh_3, TCM, $[CpFe(\eta^5\text{-}C_5H_4CH_2SSiMe_3)]$; pentane	0 °C to rt	[114]
$[Ag_{70}S_{16}(SPh)_{34}(PhCO_2)_4(triphos)_4]$ (**100**)	0D	$Ag(O_2CPh)$, $Ph(SSiMe_3)$, $S(SiMe_3)_2$, triphos, diglyme	20 °C to 0 °C to rt	[107]
$[Ag_{70}S_{20}(SPh)_{28}(dppm)_{10}](TFA)_2$ (**101**)	0D	Ag(TFA), $Ph(SSiMe_3)$, $S(SiMe_3)_2$, dppm, DME	40 °C to rt	[115]
$[Ag_{262}S_{100}(S^{t}Bu)_{62}(dppb)_6]$ (**102**)	0D	$Ag(O_2CPh)$, (^{t}Bu)S($SiMe_3$), $S(SiMe_3)_2$, dppb, THF	20 °C to rt	[115]
$[Ag_{320}S_{130}(S^{t}Bu)_{60}(dppp)_{12}]$ (**103**)	0D	$Ag(S^{t}Bu)$, $S(SiMe_3)_2$, dppp, TCM, toluene	rt	[108]
$[Ag_{123}S_{35}(S^{t}Bu)_{50}]$ (**104**)	0D	$Ag(O_2CCH_3)$, (^{t}Bu)S($SiMe_3$), $S(SiMe_3)_2$, dppxy, toluene	rt	[116]
$[Ag_{344}S_{124}(S^{t}Bu)_{96}]$ (**105**)	0D	$Ag(O_2CPh)$, (^{t}Bu)S($SiMe_3$), $S(SiMe_3)_2$, dppxy, toluene	rt	[116]
$[Ag_{490}S_{188}(S^{t}C_5H_{11})_{114}]$ (**106**)	0D	$Ag(S^{t}C_5H_{11})$, $S(SiMe_3)_2$, dppbp, THF, *p*-xylene	15 °C	[108]
$[Ag_{352}S_{128}(S^{t}C_5H_{11})_{96}]$ (**107**)	0D	$Ag(S^{t}C_5H_{11})$, $S(SiMe_3)_2$, dppbp, THF	25 °C to rt	[108]
Other Ag/S-Based Species				
$[CO_3@Ag_{20}(S^{t}Bu)_{10}(DMF)_6(NO_3)_8]$ (**108**)	0D	$AgS^{t}Bu$, $AgNO_3$, MeOH, EtOH, DMF	rt	[120]
$[CO_3@Ag_{20}(S^{t}Bu)_{10}(DOBzQA)_8(MeCN)_4]$ (**109**)	0D	$[CO_3@Ag_{20}(S^{t}Bu)_{10}(DMA)_6(NO_3)_8]$, HDOBzQA, TEA	rt	[121]
$[CO_3@Ag_{20}(S^{t}Bu)_{10}(FcC_5H_4CO_2)_8(MeCN)_4]$ (**110**)	0D	$[CO_3@Ag_{20}(S^{t}Bu)_{10}(DMA)_6(NO_3)_8]$, Ferrocenemonocarboxylic acid, TEA	rt	[121]
$[CO_3@Ag_{20}(S^{t}Bu)_{10}(BzO_2)_8(DMA)_2(MeCN)_2]$ (**111**)	0D	$[CO_3@Ag_{20}(S^{t}Bu)_{10}(DMA)_6(NO_3)_8]$, BzOH, TEA	rt	[121]
$Na_2[Ag_{39}(PFBT)_{24}(PPh_3)_8]$ (**112**)	0D	$AgNO_3$, PPh_3, PFBT, MeOH, DCM, $Na[BH_4]$, pentane	rt	[123]
$Na_2[Ag_{37}Cu_2(PFBT)_{24}(PPh_3)_8]$ (**113**)	0D	$AgNO_3$, CuCl, PPh_3, PFBT, MeOH, DCM, $Na[BH_4]$, pentane	rt	[123]
$Na_2[Ag_{37}Cu_2(PFBT)_{24}(PPh_3)_8][Ag_{14}(PFBT)_6(PPh_3)_8]$ (**114**)	0D	$AgNO_3$, $Cu(TFA)_2$, PPh_3, PFBT, MeOH, DCM, $Na[BH_4]$, pentane	rt	[123]
$[PPh_4]_4[Ag_{44}(S\text{-}C_6H_3\text{-}F_2)_{30}]$ (**115**)	0D	$AgNO_3$, 3,4-difluorobenzenethiol, PPh_4Br, DCM, MeOH, Na $[BH_4]$, TEA, hexane	4	[124]
$[PPh_4]_4[Ag_{44}(S\text{-}C_6H_4\text{-}F)_{30}]$ (**116**)	0D	$AgNO_3$, 4-fluorobenzenethiol, PPh_4Br, DCM, MeOH, $Na[BH_4]$, TEA, hexane	4	[124]
$[PPh_4]_4[Ag_{44}(S\text{-}C_6H_4\text{-}CF_3)_{30}]$ (**117**)	0D	$AgNO_3$, 4-trifluoromethylbenzenethiol, PPh_4Br, DCM, MeOH, $Na[BH_4]$, TEA, hexane	4	[124]
$[Ag_{40}(2,4\text{-DMBT})_{24}(PPh_3)_8]$ (**118**)	0D	Ag(Tos), 2,4-DMBT, PPh_3, EtOH, $Na[BH_3CN]$	rt	[125]
$[Ag_{46}(2,5\text{-DMBT})_{24}(PPh_3)_8](Tos)_2$ (**119**)	0D	Ag(Tos), 2,5-DMBT, PPh_3, EtOH, $Na[BH_3CN]$	rt	[125]
$[Ag_{43}(2,5\text{-DMBT})_{25}(PPh_3)_4]$ (**120**)	0D	$[Ag_{40}(2,4\text{-DMBT})_{24}(PPh_3)_8]$, 2,5-DMBT, DCM, MeOH	rt	[125]
$(Cat)_x[Ag_{206}(SCy)_{68}F_2Cl_2]$ (in **121**, x = 2, 3, 4, 5)	0D	$Ag[SbF_6]$, HSCy, MeOH, DCM, $Na[BH_4]$, TEA, hexane	4	[126]
$[PPh_4][Ag_{136}(S\text{-}4\text{-}^{t}BuPh)_{64}Cl_3Ag_{0.45}]$ (**122**)	0D	$[HNEt_3]_2[Ag_{10}(SPh^{t}Bu)_{12}]$, DCM, MeOH, $[PPh_4]Br$, $Na[BH_4]$, TEA, hexane	4	[127]
$[Ag_{374}(S\text{-}4\text{-}^{t}BuPh)_{113}Br_2Cl_2]$ (**123**)	0D	$[HNEt_3]_2[Ag_{10}(S\text{-}4\text{-}^{t}BuPh)_{12}]$, $AgBF_4$, DCM, MeOH, $[PPh_4]Br$, $Na[BH_4]$, TEA, hexane	4	[127]
Silver Dichalcogenolate ($Ag^{+}/(Ch_2R^{\cdot})$				
$[Ag_6(S_2P(O^{i}Pr)_2)_6]$ (**124a**)	0D	$[Ag(MeCN)_4][PF_6]$, $[NH_4][S_2P(O^{i}Pr)_2]$, DCM, H_2O	rt	[128]
$[Ag_6(Se_2P(O^{i}Pr)_2)_6]$ (**124b**)	0D	$[Ag(MeCN)_4][PF_6]$, $[NH_4][Se_2P(O^{i}Pr)_2]$, DCM, hexane	50 °C to rt	[129]
$[Ag_8(Se)(Se_2P(O^{i}Pr)_2)_6]$ (**125a**)	0D	$[Ag(MeCN)_4][PF_6]$, $[NH_4][Se_2P(O^{i}Pr)_2]$, DCM, hexane	50 °C to rt	[129]
$[Ag_8(S)(S_2P(O^{i}Pr)_2)_6]$ (**125b**)	0D	$[Ag(MeCN)_4][PF_6]$, $[NH_4][S_2P(O^{i}Pr)_2]$, THF, Na_2S	20	[130]
$[Ag_{10}(Se)(Se_2P(OEt)_2)_6]$ (**126**)	0D	$[Ag(MeCN)_4][PF_6]$, $[NH_4][Se_2P(OEt)_2]$, Et_2O, DCM, H_2O, hexane	30 °C to rt	[130]
$[Ag_{10}(Se)(Se_2P(O^{i}Pr)_2)_6]$ (**127**)	0D	$[Ag(MeCN)_4][PF_6]$, $[NH_4][Se_2P(O^{i}Pr)_2]$, Et_2O, DCM, H_2O, hexane	30 °C to rt	[130]
$[Ag_8(F)(S_2P(O^{i}Pr)_2)_6][PF_6]$ (**128a**)	0D	$[Ag(MeCN)_4][PF_6]$, $[NH_4][S_2P(O^{i}Pr)_2]$, THF	20	[130]
$[Ag_8(Cl)(S_2P(O^{i}Pr)_2)_6][PF_6]$ (**128b**)	0D	$[Ag(MeCN)_4][PF_6]$, $[NH_4][S_2P(O^{i}Pr)_2]$, THF, Benzyltriethyammonium chloride	20	[130]
$[Ag_8(Br)(S_2P(O^{i}Pr)_2)_6][PF_6]$ (**128c**)	0D	$[Ag(MeCN)_4][PF_6]$, $[NH_4][S_2P(O^{i}Pr)_2]$, THF, $[PPh_4]Br$	20	[130]
$[Ag_{10}(I)_4(S_2P(O^{i}Pr)_2)_6]$ (**129**)	0D	$[Ag(MeCN)_4][PF_6]$, $[NH_4][S_2P(O^{i}Pr)_2]$, MeOH, $[Bu_4N]I$	rt	[130]
$[Ag_{11}(Se)(I)(Se_2P(OEt)_2)_6]$ (**130**)	0D	$[Ag(MeCN)_4][PF_6]$, $[NH_4][Se_2P(OEt)_2]$, $[Bu_4N]I$, DCM, H_2O, hexane	rt	[131]
$[Ag_{11}(Se)(I)(Se_2P(O^{i}Pr)_2)_6]$ (**131**)	0D	$[Ag(MeCN)_4](PF_6)$, $[NH_4][Se_2P(O^{i}Pr)_2]$, $[Bu_4N]I$, DCM, H_2O, hexane	rt	[131]
$[Ag_7(H)(Se_2P(O^{i}Pr)_2)_6]$ (**132**)	0D	$[Ag(MeCN)_4][PF_6]$, $[NH_4][Se_2P(O^{i}Pr)_2]$, $Na[BH_4]$, DCM	rt	[132]
$[Ag_7(H)(S_2P(OEt)_2)_6]$ (**133**)	0D	$[Ag(MeCN)_4][PF_6]$, $[NH_4][S_2P(OEt)_2]$, $Na[BH_4]$, DCM	rt	[132]
$[Ag_8(H)(Se_2P(O^{i}Pr)_2)_6][PF_6]$ (**134**)	0D	$[Ag(MeCN)_4][PF_6]$, $[NH_4][Se_2P(O^{i}Pr)_2]$, $Na[BH_4]$, THF	20	[133]
$[Ag_8(H)(Se_2P(OEt)_2)_6][PF_6]$ (**135**)	0D	$[Ag(MeCN)_4][PF_6]$, $[NH_4][Se_2P(OEt)_2]$, $Na[BH_4]$, THF	20	[133]
$[Ag_{14}(S_2C_2B_{10}H_{10})_6(MeCN)_4]\bullet$4MeCN (**136**)	0D	Ag(TFA), 1-thiol-*o*-carborane, MeCN	rt	[134]

(*continued on next page*)

Table 6 (*continued*)

Compound	Dimensionality	Reactants	Temperature (°C)	Ref.
$[Ag_{14}(S_2C_2B_{10}H_{10})_6(py)_4]$ (**137**)	0D	$[Ag_{14}(S_2C_2B_{10}H_{10})(MeCN)_4]$•4MeCN, py, DCM	rt	[134]
$[Ag_{14}(S_2C_2B_{10}H_{10})_6(4\text{-}CH_3\text{-}py)_4]$ (**138**)	0D	$[Ag_{14}(S_2C_2B_{10}H_{10})(MeCN)_4]$•4MeCN, 4-$CH_3$-py, DCM	rt	[134]
$[Ag_{33}(S_2C_2B_{10}H_{10})_{12}]$ (**139**)	0D	Ag(TFA), 9,12-Dimercapto-1,2-*closo*-carborane, MeCN, PPh_3, $Na[BH_4]$	rt	[135]
Silver Polychalcogenolate $(Ag^+/(Ch_nR^-)^q$; n > 2)				
$[Ag_{30}(S_3C_2B_{10}H_9)_8(dppm)_6]$ (**140**)	0D	Ag(TFA), 8,9,12-Trimercapto-1,2-*closo*-carborane, dppm, MeCN, N_2H_4	rt	[136]
$[Ag_{18}(Mo_2O_5PTC4A)_6(EtS)_6(Tos)]$•2Ag(MeCN)$_3$•4TCM (**141**)	0D	$(AgSEt)_n$, Ag(Tos), H_4PTC4A, $[^nBu_4N]_4(\alpha\text{-}Mo_8O_{26})$, MeCN, TCM, DMF	65	[137]
$[Ag_{155}(SCy)_{40}(TC4A)_5Cl_2]$ (**142**)	0D	$(AgSCy)_n$, $AgNO_3$, ^nBuOH, H_4TC4A, TCM, $Na[BH_4]$, EtOH, NEt_3	rt	[138]

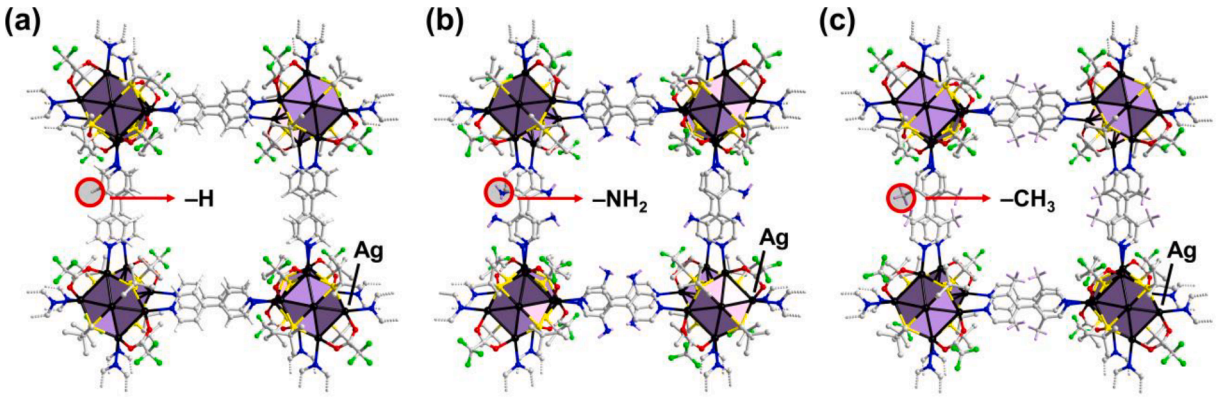

Fig. 35. Cutouts of the structures of ligand-bridged silver cluster-based polymers. (a) 2D-$[(Ag_{12}(S^tBu)_8(TFA)_4(bpy)_4]$. (b) 2D-$[(Ag_{12}(S^tBu)_8(TFA)_4(bpy\text{-}NH_2)_4]$. (c) 2D-$[(Ag_{12}(S^tBu)_8(TFA)_4(bpy\text{-}CH_3)_4]$. H atoms are omitted for clarity.

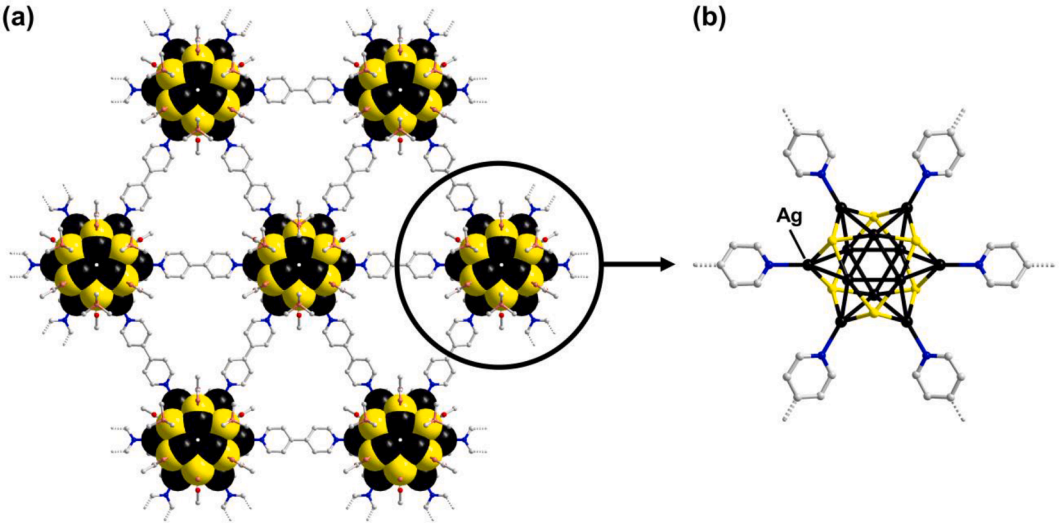

Fig. 36. Cutout of the framework of 2D-$[(Ag_{12}(S^tBu)_6(TFA)_6(bpy)_4$•$(DMA_x$•$tol_y)]$. (a) A fraction of seven linked clusters, with Ag and S atoms shown as space-filling models. (b) Zoom into one of the cluster units with half of the bridging bipy molecules drawn as ligands. H atoms are omitted for clarity.

recently also been proven feasible to link silver clusters by using carboxylate-based bridges. For instance, the two clusters were assembled into framework compounds 2D-{$[(HPO_4)_2$@$Ag_{18}(S^iPr)_8(H_2PO_4)_4(H_2$ZnTCPP(EtOH))]•2MeCN} (**154**) and 3D-$[(HPO_4)_4(H_2PO_4)_2$@$Ag_{54}(S^iPr)_{32}(TFA)_6(MeCN)_2(H_2TCPP)(TCPP)]$ (**155**; Fig. 39b) employing TCPP ligands [149]. Hence, carboxylates can also contribute to the functionalization and structural expansion of coinage metal chalcogenide cluster-based materials.

The ligand-bridged silver cluster-based polymeric compounds presented in Section 4.2 are summarized in Table 7.

5. Other ligand-functionalized and ligand-bridged transition metal chalcogenides

5.1. Ligand-functionalized and ligand-bridged {Re_6Se_8} cluster-based compounds

Among the metal chalcogenides, the octahedral {M_6Ch_8} cluster-based compounds (M = Re, Co, Mo, W, Cr; Ch = S, Se, Te) have received special attention owing to their structural beauty as well as their application potential for superconductivity [150], fast ionic conductivity [151], and chemical catalysis [152]. In the very beginning of the discovery of such compounds, cations, such as alkali metal ions, alkaline earth metal cations, were commonly used to control their

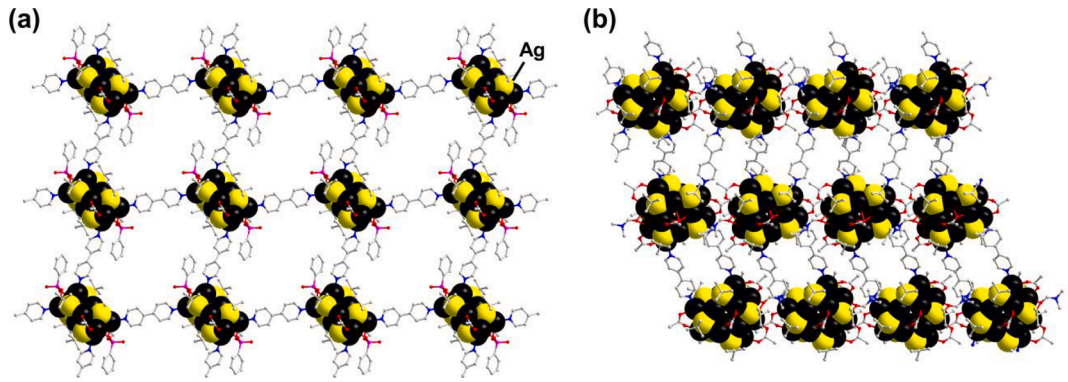

Fig. 37. View of bpy-bridged networks of silver sulfide clusters. (a) Decanuclear clusters in 2D-{[$Ag_{10}(S^tBu)_6(TFA)_2(PhPO_2(OH))_2(bpy)_2$]}. (b) Tetradecanuclear clusters in 2D-{[$Ag_{14}Cl(S^tBu)_8(TFA)_5(DMF)$]•2DMF}.

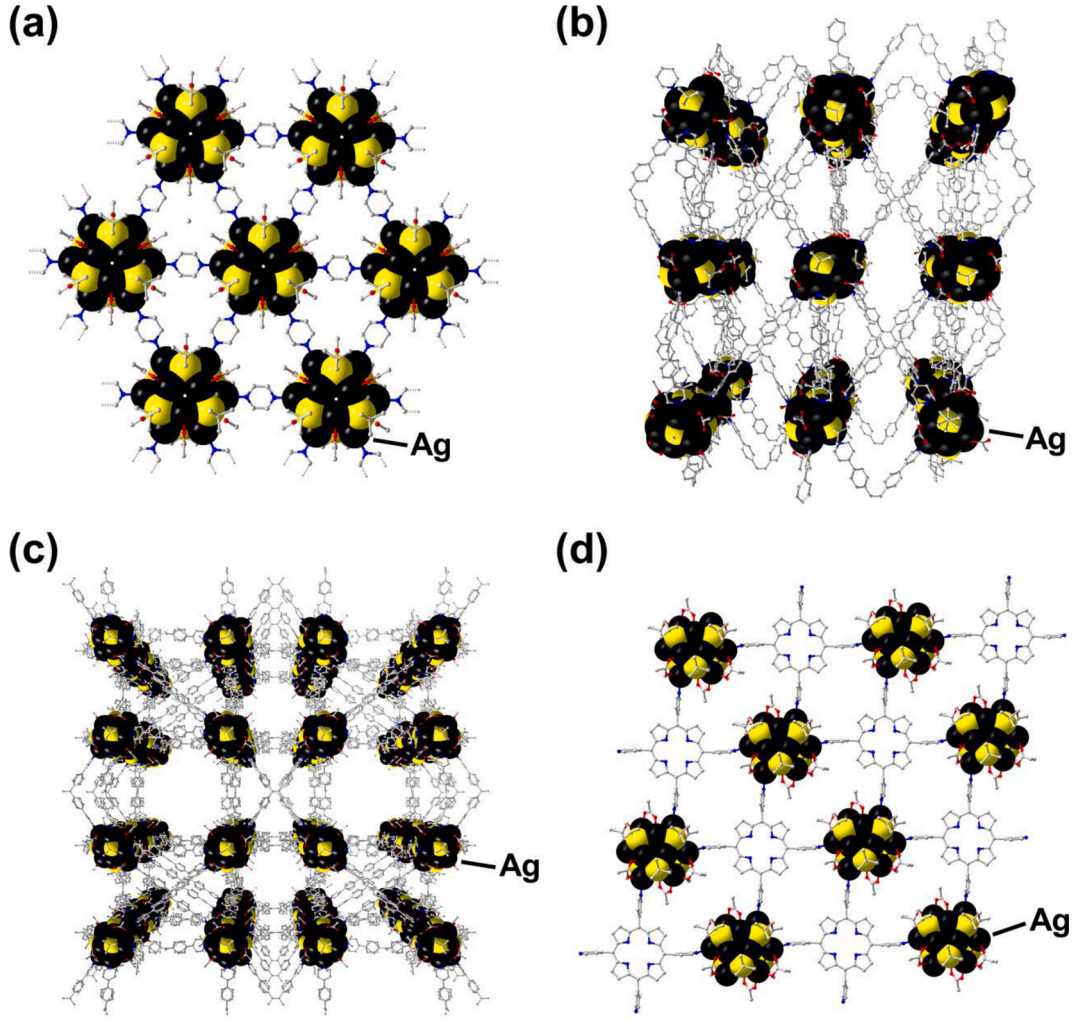

Fig. 38. Compounds comprising polymers based on dodecanuclear silver sulfide clusters. (a) 2D-{[$Ag_{12}(tbt)_6(TFA)_6(pyz)_6$]•2MeCN}. (b) 3D-{[$Ag_{12}(S^tBu)_6(TFA)$][$Ag_8(S^tBu)_4(TFA)_4$] $(tppe)_2$•10DMA}. (c) 3D-{[$Ag_{12}(S^tBu)_6(TFA)_6(tppe)_{1.5}$](DMA)}. (d) 2D-[$Ag_{12}(S^tBu)_6(TFA)_3(TPyP)$]. H atoms are omitted for clarity.

formation [153]. However, only a few cation types are available, which has been a long-term limitation for further structural expansion of such architectures. As a result, the ligand-functionalization of $\{M_6Ch_8\}$ cluster-based compounds has been adopted and proven productive. This not only led to the syntheses of new $\{M_6Ch_8\}$ cluster units [154], but also deepened our understanding regarding the activation of small molecules with such clusters [155]. In this section, we mainly focus on the syntheses of ligand-functionalized $\{Re_6Se_8\}$ and $\{Co_6Se_8\}$ cluster-based compounds. The reactivity of the latter towards carbenes is also discussed.

The naked $\{Re_6Se_8\}$ cluster unit can easily be functionalized at the open Re sites. A general schematic illustration shows the ligand-functionalization route concerning $\{Re_6Se_8\}$ moieties (Scheme 3) [156,157].

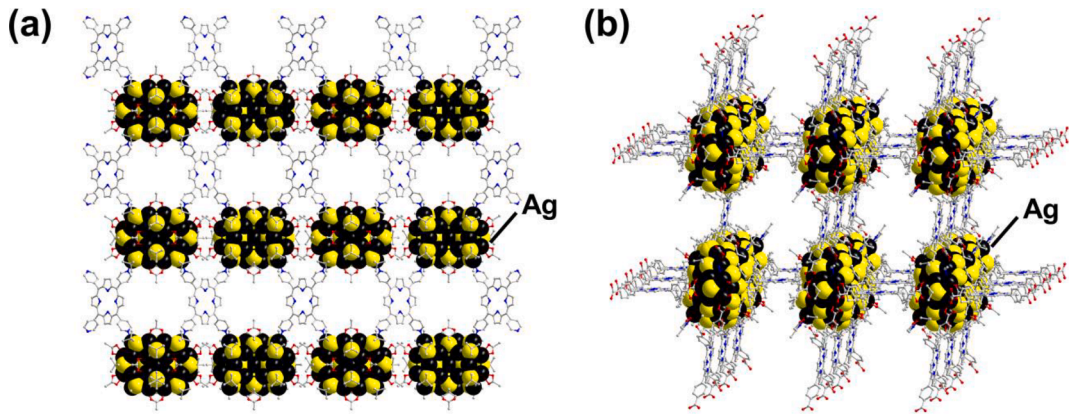

Fig. 39. Framework structures of linked silver chalcogenide cluster molecules. (a) 2D-{[$Ag_{27}S_2(S^tBu)_{14}(TFA)_8(TPyP)$](TFA)}. (b) 3D-[$(HPO_4)_4(H_2PO_4)_2$@$Ag_{54}(S^iPr)_{32}(TFA)_6(MeCN)_2(H_2$-TCPP)(TCPP)]. H atoms are omitted for clarity.

Table 7
Summary of the ligand-bridged silver cluster-based polymeric compounds presented in Section 4.2.

Compound	Dimensionality	Reactants	Temperature (°C)	Ref.
[$Ag_{12}(S^tBu)_8(TFA)_4(bpy)_4$] (**143a**)	2D	AgS^tBu, Ag(TFA), bpy, MeCN, EtOH	5–10	[139]
[$Ag_{12}(S^tBu)_8(TFA)_4$(bpy-NH_2)$_4$] (**143b**)	2D	AgS^tBu, Ag(TFA), bpy-NH_2, DCM, NH_4OH	rt	[140]
[$Ag_{12}(S^tBu)_8(TFA)_4$(bpy-CH_3)$_4$] (**143c**)	2D	AgS^tBu, Ag(TFA), bpy-CH_3, DCM, NH_4OH	rt	[140]
[$Ag_{12}(S^tBu)_8(TFA)_4$(bpy-F)$_4$] (**143d**)	2D	AgS^tBu, Ag(TFA), bpy-F, DCM, NH_4OH	rt	[140]
[$Ag_{12}(S^tBu)_6(TFA)_6$(bpy)$_4$•(DMA_x•tol_y)] (**144**)	2D	AgS^tBu, Ag(TFA), bpy, DMA, toluene	rt	[141]
[$Ag_{10}(S^tBu)_6(TFA)_2(PhPO_2(OH))_2(bpy)_2$] (**145**)	2D	AgS^tBu, Ag(TFA), bpy, MeCN, EtOH, $PhPO(OH)_2$	rt	[142]
{[$Ag_{15}Cl(S^tBu)_8(TFA)_{5.67}(NO_3)_{0.33}(bpy)_2(DMF)_2$]•4.3DMF·$H_2O$} (**146**)	1D	AgS^tBu, Ag(TFA), bpy, MeCN, DMF, PPh_4Cl	rt	[143]
{[$Ag_{14}Cl(S^tBu)_8(TFA)_5$(DMF))]•2DMF} (**147**)	2D	AgS^tBu, Ag(TFA), bpy, MeCN, DMF, PPh_4Cl	rt	[143]
[$Ag_{16}Cl(S^tBu)_8(TFA)$(DMF)$_4(H_2O)$]•1.5DMF (**148**)	0D	AgS^tBu, Ag(TFA), MeCN, DMF, PPh_4Cl	rt	[143]
{[Ag_{12}(tbt)$_6(TFA)_6$(pyz)$_6$]•2MeCN} (**149**)	2D	$Ag(tbt)_n$, Ag(TFA), pyz, MeCN, MeOH	5–15	[144]
{[$Ag_{12}(S^tBu)_6(TFA)$][$Ag_8(S^tBu)_4(TFA)_4$](tppe)$_2$•10DMA} (**150**)	3D	AgS^tBu, Ag(TFA), tppe, DMA, DCM, benzenephosphonic acid	rt	[145]
{[$Ag_{12}(S^tBu)_6(TFA)_6$(tppe)$_{1.5}$•39DMA} (**151**)	3D	AgS^tBu, Ag(TFA), tppe, DMA, DCM	rt	[146]
[$Ag_{12}(S^tBu)_6(TFA)_3$(TPyP)] (**152**)	2D	AgS^tBu, Ag(TFA), TPyP, 1,4-dioxane, TCM, CF_3COOH	rt	[147]
{[$Ag_{27}S_2(S^tBu)_{14}(TFA)_8$(TPyP)](TFA)} (**153**)	2D	AgS^tBu, Ag(TFA), TPyP, TCM, MeOH, MeCN, EtOH	rt	[148]
{[$(HPO_4)_2$@$Ag_{18}(S^iPr)_8(H_2PO_4)_4(H_2$ZnTCPP(EtOH))]•2MeCN} (**154**)	2D	AgS^iPr, Ag(TFA), ZnTCPP, MeOH, MeCN, H_3PO_4, TEA	70	[149]
[$(HPO_4)_4(H_2PO_4)_2$@$Ag_{54}(S^iPr)_{32}(TFA)_6(MeCN)_2(H_2$TCPP)(TCPP)] (**155**)	3D	AgS^iPr, Ag(TFA), H_2TCPP, MeOH, MeCN, H_3PO_4	70	[149]

2D or 3D frameworks, like the ones obtained with the face-capped $\{Re_6Se_{4+n}X_{10\ 2n}\}$ units (X = Cl, Br, I; n = 1–3) can be obtained through refluxing Re, Se, and ReX_5 at high temperatures in the presence of halide sources. Addition of TlX (X = Cl, Br, I) as a dimensional-reduction agent in some cases allows for the formation of fully capped $Tl_5[Re_6Se_8X_6]X$ monomers [156]. Alternatively, the fusion of stoichiometric amounts of Re, Se, and CsX at relatively low temperatures (400–500 °C) affords similar cluster anions as the former, for example in salts of the general formula $Cs_4[Re_6Se_8X_6]$ [156,158]. The use of CsX not only provides specific halides to cap the molecules, but the Cs^+ cations are also able to balance the negative charges and control the formation of $[Re_6Se_8X_6]^{4-}$ anions.

Given the less stable Re–X bonds, the halide ligands can be easily replaced with common ligands, like phosphines or solvent molecules (Scheme 4) [159]. This opens up opportunities for further functionalization of the clusters and obtaining oligomers, or even polymers in some specific cases.

Refluxing salts of $[Re_6Se_7(SeH)X_6]^{3-}$ with different amounts of phosphines, using DMF (Scheme 4), MeCN, or Me_2SO as solvents, affords a series of functionalized cationic clusters with $\{Re_6Se_8\}$ cores according to the general formula $\{Re_6Se_8(PEt_3)_{6-n}X_n\}$. These can react further to give $[Re_6Se_8(PEt_3)_{6-n}(solv)_n]^{2+}$ by adding $Ag[BF_4]$ or $Ag[SbF_6]$ to the reaction mixture [160].

The structures of these solvent-coordinated clusters can be further manipulated with bidentate or multidentate ligands, since the solvent molecules can be easily removed from the clusters at 180 °C *in vacuo* while keeping the corresponding Re sites open. With the use of bridging ligands, in particular comprising N-donor sites, these (partially) desolvated clusters can be transferred into dimers, trimers, tetramers, and even polymers of linked clusters. The formation and resulting structures of the desired target products depend on the structures of the specific ligands and can be controlled this way. For instance, the treatment of mono-solvated $[Re_6Se_8(PEt)_5(MeCN)]^{2+}$ with bpy in DCM and chlorobenzene allows for the isolation of ligand-functionalized monomeric $[Re_6Se_8(PEt_3)_5(bpy)]^{2+}$ and $[Re_6Se_8(PEt_3)_4(bpy)_2]^{2+}$ (in **156** and **157**; Fig. 40a 40b) and the dimeric cation $[\{Re_6Se_8(PEt_3)_5\}_2(bpy)]^{4+}$ (in **158**; Fig. 40c) [161]. Using DPE and *trans*-1,2-bis(4-pyridyl)ethane) (BPE) instead led to the formation of the similar dumbbell-shaped anionic clusters $[\{Re_6Se_8(PEt_3)_5\}_2(DPE)]^{4+}$ (in **159**) and $[\{Re_6Se_8(PEt_3)_5\}_2(BPE)]^{4+}$ (in **160**), respectively (Fig. 40c) [161]. However, the use of di-solvated *cis*-$[Re_6Se_8(PEt)_4(MeCN)_2]$ with these ligands affords a set of differently sized molecular "squares" of *cyclo*-$[\{Re_6Se_8(PEt_3)_4(bpy)\}_4]^{8+}$ (in **161**), *cyclo*-$[\{Re_6Se_8(PEt_3)_4(DPE)\}_4]^{8+}$ (in **162**), and *cyclo*-$[\{Re_6Se_8(PEt_3)_4(BPE)\}_4]^{8+}$ (in **163**) under the same reaction conditions (Fig. 40d) [162]. Refluxing di-solvated $[Re_6Se_8(PEt)_4(MeCN)_2]^{2+}$ with $[Re_6Se_8(PEt)_5(bpy)]^{2+}$ results in the formation of a rod-like trimer, $[Re_{18}Se_{24}(PEt_3)_{14}(bpy)_2]^{6+}$ (in **164**; Fig. 40e), which until now has only been identified by NMR and mass spectroscopy [161].

In terms of multidentate ligands, for example, the reaction of star-

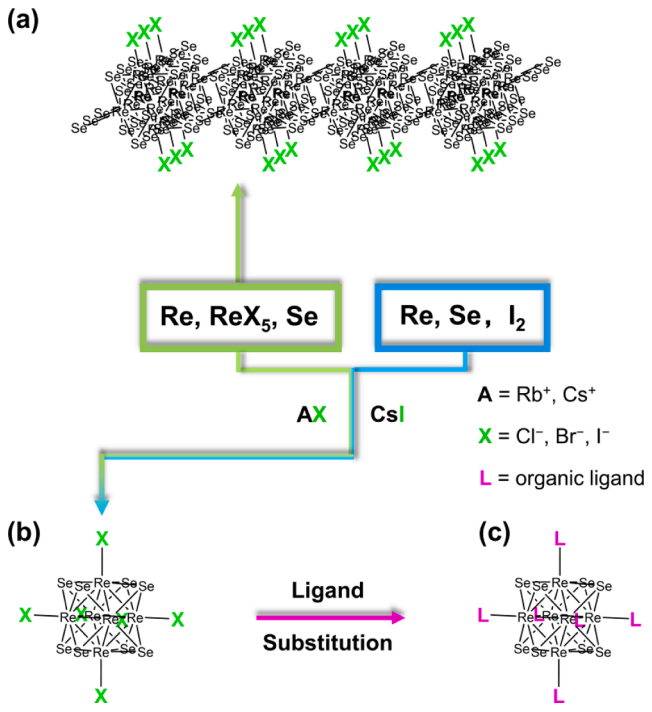

Scheme 3. Illustration for the syntheses $\{Re_6Se_8\}$ cluster-based compounds. (a) $\{Re_6Se_8\}$-based two-dimensional solid. (b) Halide-terminated anionic cluster unit $\{Re_6Se_8X_6\}$ (cations not shown here). (c) Ligand-functionalized $\{Re_6Se_8\}$ motif upon ligand substitution.

shaped 2,4,5-tri-4-pyridyl-1,3,5-trizaine (tpt) and TPyP with mono-solvated $[Re_6Se_8(PEt)_5(MeCN)]^{2+}$ led to the formation of a trimeric and a tertrameric assembly, in $[\{Re_6Se_8(PEt_3)_5\}_3(tpt)][SbF_6]_6$ (**165**; Fig. 41a) and in $[\{Re_6Se_8(PEt_3)_5\}_4(TPyP)][SbF_6]_8$ (**166**; Fig. 41b), respectively [163]. These also served to trap dicationic metal ions, like Co^{2+}, Ni^{2+}, Cu^{2+} and Zn^{2+} through a step-wise method [164]. Although no crystal structures could be obtained, CV measurements showed that the reactions were successful, as insertion of these cations caused higher current densities as compared to the non-metalated ones; this was discussed in terms of possible applications of such ligand-functionalized molecular cluster assemblies in fields such as electrocatalysis or sensing. Besides the utilization of mono- or di-solvated clusters as starting materials, the *hexa*-solvated $[Re_6Se_8(MeCN)_6]$ cluster was also prepared [160], and functionalized step-wise by replacement of the solvent molecules with even larger ligands. By using dendritic ligands, the loosely ligated solvent molecules of $[Re_6Se_8(MeCN)_6]^{2+}$ could be fully replaced, which leads to the formation of a series of dendrimers [165]. The identity of the products was confirmed by NMR and ESI-MS. Refluxing a mixture of $[Re_6Se_8(MeCN)_6]^{2+}$ with six equivalents of mono-substituted $[Re_6Se_8(MeCN)_5L]^{2+}$ (L = DPE and BPE) in chlorobenzene under inert gas afforded dendrimers with a central $[Re_6Se_8]^{2+}$ cation. By means of the bidentate N-containing ligands, this central cluster is bridged to six $[Re_6Se_8(MeCN)_5]^{2+}$ units *via* Re–L–Re connections to form $[(Re_6Se_8)\{Re_6Se_8(PEt_3)_5(DPE)\}_6]^{14+}$ (in **167**) and $[(Re_6Se_8)\{Re_6Se_8(PEt_3)_5(BPE)\}_6]^{14+}$ (in **168**) [166]. The electrochemical studies showed that the use of a ligand with a conjugated π-electron system led to strong coupled interactions between the core cluster and the terminal clusters. The fact that the interaction became weaker when using non-conjugated ligands suggested dispersive interactions between the π-electron systems of the conjugated ligands. In addition, this provided a route to related compounds using mixed $[Re_6Se_8(MeCN)_{6-n}L_n]^{2+}$ clusters as starting compounds [167].

Given the vacant N atom sites at the ligands of these multi-functionalized $[Re_8Se_6]^{2+}$ molecules, the assemblies are good candidates for further expansion into polymers. Indeed, the reaction of bpy-functionalized $[Re_6Se_8(PPh_3)_4(bpy)_2]$ with $[Cd(NO_3)_2]\bullet 4H_2O$ in a 1:1 ratio led to the crystallization of a one-dimensional polymer of corner-sharing squares, in which the octahedrally coordinated Cd^{2+} cations are bonded to four bpy ligands from the cluster units and two $[NO_3]^-$ anions, formulated as 1D-$\{[Cd(NO_3)_2\{Re_6Se_8(PPh_3)_4(bpy)_2\}_2]^{4+}\}$ (in **169**). A huge excess (over 1000 times) of $[Cd(NO_3)_2]\bullet 4H_2O$ in the reaction yields a different one-dimensional strand with the formula of 1D-$\{[Cd(NO_3)_3\{Re_6Se_8(PPh_3)_4(bpy)_2\}]^+\}$ (in **170**), in which the Cd^{2+}

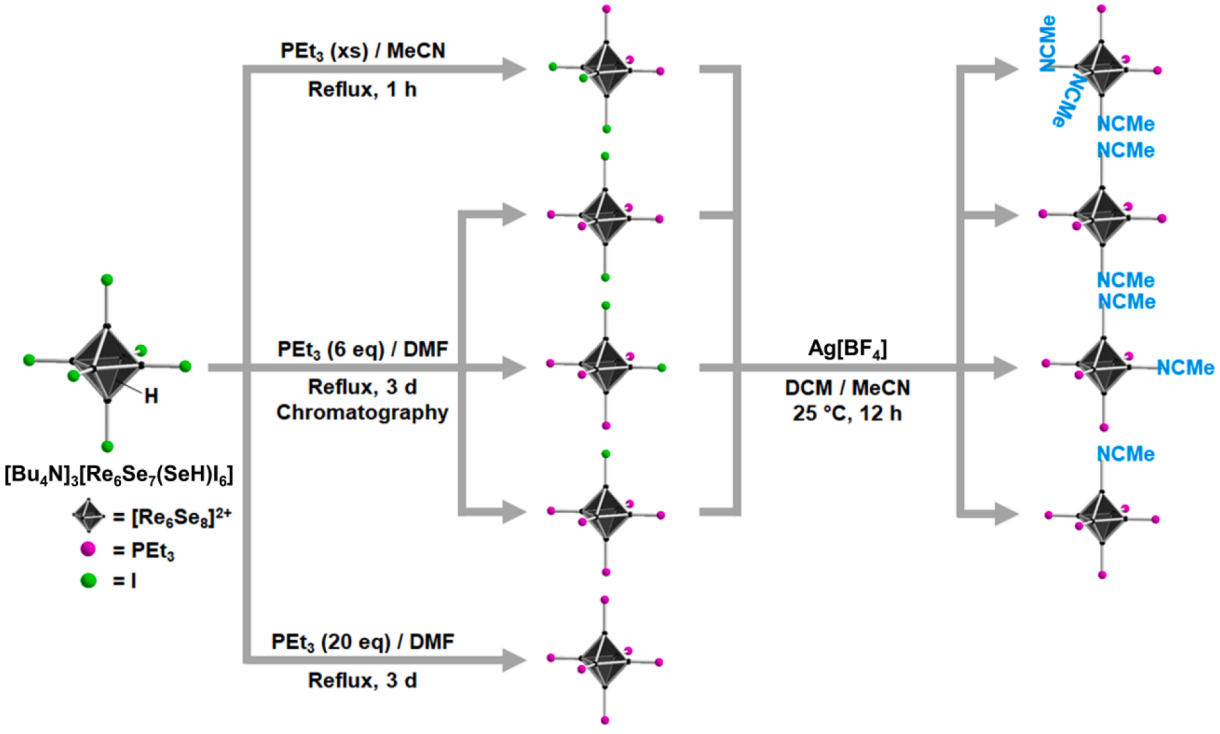

Scheme 4. Summary of substitution reactions of $[Re_6Se_7(SeH)I_6]^{3-}$ to form $[Re_6Se_8(PEt_3)_n(MeCN)_n]^{2+}$ (n 1–3).

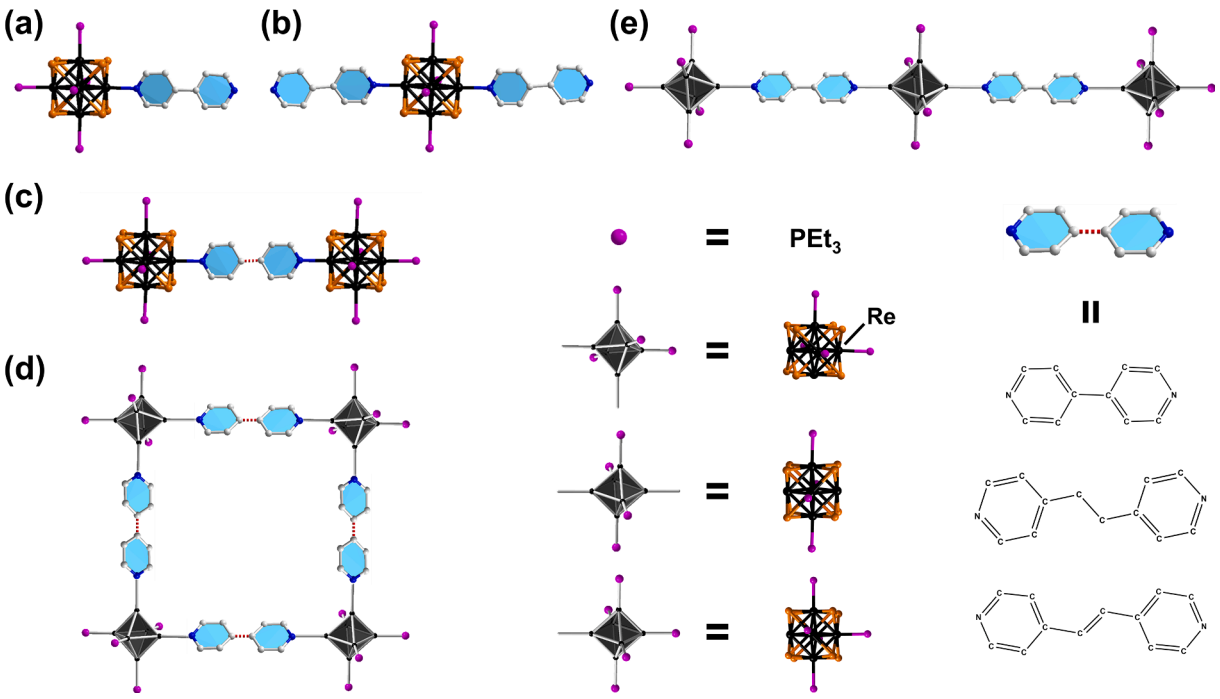

Fig. 40. Structures of bpy-decorated and bpy-linked $\{Re_6Se_8\}$ cluster units. (a) Monosubstituted $[Re_6Se_8(PEt_3)_5(bpy)]^{2+}$. (b) Disubstituted *trans*-$[Re_6Se_8(PEt_3)_4(bpy)_2]^{2+}$. (c) Ligand-bridged cluster dimer $[\{Re_6Se_8(PEt_3)_5\}_2(L)]^{4+}$. (d) Square planar cluster tetramer *cyclo*-$[\{Re_6Se_8(PEt_3)_4(L)\}_4]^{8+}$. The bidentate ligands L in the latter two cases are bpy, DPE and BPE, respectively. (e) Cluster assembly of $[\{Re_6Se_8(PEt_3)_5(bpy)\}_2\{Re_6Se_8(PEt_3)_4(bpy)_2\}]^{6+}$. H atoms are omitted for clarity.

cations are inversely coordinated—by two bpy ligands and four $[NO_3]$ anions [168]. It should be noted that adding an excess of $[Cd(NO_3)_2]\bullet 4H_2O$ in a MeOH solution of the **169** cluster assembly would also allow its direct transformation to compound **170**.

In similar ways, three one-dimensional polymers featuring the $[Re_6Se_8(PPh)_4(bpy)_2]^{2+}$ cluster nodes connected by the transition metal cations Cd^{2+}, Co^{2+}, or Zn^{2+} were also generated. The corresponding products, 1D-$\{[M(NO_3)_3\{Re_6Se_8(PEt_3)_4(bpy)_2\}]^+\}$ (M = Cd, in **171a**; M = Co, in **171b**; M = Zn, in **171c**), may serve as platforms for adsorption or activation reactions for small molecules, since the $[NO_3]$ anions can be easily removed to create free vacancies for reactivity at the Cd^{2+} sites [169].

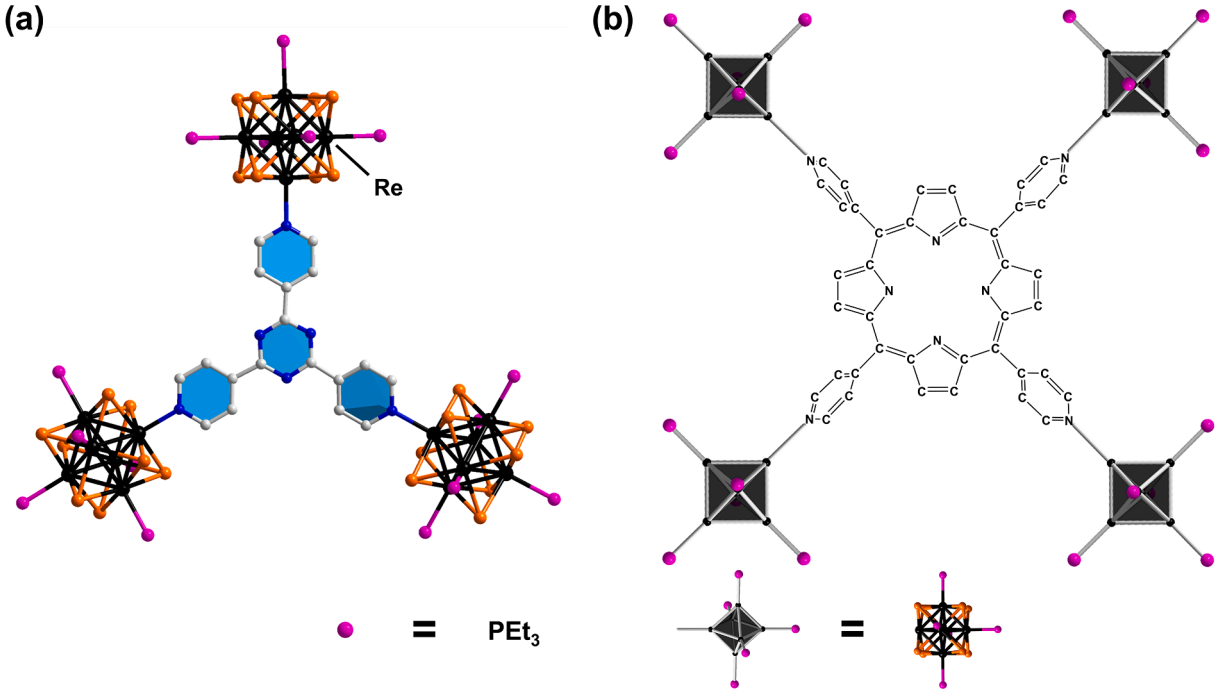

Fig. 41. Structures of cluster assemblies realized with multidentate ligands. (a) Trimer $[\{Re_6Se_8(PEt_3)_5\}_3(tpt)]^{6+}$. (b) Tetramer $[\{Re_6Se_8(PEt_3)_5\}_4(TPyP)]^{8+}$. H atoms are omitted for clarity.

More recently, the reaction of $[Re_6Se_8(CN)_6]^{2+}$ with Gd^{3+} and furan-2,5-dicarboxylate (fdc) afforded the formation of a three-dimensional framework with water molecules hosted in large pores, 3D-[{Gd$(H_2O)_3$}$_2$(fdc)$Re_6Se_8(CN)_6$]•xH_2O (**172**) [170]. The H_2O solvent molecules could be removed smoothly under vacuum to produce a porous solid, and the obtained compound showed an impressive uptake capacity and selectivity towards CO_2 at room temperature.

In addition, the redox-activity of the {Re_6Se_8} unit makes this species a potential candidate for the detection of Br_2 and N_2H_4 by color change and fluorescence response in the red region of the visible spectrum.

All ligand-functionalized and ligand-bridged octahedral transition metal chalcogenide cluster-based compounds presented in Section 5.1 are summarized in Table 8.

5.2. Ligand-functionalized and ligand-bridged {Co_6Se_8} cluster-based compounds

In comparison to the complicated procedure that was followed at the synthesis of $[Re_6Se_8(PEt_3)_{6-n}(MeCN)_n]^{2+}$, both a mild preparation method and good yields were reported for the generation of $[Co_6Se_8(PEt_3)_{6-n}(CO)_n]$ (n = 0–3; **173**). This species therefore provides better opportunities for further structural functionalization. A mixture of the clusters with varying n is obtained by treatment of $[Co_2(CO)_8]$, Se, and PEt_3 in toluene at 110 °C under inert gas (Scheme 5); the species can be obtained in pure form by fractional crystallization. Exchanging Se with S or Te led to the formation of a related series of compounds, $[Co_6S_8(PEt_3)_{6-n}(CO)_n]$ and $[Co_6Te_8(PEt_3)_{6-n}(CO)_n]$ (n = 0–3) [155,171,172].

Due to the CO ligands being easily removable *via* irradiation (Fig. 42a 42b), a wide variety of newly functionalized compounds became accessible this way. For instance, the reaction of $[Co_6Se_8(PEt_3)_5(CO)]$ with the ditopic and dianionic ligand molecules 1,4-phenylene diisocyanide (PDI) in THF under UV light irradiation resulted in a neutral ligand-bridged redox-active dimeric cluster $[Co_{12}Se_{16}(PEt_3)_{10}(PDI)]$ (**174**; Fig. 42c) [155]. The doubly-oxidized derivative, $[Co_{12}Se_{16}(PEt_3)_{10}(PDI)]^{2+}$ (in **175**), could also be isolated with the aid of $[PF_6]^-$ as anions. The fine control of the molar ratios of $[Co_6Se_8(PEt_3)_5(CO)]$ and PDI also enabled the formation of the mono-substituted species $[Co_6Se_8(PEt_3)_5(PDI)]$ [155].

Besides the variation of the molar ratios of the reactants, the use of multi-substituted clusters is another important parameter to expand the ditopic ligand-bridged structures. The reaction of two equivalents of PDI ligands with one equivalent of *trans*-$[Co_6Se_8(PEt_3)_4(CO)_2]$ yielded the PDI-capped species *trans*-$[Co_6Se_8(PEt_3)_4(PDI)_2]$ (**176**), which can then be used as a bridging unit between two coordinatively unsaturated cluster fragments, $[Co_6Se_8(PEt_3)_5(CO)]$, to form the linear trimeric assembly [{$Co_6Se_8(PEt_3)_5$}(PDI){$Co_6Se_8(PEt_3)_4$}(PDI){$Co_6Se_8(PEt_3)_5$}] = $[Co_{18}Se_{24}(PEt_3)_{14}(PDI)_2]$ (**177**) [155].

Apart from ligated dimers and trimer, the $[Co_6Se_8\{C(H)SiMe_3\}(PEt_3)_5]^+$ fragment can also be used to build a covalently linked dimer by directly fusing two monomers. The salt $[Co_6Se_8\{C(H)SiMe_3\}(PEt_3)_5][PF_6]$ (**178**) was first isolated by reacting the carbene source (trimethylsilyl)diazomethane with the mono-substituted cluster from $[Co_6Se_8(PEt_3)_5(CO)][PF_6]$ under UV irradiation at 70 °C for 5 h [173]. Upon cleaving the carbene from the monomeric unit, a fusion to form an anionic cluster dimer $[Co_{12}Se_{16}(PEt_3)_{10}]^{2+}$ (in **179**), *via* sharing an inorganic $[Co_2Se_2]$ square, can be observed *in situ* (Fig. 42d). Reacting the $[Co_{12}Se_{16}(PEt_3)_{10}]^{2+}$ cations with cobaltocene in DCM or toluene allows for the formation of the neutral $[Co_{12}Se_{16}(PEt_3)_{10}]$ (**180**) cluster dimer and the monocationic version of it, $[Co_{12}Se_{16}(PEt_3)_{10}]^+$ (in **181**) using $[PF_6]^-$ as anions, respectively. The isolation of both compounds with varied charge is attributed to the pronounced redox properties of the {Co_6Se_8} parent cluster. According to CV measurements, and as expected, the intercluster coupling within the dimers is larger than that of the ligand-bridged dimers [173].

Further investigations of the removal and replacement of carbene molecules by pyridine, 2,6-dimethylphenyl isocyanide, and cyanide ligands were also reported. In addition to $[Co_6Se_8(PEt_3)_5(CO)]$, the disubstituted $[Co_6Se_8(PEt_3)_4(CO)_2]$ (Fig. 43a) was treated with different amounts of trimethylsilyl diazomethane, which afforded derivatives $[Co_6Se_8\{C(H)SiMe_3\}(PEt_3)_4(CO)]$ (**182**; Fig. 43b), and $[Co_6Se_8\{C(H)SiMe_3\}_2(PEt_3)_4]$ (**183**; Fig. 43c) [174]. The reaction of **182** in pyridine without light illumination led to the formation of $[Co_6Se_8(py)(PEt_3)_4(CO)]$ (**184**; Fig. 43d) [174]. Upon addition of benzene to the same reaction mixture, **182** dissolved completely; addition of a trace amount of tetracyanoquinodimethane (TCNQ) in THF then triggered the fusion of the clusters by losing the carbene ligands, which yielded $[Co_{12}Se_{16}(PEt_3)_8(CO)_2][TCNQ]$ (**185**, Fig. 43e) [174]. In contrast to the either neutral or negatively charged dimeric molecules clusters discussed above, the cluster dimer is positively charged in **185**. Nevertheless, the charge as well as the decoration with ligands does not impact the general stability of the cluster, and also the effect on the electronic

Table 8
Summary of the ligand-functionalized and ligand-bridged compounds presented in Section 5.1.

Compound	Dimensionality	Reactants	Temperature (°C)	Ref.
$[Re_6Se_8(PEt_3)_5(bpy)][SbF_6]_2$ (**156**)	0D	$[Re_6Se_8(PEt_3)_5(MeCN)][SbF_6]_2$, bpy, chlorobenzene, Et_2O, DCM	reflux	[161]
$[Re_6Se_8(PEt_3)_4(bpy)_2][SbF_6]_2$ (**157**)	0D	$[Re_6Se_8(PEt_3)_4(MeCN)_2][SbF_6]_2$, bpy, chlorobenzene, Et_2O, DCM	reflux	[161]
[{$Re_6Se_8(PEt_3)_5$}$_2$(bpy)][SbF_6]$_4$ (**158**)	0D	$[Re_6Se_8(PEt_3)_5(MeCN)][SbF_6]_2$, DCM, bpy, chlorobenzene, MeCN, Et_2O	reflux	[161]
[{$Re_6Se_8(PEt_3)_5$}$_2$(DPE)][SbF_6]$_4$ (**159**)	0D	$[Re_6Se_8(PEt_3)_5(MeCN)][SbF_6]_2$, DCM, DPE, chlorobenzene, MeCN, PhH	reflux	[161]
[{$Re_6Se_8(PEt_3)_5$}$_2$(BPE)][SbF_6]$_4$ (**160**)	0D	$[Re_6Se_8(PEt_3)_5(MeCN)][SbF_6]_2$, DCM, BPE, chlorobenzene, Et_2O, MeCN	reflux	[161]
cyclo-[$Re_6Se_8(PEt_3)_4(bpy)$]$_4$[SbF_6]$_8$ (**161**)	0D	*cis*-$[Re_6Se_8(PEt_3)_4(MeCN)_2][SbF_6]_2$, bpy, chlorobenzene, Et_2O	reflux	[162]
cyclo-[$Re_6Se_8(PEt_3)_4$(DPE)]$_4$[SbF_6]$_8$ (**162**)	0D	*cis*-$[Re_6Se_8(PEt_3)_4(MeCN)_2][SbF_6]_2$, DPE, chlorobenzene, Et_2O	reflux	[162]
cyclo-[$Re_6Se_8(PEt_3)_4$(BPE)]$_4$[SbF_6]$_8$ (**163**)	0D	*cis*-$[Re_6Se_8(PEt_3)_4(MeCN)_2][SbF_6]_2$, BPE, chlorobenzene, Et_2O	reflux	[162]
$[Re_{18}Se_{24}(PEt_3)_{14}(bpy)_2][SbF_6]_6$ (**164**)	0D	*trans*-$[Re_6Se_8(PEt_3)_4(MeCN)_2][SbF_6]_2$, $[Re_6Se_8(PEt_3)_5(bpy)_2][SbF_6]_2$, chlorobenzene, Et_2O, DCM, MeCN	reflux	[161]
[{$Re_6Se_8(PEt_3)_5$}$_3$(tpt)][SbF_6]$_6$ (**165**)	0D	$[Re_6Se_8(PEt_3)_5(MeCN)][SbF_6]_2$, tpt, chlorobenzene	reflux	[163]
[{$Re_6Se_8(PEt_3)_5$}$_4$(TPyP)][SbF_6]$_6$ (**166**)	0D	$[Re_6Se_8(PEt_3)_5(MeCN)][SbF_6]_2$, TPyP, chlorobenzene	reflux	[163]
[(Re_6Se_8){$Re_6Se_8(PEt_3)_5$(DPE)}$_6$] [SbF_6]$_{14}$ (**167**)	0D	$[Re_6Se_8(MeCN)_6][SbF_6]_2$, {$[Re_6Se_8(PEt_3)_5]$(DPE)}$[SbF_6]_2$, chlorobenzene	reflux	[166]
[(Re_6Se_8){$Re_6Se_8(PEt_3)_5$(BPE)}$_6$][SbF_6]$_{14}$ (**168**)	0D	$[Re_6Se_8(MeCN)_6][SbF_6]_2$, {$[Re_6Se_8(PEt_3)_5]$(BPE)}$[SbF_6]_2$, chlorobenzene	reflux	[166]
[$Cd(NO_3)_2$\{$e_6Se_8(PPh_3)_4(bpy)_2$\}$_2$] [SbF_6]$_4$•21MeOH•21DCM (**169**)	1D	$[Re_6Se_8(PPh_3)_4(bpy)_2][SbF_6]_2$, $Cd(NO_3)_2{\cdot}4H_2O$, MeOH, DCM, Et_2O	rt	[168]
[$Cd(NO_3)_3$\{$Re_6Se_8(PPh_3)_4(bpy)_2$\}](NO_3)• 2MeOH•DCM (**170**)	1D	$[Re_6Se_8(PPh_3)_4(bpy)_2][SbF_6]_2$, $Cd(NO_3)_2{\cdot}4H_2O$, MeOH, DCM, Et_2O	rt	[168]
[$Cd(NO_3)_3$\{$Re_6Se_8(PEt_3)_4(bpy)_2$\}][SbF_6] (**171a**)	1D	$[Re_6Se_8(PEt_3)_4(bpy)_4][SbF_6]_2$, $Cd(NO_3)_2$, DCM, MeOH, Et_2O	rt	[169]
[$Co(NO_3)_3$\{$Re_6Se_8(PEt_3)_4(bpy)$\}$_2$][SbF_6]•2MeOH (**171b**)	1D	$[Re_6Se_8(PEt_3)_4(bpy)_4][SbF_6]_2$, $Co(NO_3)_2$, DCM, MeOH, Et_2O	rt	[169]
[$Zn(NO_3)_3$\{$Re_6Se_8(PEt_3)_4(bpy)$\}$_2$][SbF_6] (**171c**)	1D	$[Re_6Se_8(PEt_3)_4(bpy)_4][SbF_6]_2$, $Zn(NO_3)_2$, DCM, MeOH, Et_2O	rt	[169]
[{$Gd(H_2O)_3$}$_2$(fdc)$Re_6Se_8(CN)_6$] (**172**)	3D	$K_4[Re_6Se_8(CN)_6]$•nH_2O, $Gd(NO_3)_3$, fdc, KOH, H_2O,	rt	[170]

$$[Co_2(CO)_8] \quad + \quad PEt_3 \quad + \quad Se \xrightarrow[110\ °C]{\text{toluene}} [Co_6Se_8(PEt_3)_{8-n}(CO)_n] \quad (n = 0 - 3)$$

Scheme 5. Illustration of the access of cluster units with the general formula $[Co_6Se_8(PEt_3)_{6-n}(CO)_n]$ (n 0–3) terminated by CO and PEt_3 molecules.

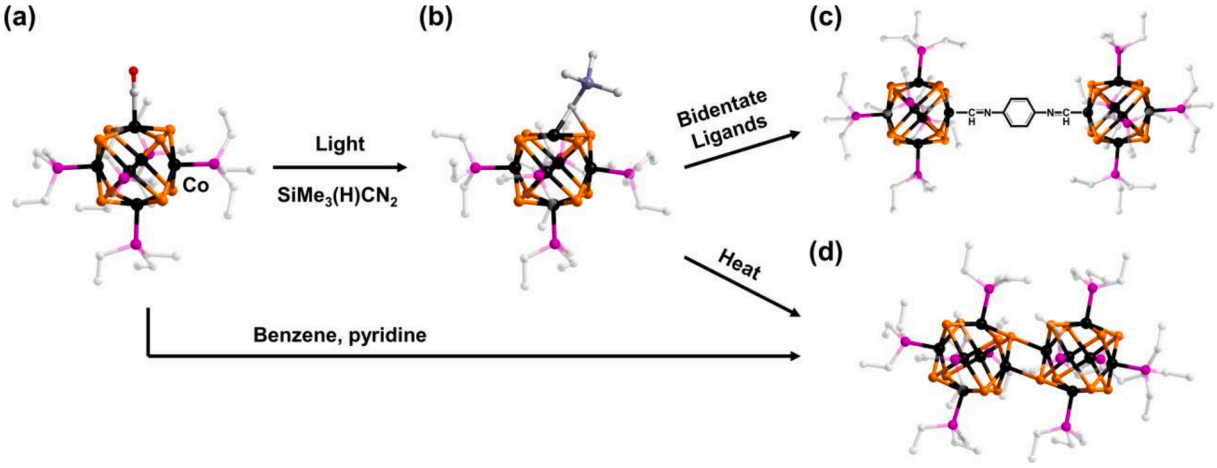

Fig. 42. Reaction path for the derivatization of $[Co_6Se_8(PEt_3)_5(CO)]$. (a) Structure of the starting compound. (b) Reaction with $SiMe_3(H)CN_2$ under treatment with light, yielding monosubstituted $[Co_6Se_8\{C(H)SiMe_3\}(PEt_3)_5]^+$. (c) Reaction with bidentate ligands to form $[Co_{12}Se_{16}(PDI)(PEt_3)_{10}]^{2+}$. (d) Subsequent heating of isolated $[Co_6Se_8\{C(H)SiMe_3\}(PEt_3)_5]^+$ to form the fused cluster dimers $[Co_{12}Se_{16}(PEt_3)_{10}]^{q+}$ (q 2, 1 and 0). H atoms are omitted for clarity.

properties of the cluster core is small, as confirmed by CV measurements.

Considering the carbonyl ligand substitution chemistry, further experiments were carried out under UV light. For instance, the reaction of *trans*-$[Co_{12}Se_{16}(PEt_3)_8(CO)_2][PF_6]$ (**186**) with two equivalents of $PEt_2(p\text{-}C_6H_4SMe)$ in THF led to the generation of *trans*-$[Co_{12}Se_{16}\{PEt_2(p\text{-}C_6H_4SMe)\}_2(PEt_3)_8]^+$ in the corresponding $[PF_6]^-$ salt (**187**, Fig. 43f) [174]. The respective *cis* isomer, *cis*-$[Co_{12}Se_{16}\{PEt_2(p\text{-}C_6H_4SMe)\}_2(PEt_3)_8]^+$ (in **188**), could also be isolated through another step-wise route. In terms of the mechanism, it was suggested that *cis*-$[Co_6Se_8(PEt)_4(CO)_2]$ (Fig. 43g) was functionalized with $PEt_2(p\text{-}C_6H_4SMe)$ (Fig. 43h) in a first step, while further removal of carbonyl ligands and the formation of Se–Co bonds, allowed for the formation of *cis*-$[Co_{12}Se_{16}\{PEt_2(p\text{-}C_6H_4SMe)\}_2(PEt_3)_8][PF_6]$ (Fig. 43i). The redox activity of the latter two is almost identical, which again indicates that capping the open cluster faces with ligands has little influence on the electronic properties of the cluster core [174].

Apart from the rational design of cluster oligomers, recent efforts have also been dedicated to obtaining extended solids. The functional ligand is thus supposed to possess a secondary coordination position. With the use of *trans*-$[Co_6Se_8(PEt_3)_4(PDI)_2]$ as bridging moieties and anionic $[Mo_6O_{19}]^2$ in an electro-crystallization cell, the bidentate PDI ligands serve to link the clusters to form polymer strands, which further interweave to give two-dimensional sheets of $\{[Co_6Se_8(PEt_3)_4](PDI)_{1.64}\}_2[Mo_6O_{19}]$ (**189**) [175]. Besides the use of bis-isocyanide functionalized clusters as nodes, the carboxylic acid-decorated $[Co_6Se_8\{PEt_2(4\text{-}C_6H_4COOH)\}_6]$ (**190**; Fig. 44b) was also obtained and is regarded as a suitable candidate for the formation of framework compounds [176]. The reactions of **190** with Zn^{2+} in DMF/MeOH and DMF/EtOH afforded a 3D solid and a 2D layer, with the formula 3D-$[Zn_3\{Co_6Se_8\{PEt_2(4\text{-}C_6H_4COOH)\}_3\}]\bullet 2MeOH$ (**191**) and 2D-$[Zn_3\{Co_6Se_8\{PEt_2(4\text{-}C_6H_4COOH)\}_6\}]$ (**192**), respectively (Fig. 44a, 44c). It has to be noted, that the latter can be further exfoliated to form soluble ultrathin nanosheets that display excellent redox-activity (Fig. 44d).

All ligand-functionalized and ligand-bridged octahedral transition metal chalcogenide cluster-based compounds presented in Section 5.2 are summarized in Table 9.

5.3. Ligand-functionalized and ligand-bridged $\{Mo_3Ch_x\}$, $\{Fe_4S_4\}$, ans $\{Co_4S_4\}$ cluster-based compounds (x = 4, 7)

Transition metal dichalcogenides (TMDCs) with layered structures, such as MoS_2, are investigated with respect to applications like electrocatalysis and photocatalysis [177,178]. As a fragment of the two-dimensional MoS_2 surface, $[Mo_3S_{13}]^2$ cluster molecules not only mimic the catalytic properties of TMDCs, but also are easily prepared and modified. They also possess good solubility making it an ideal molecular model for structure and material design. Upon decorating this type of clusters with surface ligands, further interesting properties can be introduced. Scheme 6 shows one possible general approach for this [179].

In a first step, the reaction of ammonium molybdate tetrahydrate and ammonium polysulfide at 90 °C for 20 h allows for the formation of $(NH_4)_2[Mo_3S_{13}]$, comprising a $[Mo_3S_7]^{4+}$ core and three S_2^2 disulfide ligands. In a second step, $(NH_4)_2[Mo_3S_{13}]$ is treated with an HBr solution to afford $[Mo_3S_7Br_6]^2$. Here, the three S_2^2 ligands were replaced by six Br anions. In a last step, dithiolene or oxalate ligands are used to replace the bromide anions [179,180]. The structural expansion and properties of clusters of the type $[Mo_3S_7R_3]^2$ (Fig. 45a) strongly depend on the ligands employed (Fig. 45b). Herein, we give a brief introduction to such functionalized sulfido molybdate clusters and to the polymers derived thereof.

The treatment of $[Mo_3S_7Br_6]^2$ and $[Zn(dmit)_2]^2$ (**193**; dmit = 1,3-dithia-2-thione-4,5-dithiolate) in acetonitrile allows for the formation of $[Mo_3S_7(dmit)_3]^2$ dianions. The ligand-functionalized cluster forms a dimeric assembly by interaction of the sulfur atoms from the $[Mo_3S_7]^{4+}$ core with the dmit ligands. Further interactions between the dmit ligands led to the formation of a chain [181]. These interactions within the molecular units cause a significant electron delocalization and make this compound a "single-component molecular conductor". Reactions of $[Mo_3S_7Br_6]^2$ with other dithiolates, bis(trifluoromethyl)-1,2-dithiolate (tfd), 1,2-benzenedithiolate (BDT), 1,3-dithia-2-one-4,5-dithiolate (dmid), and 1,3-dithia-2-thione-4,5-diselenolate (dsit), as functional ligands led to the formation of $[Mo_3S_7(tfd)_3]^2$ (in **194**), $[Mo_3S_7(BDT)_3]^2$ (in **195**), $[Mo_3S_7(dmid)_3]^2$ (in **196**), and $[Mo_3S_7(dsit)_3]^2$ (in **197**) [182]. Again, the highest occupied molecular orbitals (HOMOs) in these four anions are delocalized over the inorganic $[Mo_3S_7]^{4+}$ cluster cores and

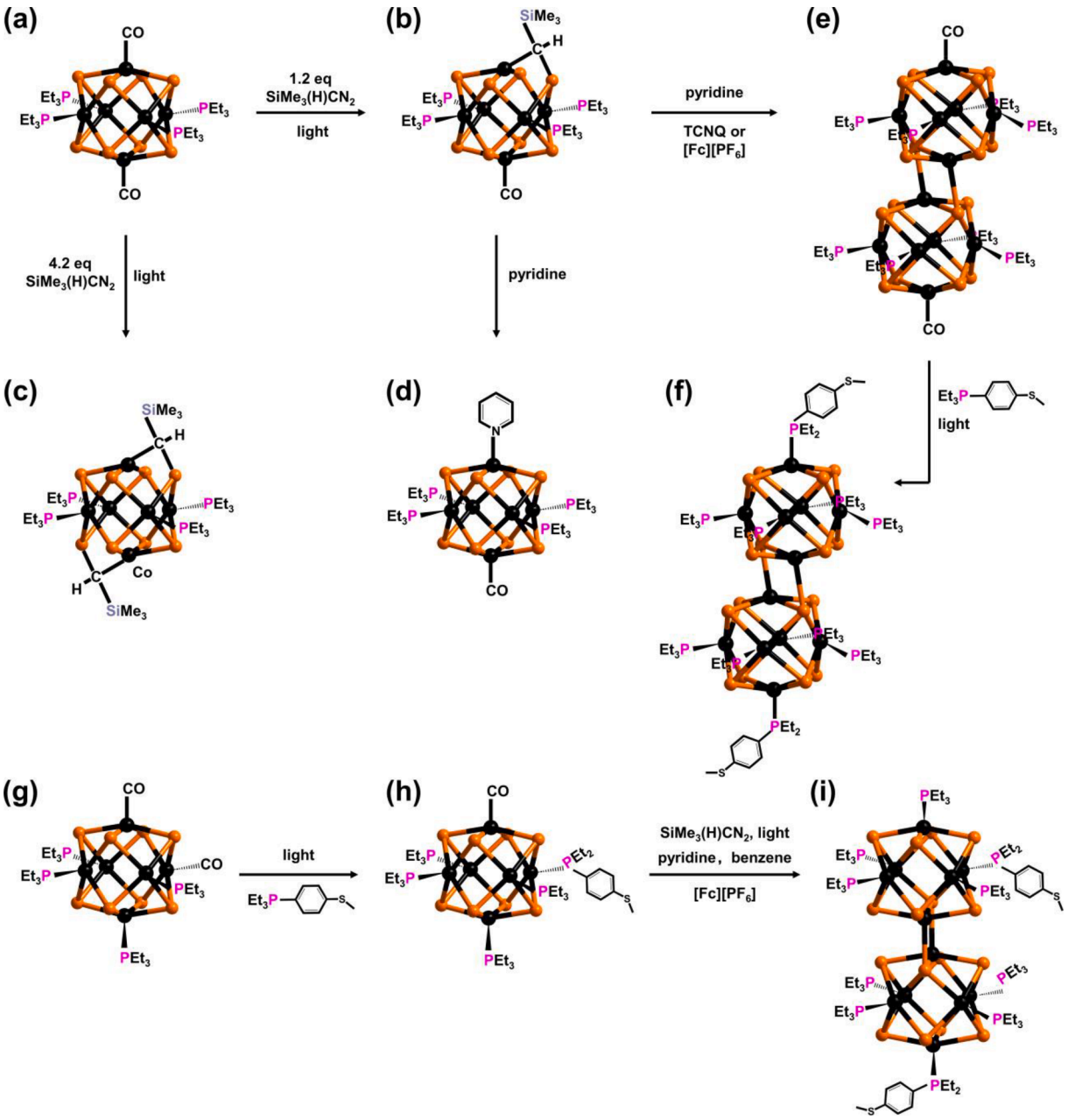

Fig. 43. Reactivity of clusters based on ligand-decorated $\{Co_6Se_8\}$ moieties. (a) Structure of the starting compound *trans*-$[Co_6Se_8(PEt_3)_4(CO)_2]$. (b) Reaction of *trans*-$[Co_6Se_8(PEt_3)_4(CO)_2]$ with 1.2 equivalents of $SiMe_3(H)CN_2$ yielding $[Co_6Se_8(PEt_3)_4\{C(H)SiMe_3\}(CO)]$. (c) Reaction of *trans*-$[Co_6Se_8(PEt_3)_4(CO)_2]$ with 4.2 equivalents of $SiMe_3(H)CN_2$ yielding *trans*-$[Co_6Se_8(PEt_3)_4\{C(H)SiMe_3\}_2]$. (d) Pyridyl-functionalized $[Co_6Se_8(py)(CO)(PEt_3)_4]$. (e) Subsequent removal of carbene from $[Co_6Se_8(PEt_3)_8(CO)_2]$ affording dimeric $[Co_{12}Se_{16}(PEt_3)_8(CO)_2]^+$. (f) Further substitution of CO to form [*trans*-$Co_{12}Se_{16}(PEt_2(p\text{-}C_6H_4SMe))_2(PEt_3)_8]^+$. (g) Structure of the starting compound *cis*-$[Co_6Se_8(PEt_3)_4(CO)_2]$. (h) Reaction of *cis*-$[Co_6Se_8(PEt_3)_4(CO)_2]$ with $PEt_2(p\text{-}C_6H_4SMe)$ to form *cis*-$[Co_6Se_8\{PEt_2(^pC_6H_4SMe)\}(CO)(PEt_3)_4]$. (i) Further fusion affording *cis*-$[Co_{12}Se_{16}(PEt_2(p\text{-}C_6H_4SMe))_2(PEt_3)_8]^+$. H atoms are omitted for clarity.

the surface-capping ligands. The contribution of the respective ligands to the HOMO, ranging from 61.67% in **195** to 65.16% in **194** to 77.8% in **196** to 82.07% in **197**, allows for tuning the electronic and magnetic properties over the four ligand-functionalized compounds. Similar ditopic ligands, such as 1,2,5-thiadizole-3,4-dithiol (tdas) and maleonitriledithiolate (mnt) are also capable of decorating the surface of $\{Mo_3S_7\}$ cluster cores. This way, $(N^nBu_4)_2[Mo_3S_7(tdas)_3]$ (**198**) and $(N^nEt_4)_2[Mo_3S_7(mnt)_3]$ (**199**) can be obtained.

Besides the functionalization with dithiolate ligands, the use of oxalate or dicarboxylic ligands enabled the isolation of a series of similar compounds. The reaction of 1D-$\{[Mo_3S_7Br_4]^2\}$, instead of 0D-$[Mo_3S_{13}]^2$, with $K_2C_2O_4$ (K_2ox) in water at 5 °C afforded crystals of $K_2[Mo_3S_7(ox)_3]$ (**200**) [180]. Analogous salts of cluster anions $[Mo_3Se_7(ox)_3]^2$ (in **201**) and $[W_3S_7(ox)_3]^2$ (in **202**) were also isolable by varying the compositions of the starting materials [183]. With the use of more complex dicarboxylic ligands, like mercaptosuccinic acid (H_3msa), the anion $[Mo_3S_7(Hmsa)_3]^2$ (in **203**) with accessible oxygen donor atoms on the ligands can be formed [179]. Smaller clusters $[M_3S_4]^{4+}$ (M = W, Mo) were also decorated with nitrilotriacetic ligands (H_3nta) [184].

Taking advantage of the accessible oxygen donor atoms of functional ligands, such clusters are considered as perfect building units for the design of cluster-based molecules or polymer compounds. The reactions of **202** with La^{3+} or Ce^{3+} cations in water afforded 2D-polymeric cationic species $\{[La(H_2O)_6]_3[W_3S_7(ox)_3]_4\}^+$ (in **204**) and $\{[Ce(H_2O)_6]_3[W_3S_7(ox)_3]_4\}^+$ (in **205**) [185], respectively. Notably, a series

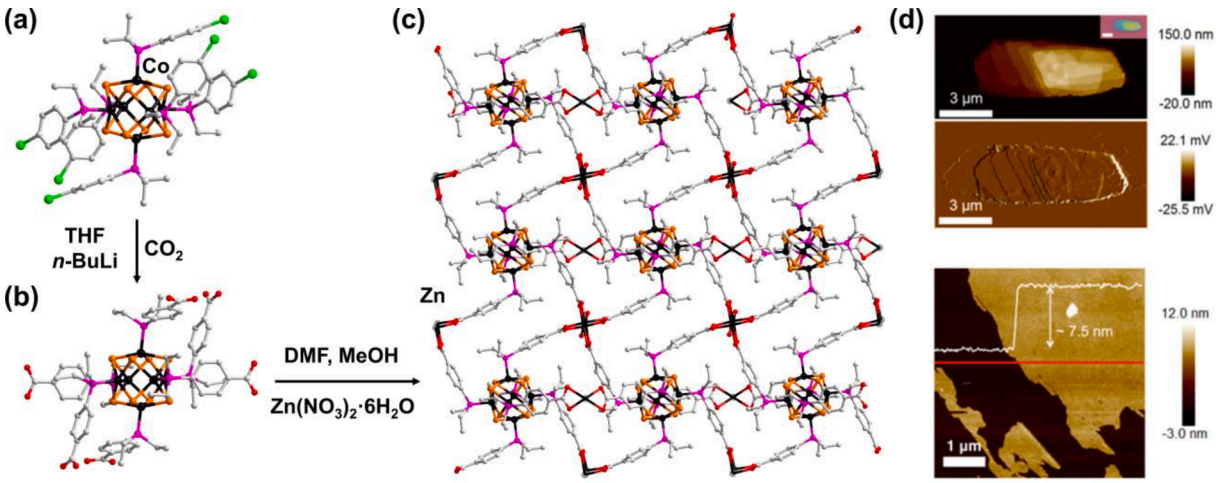

Fig. 44. Reactivity of $[Co_6Se_8\{PEt_2(4\text{-}C_6H_4Br)\}_6]$. (a) Structure of the starting species. (b) Structure of the species $[Co_6Se_8\{PEt_2(4\text{-}C_6H_4COOH)\}_6]$ obtained by reaction with *n*-BuLi and CO_2 in THF. (c) Formation of the Zn^{2+}-bridged two-dimensional network $\{Zn_3[Co_6Se_8(PEt_2\{4\text{-}C_6H_4COOH\}_3)\}$. (d) Results of atomic force microscopy (AFM) images of the exfoliated nanosheet formed from the latter, reproduced from Ref. [176] with permission from American Chemical Society. H atoms are omitted for clarity.

Table 9
Summary of the ligand-functionalized and ligand-bridged compounds presented in Section 5.2.

Compound	Dimensionality	Reactants	Temperature (°C)	Ref.
$[Co_6Se_8(PEt_3)_{6-n}(CO)_n]$ (**173**)	0D	$[Co_6S_8(PEt_3)_6]$, Se, CO, toluene	100	[171]
$[Co_{12}Se_{16}(PEt_3)_{10}(PDI)]$ (**174**)	0D	$[Co_6Se_8(PEt_3)_5(CO)]$, PDI, THF	rt (with UV lamp irradiation)	[155]
$[Co_{12}Se_{16}(PEt_3)_{10}(PDI)][PF_6]_2$ (**175**)	0D	$[Co_6Se_8(PEt_3)_5(CO)][PF_6]$, PDI, THF	rt (with UV lamp irradiation)	[155]
$[Co_6Se_8(PEt_3)_4(PDI)_2]$ (**176**)	0D	$[Co_6Se_8(PEt_3)_4(CO)_2]$, PDI, THF	rt (with UV lamp irradiation)	[155]
$[Co_{18}Se_{24}(PEt_3)_{14}(PDI)_2]$ (**177**)	0D	$[Co_6Se_8(PEt_3)_4(PDI)_2]$, $[Co_6Se_8(PEt_3)_5(CO)]$, THF	rt	[155]
$[Co_6Se_8\{C(H)SiMe_3\}(PEt_3)_5][PF_6]$ (**178**)	0D	$[Co_6Se_8(PEt_3)_5(CO)][PF_6]$, THF, TMSD	rt (with UV lamp irradiation)	[173]
$[Co_{12}Se_{16}(PEt_3)_{10}][PF_6]_2$ (**179**)	0D	$[Co_6Se_8(PEt_3)_5(CO)][PF_6]$, MeCN	70	[173]
$[Co_{12}Se_{16}(PEt_3)_{10}]$ (**180**)	0D	$[Co_{12}Se_{16}(PEt_3)_{10}][PF_6]_2$, $Co(Cp)_2$, toluene, MeCN	rt	[173]
$[Co_{12}Se_{16}(PEt_3)_{10}][PF_6]$ (**181**)	0D	$[Co_{12}Se_{16}(PEt_3)_{10}][PF_6]_2$, $Co(Cp)_2$, DCM, toluene, pentane	rt	[173]
$[Co_6Se_8\{C(H)SiMe_3\}(PEt_3)_4(CO)]$ (**182**)	0D	$[Co_6Se_8(PEt_3)_4(CO)_2]$, THF, TMSD, hexane	0 (with UV lamp irradiation)	[174]
$[Co_6Se_8\{C(H)SiMe_3\}_2(PEt_3)_4]$ (**183**)	0D	$[Co_6Se_8(PEt_3)_4(CO)_2]$, THF, TMSD	0 (with UV lamp irradiation)	[174]
$[Co_6Se_8(py)(PEt_3)_4(CO)]$ (**184**)	0D	$[Co_6Se_8\{C(H)SiMe_3\}(PEt_3)_4(CO)]$, py	rt	[174]
$[Co_{12}Se_{16}(PEt_3)_8(CO)_2][TCNQ]$ (**185**)	0D	$[Co_6Se_8\{C(H)SiMe_3\}(PEt_3)_4(CO)]$, benzene, py, THF, TCNQ, MeCN	rt	[174]
trans-$[Co_{12}Se_{16}(PEt_3)_8(CO)_2][PF_6]$ (**186**)	0D	$[Co_6Se_8\{C(H)SiMe_3\}(PEt_3)_4(CO)]$, benzene, py, THF, $[Fc][PF_6]$, MeCN	rt	[174]
trans-$[Co_{12}Se_{16}\{PEt_2(p\text{–}C_6H_4SMe)\}_2(PEt_3)_8][PF_6]$ (**187**)	0D	*trans*-$[Co_{12}Se_{16}(PEt_3)_8(CO)_2][PF_6]$, $PEt_2(p\text{-}C_6H_4SMe)$, THF	rt	[174]
cis-$[Co_{12}Se_{16}\{PEt_2(p\text{–}C_6H_4SMe)\}_2(PEt_3)_8]$ (**188**)	0D	*cis*-$[Co_{12}Se_{16}(CO)(PEt_3)_8][PF_6]$, $[Fc][PF_6]$, THF,	27	[174]
$\{[Co_6Se_8(PEt_3)_4](PDI)_{1.64}\}_2[Mo_6O_{19}]\bullet$THF (**189**)	2D	$[Co_6Se_8(PEt_3)_4(PDI)_2]$, $[^nBu_4N]_2[Mo_6O_{19}]$, THF	20	[175]
$[Co_6Se_8\{PEt_2(4\text{-}C_6H_4COOH)\}_6]$ (**190**)	0D	$[Co_6Se_8\{PEt_2(4\text{-}C_6H_4Br)\}_6]$, THF, *n*-BuLi, CO_2	78	[176]
$[Zn_3[Co_6Se_8\{PEt_2(4\text{-}C_6H_4COOH)\}_6]\bullet 2$MeOH (**191**)	3D	$[Co_6Se_8\{PEt_2(4\text{-}C_6H_4COOH)\}_6]$, DMF, $Zn(NO_3)_3{\cdot}6H_2O$, MeOH	65	[176]
$\{Zn_3[Co_6Se_8\{PEt_2(4\text{-}C_6H_4COOH)\}_6\}$ (**192**)	2D	$[Co_6Se_8\{PEt_2(4\text{-}C_6H_4COOH)\}_6]$, DMF, $Zn(NO_3)_3{\cdot}6H_2O$, EtOH, HCl	65	[176]

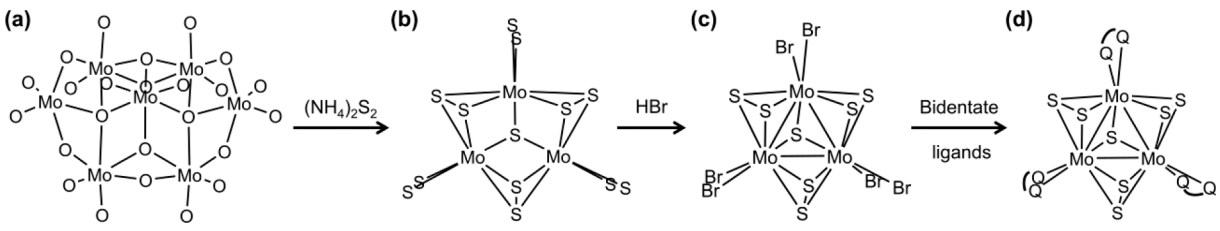

Scheme 6. Generation and ligand-functionalization process of the clucter anion $[Mo_3S_{13}]^{2-}$. (a) Reaction of $[Mo_7O_{24}]^{6-}$ with $(NH_4)_2S_2$ yielding $[Mo_3S_{13}]^{2-}$. (b) Structure diagram of $[Mo_3S_{13}]^{2-}$. (c) Reaction with HBr to form $[Mo_3S_7Br_6]^{2-}$. (c) Treatment with bidentate ligands (L; indicated as "Q—Q" in the scheme) yielding $[Mo_3S_7L_3]^{2-}$.

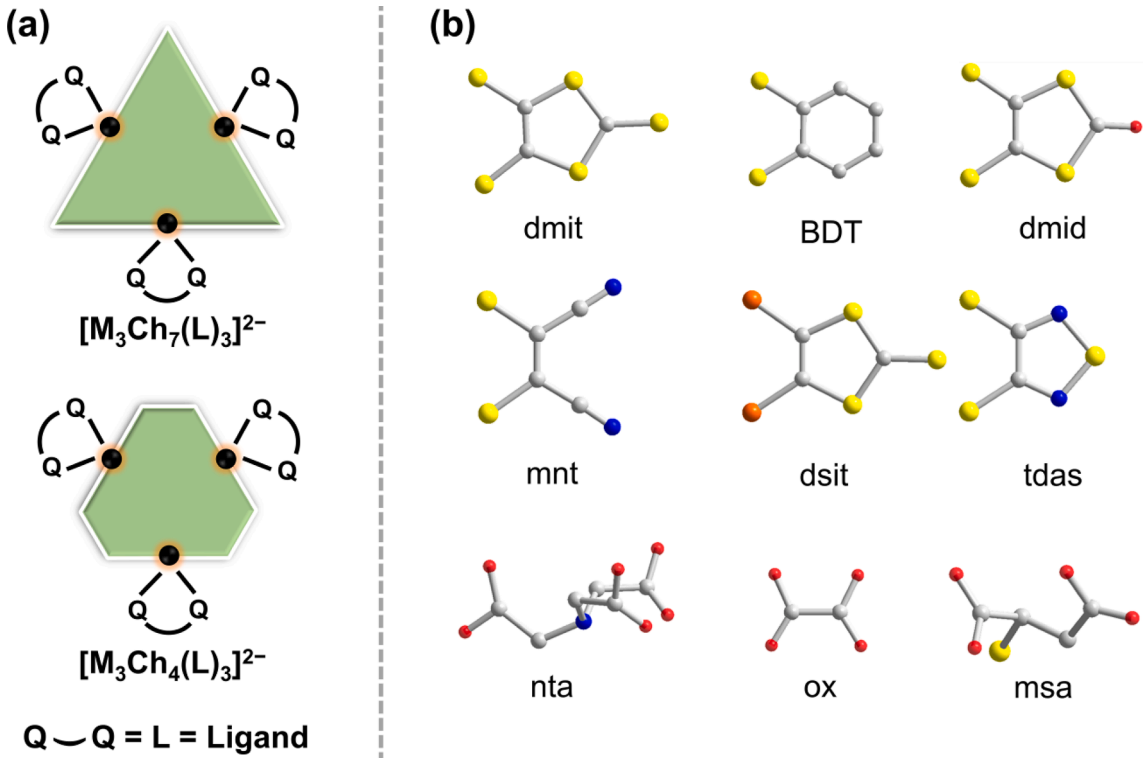

Fig. 45. (a) Schematic illustrations of ligand-functionalized $[M_3Ch_7]^{2-}$ and $[M_3Ch_4]^{2-}$ clusters (M W, Mo; Ch S, Se), (b) Survey of commonly used dithiolene, oxalate and dicarboxylic ligands. H atoms are omitted for clarity.

of weakly interacting neutral strands, instead of the analogous 2D-polymers, were obtained by reacting Pr^{3+}, Nd^{3+}, Sm^{3+}, or Gd^{3+} instead with the general formula 1D-{$[W_3S_7(ox)_3][Ln(H_2O)_5](ox)$} (Ln = Pr^{3+}; Nd^{3+}; Sm^{3+} and Ga^{3+}). The treatment of $[W_3S_7(ox)_3]^2$ with highly positively charged Th^{4+} cations afforded the complex anion $[\{W_3S_7(ox)_3\}_4Th_2(OH)_2(H_2O)_{10}]^2$ (in **206**), which consists of four ligand-functionalized $[W_3S_7(ox)_3]^2$ wings and one dinuclear $[Th_2(OH)_2]^{6+}$ unit [185]. In aqueous solutions with pH < 10, by treating $[Mo_3S_4(Hnta)_3]^2$ with La^{3+} can also form a layer-type coordination polymer, 2D-{$[(Mo_3S_4)La_{0.75}(Hnta)_3]^{0.25+}$} (in **207**) [184]. Even though rare, the tunable compositions in the cluster cores, the wide variety of dicarboxylic ligands, and the diverse number of possible bridging metal cations endow a great potential for the development of such cluster-based polymer materials.

To simplify the reaction processes and further expand the ligand-functionalization of trinuclear $[Mo_3S_7]^{4+}$ clusters, $[Mo_3S_7Br_6]^2$ was reacted directly with benzenedithiol, which yielded salts of cluster dimers, $[Mo_3S_7Br_3(m\text{-BDT})_{1.5}]_2^4$ (in **208**; Fig. 46a) and $[Mo_3S_7Br_3(p\text{-BDT})]_2^4$ (in **209**; Fig. 46b), as well as a polymeric 1D-{$[Mo_3S_7Br_3(p\text{-BDT})_{1.5}]^2$ }$_n$ strand (in **210**; Fig. 46c) in decent yields [186]. Notably,

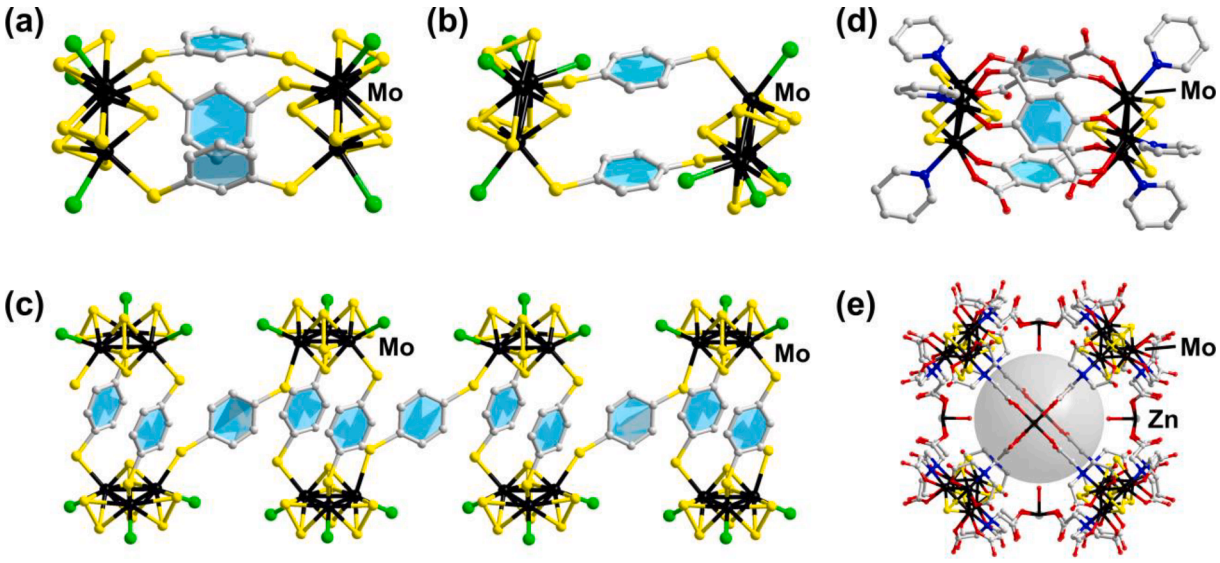

Fig. 46. Ligand-functionalized cluster assemblies based on $\{Mo_3S_4\}$ sulfido molybdate units. (a) Two $[Mo_3S_7Br_3]^-$ units bridged by two *m*-BDT molecules. (b) Two $[Mo_3S_7Br_3]^-$ units bridged by two *p*-BDT molecules. (c) Polymeric strand upon bridging of $[Mo_3S_7Br_3]^-$ by *p*-BDT molecules. (d) Two $[Mo_3S_4(py)_3]^{4+}$ units bridged by three DOT anions. (e) cage-type assembly upon linkage of $[Zn(H_2O)]^{2+}$ and $[Mo_3S_4]^{4+}$ units *via* nta anions. H atoms are omitted for clarity.

the polymeric compound shows a nearly 40-fold enhancement of the turnover frequency in electrocatalytic hydrogen evolution reactions properties as compared to the performance of non-functionalized cluster analogs. It was assumed that the alignment of the clusters by benzenedithiol bridges cause long-range order on the electrode, which allowed for a better electrocatalytic performance. With the use of different carboxylic ligands as bridges, for instance, in the presence of dicarboxylic ligand (H_2DOT), the dimeric molecules $[Mo_3S_4(py)_3(DOT)_{1.5}]_2^4$ (in **211**; Fig. 46d) could be obtained. By linking carboxylic functionalized tridentate $[Mo_3S_4(nta)_3]^5$ units with Zn^{2+}, the $[Mo_3S_4(nta)_3]_8[Zn(H_2O)]_6^{28}$ anionic cage molecule (in **212**; Fig. 46e) was isolated as its salt from similar reactions [186].

Not only the mentioned sulfido molybdate cluster and its derivatives serve as building blocks for the generation of polymer compounds, but also classical sulfido ferrate and cobaltate cluster units can be assembled with different dimensionalities. The reaction of $(R_4N)_2[Fe_4S_4(SPh)_4]$ (**213**, R = ^{n}Bu; **214**, R = Me; Fig. 47a, 47b) with 1,4-benzenedithiol (*p*-BDT) in MeCN at an excess of $Li[CF_3SO_3]$ led to the crystallization of the respective ammonium salts of polymeric strands. [187] Even though they possess the same inorganic skeletons, the solubilities differed notably owing to the size discrepancy of the cations; only the $[Bu_4N]^+$ salt dissolves in DMF without decomposition. Additionally, reduction of the $\{Fe_4S_4\}$ cluster units resulted in a conductivity increase of the material by up to 4 orders of magnitude (from $3(4)\bullet10^{-9}$ to $1.5(5)\bullet10^{-5}$ S/cm). The use of alkylate derivatives of the bridging molecules, namely 2,5-dimethyl-1,4-benzenedithiol (DMBDT) or 2,3,5,6-tetramethyl-1,4-benzenedithiol (TMBDT), afforded similar strand-like structures in $(^nBu_4N)_2[(Fe_4S_4)(DMBDT)_2]$ (**215**; Fig. 47c) like the ones in **213** and **214** [188]. However, the isolation of single crystals of **215** was unsuccessful, hence synchrotron powder X-ray diffraction was performed to reveal the molecular structure by combining rigorous *ab initio* calculations with Rietveld refinement. Both compounds exhibit redox activity but differ from each in terms of their reduction potential: the more electron-donating alkyl-substituted linkers lead to more electron-rich compounds. These results indicated the subtle influence of the alkylation of the bridging ligands for modifying the electrochemical properties of redox-active compounds.

Most recently, neutral $[Co_4S_4(P^iPr_3)_4]$ clusters were used to build cluster-based oligomeric and polymeric compounds. The P^iPr_3 ligands of $[Co_4S_4(P^iPr_3)_4]$ can be easily substituted with N-heterocyclic carbenes (NHCs) and bis-NHCs in benzene upon heating. Ligand-functionalized $[Co_4S_4(^iPr_2NHCBz)_4]$ (**216**) and ligand-bridged $[Co_4S_4\{^iPr_2(NHC)_2Bz\}_2]$ (**217**) were isolable this way. Although the carbene-substituted clusters have been previously reported, these were the first $[Co_4S_4]$-based polymers comprising bis-NHC bridges [189].

All compounds presented in Section 5.3 are summarized in Table 10.

6. Conclusion and perspectives

In conclusion, we have reviewed recent development in the field of ligand-functionalized and ligand-bridged or organyl-separated chalcogenido metalate-based clusters, for which we selected certain cluster families that have emerged as being particularly focused on. These were supertetrahedral chalcogenido metalate clusters of d^{10} metals and related clusters based on other structural motifs, coinage metal chalcogenide clusters as well as several examples of chalcogenido metalate clusters based on well-known octahedral or (semi-)cubic arrangements of Re, Mo, Fe, or Co ions.

The broad spectrum of terminal, capping, or bridging ligands serves to widen the accessibility of these cluster-based compounds on the one hand, and play a significant role in modifying their chemical and physical properties on the other hand. The attachment of either

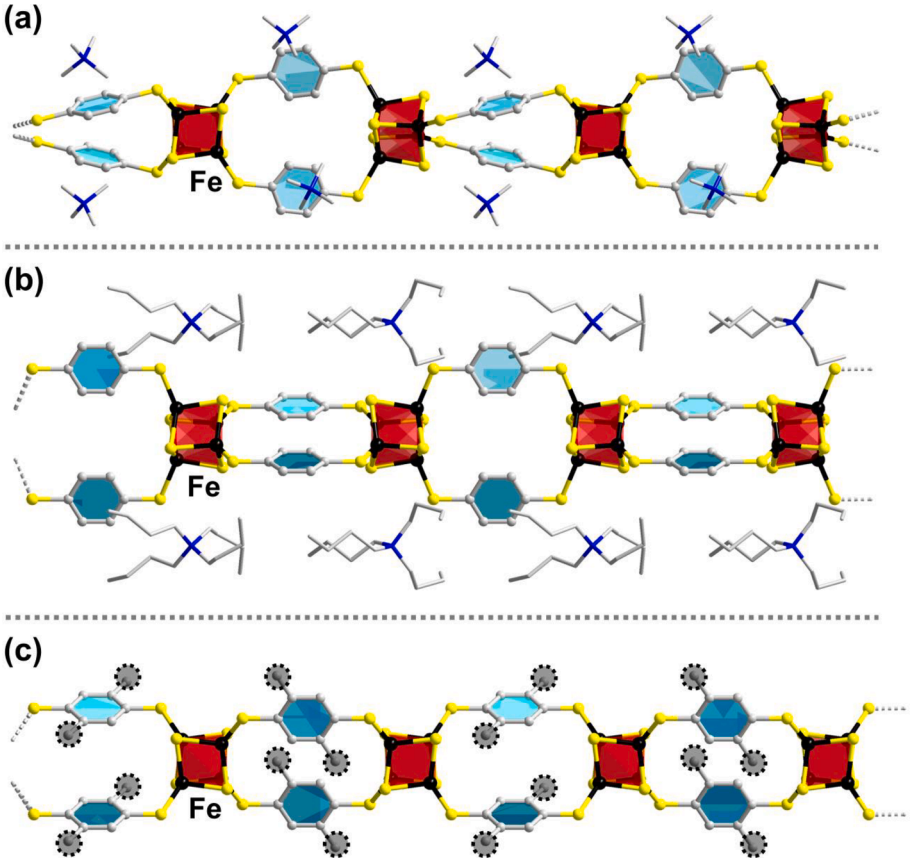

Fig. 47. Polymer strands formed through bridging $\{Fe_4S_4\}$ clusters. (a) $[Me_4N]^+$ Salts of *p*-BDT-bridged strands. (b) $[^nBu_4N]^+$ Salts of *p*-BDT-bridged strands. (c) Structure of the polymer strand formed by bridging $\{Fe_4S_4\}$ clusters with DMBDT. H atoms are omitted for clarity.

Table 10
Summary of the ligand-functionalized and ligand-bridged compounds presented in Section 5.3.

Compound	Dimensionality	Reactants	Temperature (°C)	Ref.
$[^nBu_4N]_2[Mo_3S_7(dmit)_3]$ (**193**)	0D	$(^nBu_4)_2Sn(dmit)$, $[^nBu_4N]_2[Mo_3S_7Br_6]$, MeCN	reflux	[181]
$[^nBu_4N]_2[Mo_3S_7(tfd)_3]$ (**194**)	0D	$(^nBu_4)_2Sn(tfd)$, $[^nBu_4N]_2[Mo_3S_7Br_6]$, MeCN	reflux	[182]
$[^nBu_4N]_2[Mo_3S_7(BDT)_3]$ (**195**)	0D	$(^nBu_4)_2Sn(BDT)$, $[^nBu_4N]_2[Mo_3S_7Br_6]$, MeCN	reflux	[182]
$[^nBu_4N]_2[Mo_3S_7(dmid)_3]$ (**196**)	0D	$(^nBu_4)_2Sn(dmid)$, $[^nBu_4N]_2[Mo_3S_7Br_6]$, MeCN	reflux	[182]
$[^nBu_4N]_2[Mo_3S_7(dsit)_3]$ (**197**)	0D	$(^nBu_4N)_2[Zn(dsit)_2]$, $[^nBu_4N]_2[Mo_3S_7Br_6]$, MeCN	reflux	[182]
$[^nBu_4N]_2[Mo_3S_7(tdas)_3]$ (**198**)	0D	$(^nBu_4N)_2[Zn(tdas)_2]$, $[^nBu_4N]_2[Mo_3S_7Br_6]$, MeCN	reflux	[182]
$[Et_4N]_2[Mo_3S_7(mnt)_3]$ (**199**)	0D	$(BEt_4N)_2[Mo_3S_7Br_6]$, Na_2mnt, MeCN	reflux	[180]
$K_2[Mo_3S_7(ox)_3]\bullet 0.5KBr\cdot 3H_2O$ (**200**)	0D	$Mo_3S_7Br_4$, K_2ox, H_2O	5	[180]
$K_2[Mo_3Se_7(ox)_3]\bullet 0.5KBr\cdot 4H_2O$ (**201**)	0D	$Mo_3Se_7Br_4$, K_2ox, H_2O	5	[180]
$K_2[W_3S_7(ox)_3]\bullet 0.5KBr\cdot 5H_2O$ (**202**)	0D	$W_3S_7Br_4$, K_2ox, H_2O	5	[180]
$(Et_4N)_2[Mo_3S_7(Hmsa)_3]$ (**203**)	0D	$(Et_4N)_2Mo_3S_7Br_6\bullet$MeCN, H_3msa, MeCN, TEA	70	[179]
$\{[La(H_2O)_6]_3[W_3S_7(ox)_3]_4\}Br\cdot 24.35H_2O$ (**204**)	2D	$K_2[W_3S_7(ox)_3]\bullet 0.5KBr\cdot 5H_2O$, $La(NO_3)_3\cdot 6H_2O$, H_2O	rt	[185]
$\{[Ce(H_2O)_6]_3[W_3S_7(ox)_3]_4\}Br\cdot 24.95H_2O$ (**205**)	2D	$K_2[W_3S_7(ox)_3]\bullet 0.5KBr\cdot 5H_2O$, $Ce(NO_3)_3\cdot 6H_2O$, H_2O	rt	[185]
$K[(W_3S_7(ox)_3)_4Th(OH)_2(H_2O)_{10}(\mu\text{- ox})]$ $Br\cdot 14.33H_2O$ (**206**)	0D	$K_2[W_3S_7(ox)_3]\bullet 0.5KBr\cdot 5H_2O$, $ThCl_4\cdot 8H_2O$, H_2O	rt	[185]
$[(Mo_3S_4)La_{0.75}(Hnta)_3]\cdot Cl_{0.25}\cdot 18H_2O$ (**207**)	2D	$Na_2[Mo_3S_4(Hnta)_3]\bullet 7H_2O$, $LaCl_3$, H_2O, HCl	Rt	[184]
$(Et_4N)_4[Mo_3S_7Br_3(m\text{-BDT})_{1.5}]_2$ (**208**)	0D	$(Et_4N)_2[Mo_3S_7Br_6]$, *m*-BDT, $[Et_4N]Br$, DMF, py	rt	[186]
$(Et_4N)_4[Mo_3S_7Br_3(p\text{-BDT})]_2$ (**209**)	0D	$(Et_4N)_2[Mo_3S_7Br_6]$, *p*-BDT, $[Et_4N]Br$, MeCN, 2,6-lutidine	rt	[186]
$(Et_4N)_2[Mo_3S_7Br_3(p\text{-BDT})_{1.5}]$ (**210**)	1D	$(Et_4N)_2[Mo_3S_7Br_6]$, *p*-BDT, $[Et_4N]Br$, DMF, py	rt	[186]
$(Et_4N)_2[Mo_3S_4(py)_3(DOT)_{1.5}]_2$ (**211**)	0D	$(Et_4N)_2[Mo_3S_7Br_6]$, H_2DOT, $[Et_4N]Br$, DMF, py	120	[186]
$Na_{28}[Mo_3S_4(nta)]_8[Zn(H_2O)]_2$ (**212**)	0D	$Na_2[Mo_3S_4(Hnta)_3]$, DMF, $Zn(OAc)_2$, DMF, py	rt	[186]
$(^nBu_4N)_2[(Fe_4S_4)(BDT)_2]$ (**213**)	1D	$(^nBu_4N)_2[Fe_4S_4(SPh)_4]$, $Li[CF_3SO_3]$, DMF, BDT	140	[187]
$(Me_4N)_2[(Fe_4S_4)(BDT)_2]$ (**214**)	1D	$(Me_4N)_2[Fe_4S_4(SPh)_4]$, $Li[CF_3SO_3]$, MeCN, BDT	100	[187]
$(^nBu_4N)_2[(Fe_4S_4)(DMBDT)_2]$ (**215**)	1D	$(^nBu_4N)_2[Fe_4S_4(SPh)_4]$, $Li[CF_3SO_3]$, MeCN, DMBDT	100	[188]
$[Co_4S_4(^iPr_2NHCBz)_4]$ (**216**)	0D	$Co_4S_4(P^iPr_3)$, Pr^i(NHCBz), THF	60 °C for two days, then 78 °C for two days	[189]
$[Co_4S_4\{^iPr_2(NHC)_2Bz\}_2]$ (**217**)	3D	$Co_4S_4(P^iPr_3)$, 1,1′,3,3-tetra-isopropyl-5,5′-bibenzimidazolium bromide, benzene	100	[189]

monodentate or multidentate ligands can be achieved by using different approaches for each specific cluster. For instance, the functionalization of supertetrahedral clusters normally follows facile ionothermal or solvothermal routes and the capping agents are usually transferred from the reaction media *in situ*. Surfactant-type reaction media or auxiliaries are (additionally) capable of separating the inorganic cluster units into lamellar arrangements and also help to obtain functionalized and bridged compounds. Silver chalcogenide clusters, in particular, can be isolated as ligand-functionalized molecules, using monodentate chalcogenolates, or as ligand-bridged polymers if multidentate ligands are employed in the reactions. The decoration of other transition metal-based clusters units, like $\{M_6Ch_8\}$ (M = Re, Co), $\{M_3Ch_{13}\}$ or $\{M_3Ch_4\}$ (M = Mo, W), follows pretty controllable step-wise processes that include the installation of removable inorganic ligands at the corners of the respective clusters (e.g., halides) and the replacement of these ligands with monodentate or multidentate ligands. The pre-customized inorganic ligands are instrumental, as they afford to a well-designable platform for further structural modifications.

Even though many ligand-functionalized clusters have been synthesized using these methods in the past, there is still room for further development: First, one may take advantage of the different solubilities of different clusters to investigating possible intermediates and the still widely unknown formation of such compounds *in situ*. Second, the preparation of chalcogenido metalate supertetrahedra and coinage metal chalcogenide clusters with removable inorganic halides would allow for further avenues into substitution reactions with either capping or bridging ligands. Third, the decoration of the ligands with fluorescent, catalytically active, or highly reactive groups might help to introduce and control corresponding properties and reactivities. Moreover, ligand engineering for cluster-based polymers would be benficial for designing their specific gas adsorption/separation properties, and finally, the presence of long-alkyl chains from ionic liquid cations or surfactants may be useful for the exfoliation of lamellar sheets comprising semiconductor-based cluster units. All of the mentioned directions are in line with open questions and long-term goals for inorganic and material chemistry.

Color code: H — white; C — gray; N — blue; O — red; P — pink; S — gold; Ga — sea green; Ge — plum; As — sky blue; Se — orange; In — rose; Sn — dark blue; Sb — light blue; Te — blue-gray. Transition metal atoms are shown in black color and defined in each figure specifically. Halide atoms are given in bright green color. Carbon atoms of chalcogenolate alkyl groups in Figs. 5–6, 15–16 are presented in turquoise color.

Declaration of Competing Interest

The authors declare that they have no known competing financial interests or personal relationships that could have appeared to influence the work reported in this paper.

Data availability

No data was used for the research described in the article.

Acknowledgments

This work was financially supported by the German Research Foundation (Deutsche Forschungsgemeinschaft, DFG). Z. W. acknowledges a Ph.D. fellowship by the China Scholarship Council (CSC no. 202006920030). We are indepted to Dr. Lukas Guggolz, Dr. Benjamin Peerless, and Dr. Niklas Rinn for their help with the manuscript.

References

[1] R.J. Wilson, N. Lichtenberger, B. Weinert, S. Dehnen, Chem. Rev. 119 (2019) 8506–8554.
[2] A. Pinkard, A.M. Champsaur, X. Roy, Acc. Chem. Res. 51 (2018) 919–929.
[3] J. Zhang, X. Bu, P. Feng, T. Wu, Acc. Chem. Res. 53 (2020) 2261–2272.
[4] S. Hossain, Y. Niihori, L.V. Nair, B. Kumar, W. Kurashige, Y. Negishi, Acc. Chem. Res. 51 (2018) 3114–3124.
[5] S.E. Latturner, Acc. Chem. Res. 51 (2018) 40–48.
[6] R.S. Dhayal, W.E. van Zyl, C.W. Liu, Acc. Chem. Res. 49 (2016) 86–95.
[7] S.-F. Yuan, Z.-J. Guan, Q.-M. Wang, J. Am. Chem. Soc. 144 (2022) 11405–11412.
[8] X. Xu, W. Wang, D. Liu, D. Hu, T. Wu, X. Bu, P. Feng, J. Am. Chem. Soc. 140 (2018) 888–891.
[9] R. Zhang, M. Murata, T. Aharen, A. Wakamiya, T. Shimoaka, T. Hasegawa, Y. Murata, Nat. Chem. 8 (2016) 435–441.

[10] H.-J. Zhai, Y.-F. Zhao, W.-L. Li, Q. Chen, H. Bai, H.-S. Hu, Z.A. Piazza, W.-J. Tian, H.-G. Lu, Y.-B. Wu, Y.-W. Mu, G.-F. Wei, Z.-P. Liu, J. Li, S.-D. Li, L.-S. Wang, Nat. Chem. 6 (2014) 727–731.
[11] Z. Wu, F. Weigend, D. Fenske, T. Naumann, J.M. Gottfried, S. Dehnen, J. Am. Chem. Soc. 145 (2023) 3802–3811.
[12] J.-X. Liu, X.-B. Zhang, Y.-L. Li, S.-L. Huang, G.-Y. Yang, Coord. Chem. Rev. 414 (2020), 213260.
[13] B. Peerless, A. Schmidt, Y.J. Franzke, S. Dehnen, Nat. Chem. 15 (2023) 347–356.
[14] N. Zheng, X. Bu, B. Wang, P. Feng, Science 298 (2002) 2366–2369.
[15] O. Fuhr, S. Dehnen, D. Fenske, Chem. Soc. Rev. 42 (2013) 1871–1906.
[16] X. Zhou, V.S.C. Kolluru, W. Xu, L. Wang, T. Chang, Y.-S. Chen, L. Yu, J. Wen, M.K. Y. Chan, D.Y. Chung, M.G. Kanatzidis, Nature 612 (2022) 72–77.
[17] J.F. Corrigan, O. Fuhr, D. Fenske, Adv. Mater. 21 (2009) 1867–1871.
[18] C. Wang, X. Bu, N. Zheng, P. Feng, J. Am. Chem. Soc. 124 (2002) 10268–10269.
[19] E. Dornsiepen, F. Pieck, R. Tonner, S. Dehnen, J. Am. Chem. Soc. 141 (2019) 16494–16500.
[20] X. Bu, N. Zheng, P. Feng, Chem Eur J 10 (2004) 3356–3362.
[21] S.-S. Zhang, R.-C. Liu, X.-C. Zhang, L. Feng, Q.-W. Xue, Z.-Y. Gao, C.-H. Tung, D. Sun, Sci. China Chem. 64 (2021) 2118–2124.
[22] C. Sun, B.K. Teo, C. Deng, J. Lin, G.-G. Luo, C.-H. Tung, D. Sun, Coord. Chem. Rev. 427 (2021), 213576.
[23] Y.-L. Tan, L. Yang, T.-C. Yu, H. Yu, X.-Y. Wang, Y.-L. Song, Z. Niu, J.-P. Lang, Sci. China Chem. 64 (2021) 948–952.
[24] Z. Wang, Q.-P. Qu, H.-F. Su, P. Huang, R.K. Gupta, Q.-Y. Liu, C.-H. Tung, D. Sun, L.-S. Zheng, Sci. China Chem. 63 (2020) 16–20.
[25] Z. Wang, H.-F. Su, Y.-Z. Tan, S. Schein, S.-C. Lin, W. Liu, S.-A. Wang, W.-G. Wang, C.-H. Tung, D. Sun, L.-S. Zheng, Proc. Natl. Acad. Sci. 114 (2017) 12132–12137.
[26] O. Peña, Physica C (Amsterdam, Neth.) 514 (2015) 95–112.
[27] T. Wu, L. Wang, X. Bu, V. Chau, P. Feng, J. Am. Chem. Soc. 132 (2010) 10823–10831.
[28] Y. Lin, W. Massa, S. Dehnen, J. Am. Chem. Soc. 134 (2012) 4497–4500.
[29] T. Wu, F. Zuo, L. Wang, X. Bu, S.-T. Zheng, R. Ma, P. Feng, J. Am. Chem. Soc. 133 (2011) 15886–15889.
[30] Y.-P. Xie, J.-L. Jin, G.-X. Duan, X. Lu, T.C.W. Mak, Coord. Chem. Rev. 331 (2017) 54–72.
[31] W. Kurashige, Y. Niihori, S. Sharma, Y. Negishi, Coord. Chem. Rev. 320–321 (2016) 238–250.
[32] O. Veselska, A. Demessence, Coord. Chem. Rev. 355 (2018) 240–270.
[33] Y. Jin, C. Zhang, X.-Y. Dong, S.-Q. Zang, T.C.W. Mak, Chem. Soc. Rev. 50 (2021) 2297–2319.
[34] B. Peters, G. Stuhrmann, F. Mack, F. Weigend, S. Dehnen, Angew. Chem. Int. Ed. 60 (2021) 17622–17628.
[35] Y. Wang, Z. Zhu, Z. Sun, Q. Hu, J. Li, J. Jiang, X. Huang, Chem Eur J 26 (2020) 1624–1632.
[36] J. Zhang, P. Feng, X. Bu, T. Wu, Natl. Sci. Rev. 9 (2022) nwab076.
[37] H. Li, A. Laine, M. O'Keeffe, O.M. Yaghi, Science 283 (1999) 1145–1147.
[38] G.S.H. Lee, D.C. Craig, I. Ma, M.L. Scudder, T.D. Bailey, I.G. Dance, J. Am. Chem. Soc. 110 (1988) 4863–4864.
[39] O. Palchik, R.G. Iyer, J.H. Liao, M.G. Kanatzidis, Inorg. Chem. 42 (2003) 5052–5054.
[40] N.W. Rosemann, J.P. Eußner, E. Dornsiepen, S. Chatterjee, S. Dehnen, J. Am. Chem. Soc. 138 (2016) 16224–16227.
[41] P. Vaqueiro, M.L. Romero, Chem. Commun. (2007) 3282–3284.
[42] T. Wu, X. Bu, P. Liao, L. Wang, S.-T. Zheng, R. Ma, P. Feng, J. Am. Chem. Soc. 134 (2012) 3619–3622.
[43] W.-W. Xiong, J.-R. Li, B. Hu, B. Tan, R.-F. Li, X.-Y. Huang, Chem. Sci. 3 (2012) 1200–1204.
[44] B. Peters, N. Lichtenberger, E. Dornsiepen, S. Dehnen, Chem. Sci. 11 (2020) 16–26.
[45] Z. Wu, G. Stuhrmann, S. Dehnen, Chem. Commun. 58 (2022) 11609–11624.
[46] N.-N. Shen, B. Hu, C.-C. Cheng, G.-D. Zou, Q.-Q. Hu, C.-F. Du, J.-R. Li, X.-Y. Huang, Cryst. Growth Des. 18 (2018) 962–968.
[47] B. Peters, S. Santner, C. Donsbach, P. Vöpel, B. Smarsly, S. Dehnen, Chem. Sci. 10 (2019) 5211–5217.
[48] T. Kaib, M. Kapitein, S. Dehnen, Z. Anorg, Allg. Chem. 637 (2011) 1683–1686.
[49] J.B. Parise, Y. Ko, Chem. Mater. 6 (1994) 718–720.
[50] W. Schiwy, B. Krebs, Angew. Chem. Int. Ed. 14 (1975) 436.
[51] B. Peters, S. Reith, S. Dehnen, Z. Anorg, Allg. Chem. 646 (2020) 964–967.
[52] G. Stuhrmann, private communication. Karlsruhe (2023).
[53] Z. Wu, M. Luo, C. Xue, J. Zhang, J. Lv, X. Wang, T. Wu, Cryst. Growth Des. 19 (2019) 4151–4156.
[54] C.-Y. Yue, X.-W. Lei, L.-J. Feng, C. Wang, Y.-P. Gong, X.-Y. Liu, Dalton Trans. 44 (2015) 2416–2424.
[55] X. Bu, N. Zheng, Y. Li, P. Feng, J. Am. Chem. Soc. 124 (2002) 12646–12647.
[56] C. Wang, Y. Li, X. Bu, N. Zheng, O. Zivkovic, C.-S. Yang, P. Feng, J. Am. Chem. Soc. 123 (2001) 11506–11507.
[57] Y. Peng, Q. Hu, Y. Liu, J. Li, X. Huang, ChemPlusChem 85 (2020) 2487–2498.
[58] P. Feng, X. Bu, N. Zheng, Acc. Chem. Res. 38 (2005) 293–303.
[59] G.S.H. Lee, K.J. Fisher, D.C. Craig, M.L. Scudder, I.G. Dance, J. Am. Chem. Soc. 112 (1990) 6435–6437.
[60] A. Eichhöfer, D. Fenske, J. Chem. Soc. Dalton Trans. (2000) 941–944.
[61] P. Vaqueiro, M.L. Romero, J. Am. Chem. Soc. 130 (2008) 9630–9631.
[62] P. Vaqueiro, M.L. Romero, Inorg. Chem. 48 (2009) 810–812.
[63] P. Vaqueiro, S. Makin, Y. Tong, S.J. Ewing, Dalton Trans. 46 (2017) 3816–3819.
[64] P. Vaqueiro, M.L. Romero, B.C. Rowan, B.S. Richards, Chem Eur J 16 (2010) 4462–4465.
[65] C. Xu, N. Hedin, H.-T. Shi, Q.-F. Zhang, Chem. Commun. 50 (2014) 3710–3712.
[66] Z.-K. Wang, M.-M. Sheng, S.-S. Qin, H.-T. Shi, M. Strømme, Q.-F. Zhang, C. Xu, Inorg. Chem. 59 (2020) 2121–2126.
[67] C. Xu, M.-M. Sheng, H.-T. Shi, M. Strømme, Q.-F. Zhang, Dalton Trans. 48 (2019) 5505–5510.
[68] Y.-L. Li, P.-T. Sheng, F.-A. Li, R.-B. Bai, X.-M. Gao, Y.-J. Han, Inorg. Chem. 62 (2023) 4043–4047.
[69] T. Wu, R. Khazhakyan, L. Wang, X. Bu, S.-T. Zheng, V. Chau, P. Feng, Angew. Chem. Int. Ed. 50 (2011) 2536–2539.
[70] J. Zhang, W. Wang, C. Xue, M. Zhao, D. Hu, J. Lv, X. Wang, D. Li, T. Wu, Inorg. Chem. 57 (2018) 9790–9793.
[71] X. Liu, C. Xue, X. Wang, J. Zhang, T. Wu, Dalton Trans. 49 (2020) 11489–11492.
[72] H. Yang, J. Zhang, M. Luo, W. Wang, H. Lin, Y. Li, D. Li, P. Feng, T. Wu, J. Am. Chem. Soc. 140 (2018) 11189–11192.
[73] X. Han, Z. Wang, D. Liu, J. Xu, Y. Liu, C. Wang, Chem. Commun. 50 (2014) 796–798.
[74] X.-M. Zhang, D. Sarma, Y.-Q. Wu, L. Wang, Z.-X. Ning, F.-Q. Zhang, M. G. Kanatzidis, J. Am. Chem. Soc. 138 (2016) 5543–5546.
[75] Y.-H. Wang, J.-B. Jiang, P. Wang, X.-L. Sun, Q.-Y. Zhu, J. Dai, CrstEngComm 15 (2013) 6040–6045.
[76] Y. Zhang, D. Hu, C. Xue, H. Yang, X. Wang, T. Wu, Dalton Trans. 47 (2018) 3227–3230.
[77] J. Li, C. Liu, X. Wang, Y. Ding, Z. Wu, P. Sun, J. Tang, J. Zhang, D.-S. Li, N. Chen, T. Wu, Dalton Trans. 51 (2022) 978–985.
[78] J. Xie, X. Bu, N. Zheng, P. Feng, Chem. Commun. (2005) 4916–4918.
[79] Q. Zhang, X. Bu, Z. Lin, T. Wu, P. Feng, Inorg. Chem. 47 (2008) 9724–9726.
[80] N. Zheng, X. Bu, H. Lu, L. Chen, P. Feng, J. Am. Chem. Soc. 127 (2005) 14990–14991.
[81] N. Zheng, X. Bu, P. Feng, J. Am. Chem. Soc. 124 (2002) 9688–9689.
[82] H. Döllefeld, H. Weller, A. Eychmüller, J. Phys. Chem. B 106 (2002) 5604–5608.
[83] C.-F. Du, N.-N. Shen, J.-R. Li, M.-T. Hao, Z. Wang, X.-Y. Huang, Chem. Asian J. 11 (2016) 1555–1564.
[84] C. Donsbach, S. Dehnen, Eur. J. Inorg. Chem. 2018 (2018) 4429–4433.
[85] M. Tallu, B. Peters, A. Friedrich, S. Dehnen, Inorg. Chem. 62 (2023) 13943–13952.
[86] C. Donsbach, K. Reiter, D. Sundholm, F. Weigend, S. Dehnen, Angew. Chem. Int. Ed. 57 (2018) 8770–8774.
[87] W.-W. Xiong, Q. Zhang, Angew. Chem. Int. Ed. 54 (2015) 11616–11623.
[88] J. Li, B. Marler, H. Kessler, M. Soulard, S. Kallus, Inorg. Chem. 36 (1997) 4697–4701.
[89] F. Bonhomme, M.G. Kanatzidis, Chem. Mater. 10 (1998) 1153–1159.
[90] K.K. Rangan, M.G. Kanatzidis, Inorg. Chim. Acta 357 (2004) 4036–4044.
[91] M.-J. Suh, V. Vien, S. Huh, Y. Kim, S.-J. Kim, Eur. J. Inorg. Chem. 2008 (2008) 686–692.
[92] W.-W. Xiong, E.U. Athresh, Y.T. Ng, J. Ding, T. Wu, Q. Zhang, J. Am. Chem. Soc. 135 (2013) 1256–1259.
[93] J. Gao, Q. Tay, P.-Z. Li, W.-W. Xiong, Y. Zhao, Z. Chen, Q. Zhang, Chem. Asian J. 9 (2014) 131–134.
[94] Z. Wang, G. Xu, Y. Bi, C. Wang, CrstEngComm 12 (2010) 3703–3707.
[95] G. Zhang, P. Li, J. Ding, Y. Liu, W.-W. Xiong, L. Nie, T. Wu, Y. Zhao, A.I.Y. Tok, Q. Zhang, Inorg. Chem. 53 (2014) 10248–10256.
[96] L. Nie, W.-W. Xiong, P. Li, J. Han, G. Zhang, S. Yin, Y. Zhao, R. Xu, Q. Zhang, J. Solid State Chem. 220 (2014) 118–123.
[97] M.J. Manos, M.G. Kanatzidis, Inorg. Chem. 48 (2009) 4658–4660.
[98] Y. Liu, P.D. Kanhere, C. Ling Wong, Y. Tian, Y. Feng, F. Boey, T. Wu, H. Chen, T. J. White, Z. Chen, Q. Zhang, J. Solid State Chem. 183 (2010) 2644–2649.
[99] Y. Liu, Y. Tian, F. Wei, M.S.C. Ping, C. Huang, F. Boey, C. Kloc, L. Chen, T. Wu, Q. Zhang, Inorg. Chem. Commun. 14 (2011) 884–888.
[100] C. Tang, Y. Shen, P. Sun, S. Liu, J. Han, Y. Liu, H. Sun, D. Jia, Eur. J. Inorg. Chem. 2016 (2016) 3921–3926.
[101] J. Han, S. Li, C. Tang, W. Zheng, W. Jiang, D. Jia, RSC Adv. 8 (2018) 34078–34087.
[102] P. Sun, S. Liu, S. Li, L. Zhang, H. Sun, D. Jia, Inorg. Chem. 56 (2017) 6152–6162.
[103] P. Sun, J. Wu, Z. Wang, X. Wang, N. Chen, T. Wu, Dalton Trans. 50 (2021) 16473–16477.
[104] R. Jin, G. Li, S. Sharma, Y. Li, X. Du, Chem. Rev. 121 (2021) 567–648.
[105] I. Chakraborty, T. Pradeep, Chem. Rev. 117 (2017) 8208–8271.
[106] J. Yan, B.K. Teo, N. Zheng, Acc. Chem. Res. 51 (2018) 3084–3093.
[107] X.-J. Wang, T. Langetepe, C. Persau, B.-S. Kang, G.M. Sheldrick, D. Fenske, Angew. Chem. Int. Ed. 41 (2002) 3818–3822.
[108] C.E. Anson, A. Eichhöfer, I. Issac, D. Fenske, O. Fuhr, P. Sevillano, C. Persau, D. Stalke, J. Zhang, Angew. Chem. Int. Ed. 47 (2008) 1326–1331.
[109] P. Sun, X. Tang, W. Yang, X. Wang, R. Zhou, N. Chen, S.-F. Yuan, Inorg. Chem. 61 (2022) 9251–9256.
[110] P. Sun, M. Xie, L.-M. Zhang, J.-X. Liu, J. Wu, D.-S. Li, S.-F. Yuan, T. Wu, D. Li, Angew. Chem. Int. Ed. 61 (2022) e202209971.
[111] R. Langer, B. Breitung, L. Wünsche, D. Fenske, O. Fuhr, Z. Anorg, Allg. Chem. 637 (2011) 995–1006.
[112] K. Tang, X. Xie, L. Zhao, Y. Zhang, X. Jin, Eur. J. Inorg. Chem. 2004 (2004) 78–85.
[113] S. Chitsaz, D. Fenske, O. Fuhr, Angew. Chem. Int. Ed. 45 (2006) 8055–8059.
[114] S. Ahmar, D.G. MacDonald, N. Vijayaratnam, T.L. Battista, M.S. Workentin, J. F. Corrigan, Angew. Chem. Int. Ed. 49 (2010) 4422–4424.
[115] D. Fenske, C. Persau, S. Dehnen, C.E. Anson, Angew. Chem. Int. Ed. 43 (2004) 305–309.
[116] D. Fenske, C.E. Anson, A. Eichhöfer, O. Fuhr, A. Ingendoh, C. Persau, C. Richert, Angew. Chem. Int. Ed. 44 (2005) 5242–5246.

[117] J.-W. Liu, Z. Wang, Y.-M. Chai, M. Kurmoo, Q.-Q. Zhao, X.-P. Wang, C.-H. Tung, D. Sun, Angew. Chem. Int. Ed. 58 (2019) 6276–6279.
[118] H. Yang, J. Lei, B. Wu, Y. Wang, M. Zhou, A. Xia, L. Zheng, N. Zheng, Chem. Commun. 49 (2013) 300–302.
[119] W.-J. Zhang, Z. Liu, K.-P. Song, C.M. Aikens, S.-S. Zhang, Z. Wang, C.-H. Tung, D. Sun, Angew. Chem. Int. Ed. 60 (2021) 4231–4237.
[120] S. Yuan, Y.-K. Deng, X.-P. Wang, D. Sun, New J. Chem. 37 (2013) 2973–2977.
[121] S. Li, X.-S. Du, B. Li, J.-Y. Wang, G.-P. Li, G.-G. Gao, S.-Q. Zang, J. Am. Chem. Soc. 140 (2018) 594–597.
[122] H. Yang, Y. Wang, N. Zheng, Nanoscale 5 (2013) 2674–2677.
[123] X.-H. Ma, Y. Si, L.-L. Luo, Z.-Y. Wang, S.-Q. Zang, T.C.W. Mak, ACS Nano 16 (2022) 5507–5514.
[124] H. Yang, Y. Wang, H. Huang, L. Gell, L. Lehtovaara, S. Malola, H. Häkkinen, N. Zheng, Nat. Commun. 4 (2013) 2422.
[125] J. Chai, S. Yang, Y. Lv, T. Chen, S. Wang, H. Yu, M. Zhu, J. Am. Chem. Soc. 140 (2018) 15582–15585.
[126] J. Yan, J. Zhang, X. Chen, S. Malola, B. Zhou, E. Selenius, X. Zhang, P. Yuan, G. Deng, K. Liu, H. Su, B.K. Teo, H. Häkkinen, L. Zheng, N. Zheng, Natl. Sci. Rev. 5 (2018) 694–702.
[127] H. Yang, Y. Wang, X. Chen, X. Zhao, L. Gu, H. Huang, J. Yan, C. Xu, G. Li, J. Wu, A.J. Edwards, B. Dittrich, Z. Tang, D. Wang, L. Lehtovaara, H. Häkkinen, N. Zheng, Nat. Commun. 7 (2016) 12809.
[128] C.W. Liu, J.T. Pitts, J.P. Fackler, Polyhedron 16 (1997) 3899–3909.
[129] C.W. Liu, I.-J. Shang, J.-C. Wang, T.-C. Keng, Chem. Commun. (1999) 995–996.
[130] J.-H. Liao, H.-W. Chang, Y.-J. Li, C.-S. Fang, B. Sarkar, W.E. van Zyl, C.W. Liu, Dalton Trans. 43 (2014) 12380–12389.
[131] C.W. Liu, I.-J. Shang, R.-J. Fu, B.-J. Liaw, J.-C. Wang, I.J. Chang, Inorg. Chem. 45 (2006) 2335–2340.
[132] C.W. Liu, Y.-R. Lin, C.-S. Fang, C. Latouche, S. Kahlal, J.-Y. Saillard, Inorg. Chem. 52 (2013) 2070–2077.
[133] C.W. Liu, H.-W. Chang, B. Sarkar, J.-Y. Saillard, S. Kahlal, Y.-Y. Wu, Inorg. Chem. 49 (2010) 468–475.
[134] Z.-Y. Wang, M.-Q. Wang, Y.-L. Li, P. Luo, T.-T. Jia, R.-W. Huang, S.-Q. Zang, T.C. W. Mak, J. Am. Chem. Soc. 140 (2018) 1069–1076.
[135] J.-H. Huang, Y. Si, X.-Y. Dong, Z.-Y. Wang, L.-Y. Liu, S.-Q. Zang, T.C.W. Mak, J. Am. Chem. Soc. 143 (2021) 12439–12444.
[136] J.-H. Huang, Z.-Y. Wang, S.-Q. Zang, T.C.W. Mak, A.C.S. Cent, Sci. 6 (2020) 1971–1976.
[137] Z. Wang, L. Li, L. Feng, Z.-Y. Gao, C.-H. Tung, L.-S. Zheng, D. Sun, Angew. Chem. Int. Ed. 61 (2022) e202200823.
[138] Z. Wang, F. Alkan, C.M. Aikens, M. Kurmoo, Z.-Y. Zhang, K.-P. Song, C.-H. Tung, D. Sun, Angew. Chem. Int. Ed. 61 (2022) e202206742.
[139] R.-W. Huang, Y.-S. Wei, X.-Y. Dong, X.-H. Wu, C.-X. Du, S.-Q. Zang, T.C.W. Mak, Nat. Chem. 9 (2017) 689–697.
[140] X.-Y. Dong, Y. Si, J.-S. Yang, C. Zhang, Z. Han, P. Luo, Z.-Y. Wang, S.-Q. Zang, T.C. W. Mak, Nat. Commun. 11 (2020) 3678.
[141] R.-W. Huang, X.-Y. Dong, B.-J. Yan, X.-S. Du, D.-H. Wei, S.-Q. Zang, T.C.W. Mak, Angew. Chem. Int. Ed. 57 (2018) 8560–8566.
[142] X.-Y. Dong, H.-L. Huang, J.-Y. Wang, H.-Y. Li, S.-Q. Zang, Chem. Mater. 30 (2018) 2160–2167.
[143] M.J. Alhilaly, R.-W. Huang, R. Naphade, B. Alamer, M.N. Hedhili, A.-H. Emwas, P. Maity, J. Yin, A. Shkurenko, O.F. Mohammed, M. Eddaoudi, O.M. Bakr, J. Am. Chem. Soc. 141 (2019) 9585–9592.
[144] W.A. Dar, A. Jana, K.S. Sugi, G. Paramasivam, M. Bodiuzzaman, E. Khatun, A. Som, A. Mahendranath, A. Chakraborty, T. Pradeep, Chem. Mater. 34 (2022) 4703–4711.
[145] X.-H. Wu, P. Luo, Z. Wei, Y.-Y. Li, R.-W. Huang, X.-Y. Dong, K. Li, S.-Q. Zang, B. Z. Tang, Adv. Sci. 6 (2019) 1801304.
[146] X.-H. Wu, Z. Wei, B.-J. Yan, R.-W. Huang, Y.-Y. Liu, K. Li, S.-Q. Zang, C.W. Mak Thomas, CCS Chem. 1 (2019) 553–560.
[147] M. Cao, R. Pang, Q.-Y. Wang, Z. Han, Z.-Y. Wang, X.-Y. Dong, S.-F. Li, S.-Q. Zang, T.C.W. Mak, J. Am. Chem. Soc. 141 (2019) 14505–14509.
[148] M. Zhao, S. Huang, Q. Fu, W. Li, R. Guo, Q. Yao, F. Wang, P. Cui, C.-H. Tung, D. Sun, Angew. Chem. Int. Ed. 59 (2020) 20031–20036.
[149] C.-H. Gong, Z.-B. Sun, M. Cao, X.-M. Luo, J. Wu, Q.-Y. Wang, S.-Q. Zang, T.C. W. Mak, Chem. Commun. 58 (2022) 9806–9809.
[150] Ø. Fischer, A. Treyvaud, R. Chevrel, M. Sergent, Superconductivity in the RexMo6S8, in: H.R. Ott (Ed.), Ten Years of Superconductivity: 1980–1990, Springer, Netherlands, Dordrecht, 1993, pp. 53–56.
[151] R. Chevrel, M. Hirrien, M. Sergent, Polyhedron 5 (1986) 87–94.
[152] E.A. Doud, A. Voevodin, T.J. Hochuli, A.M. Champsaur, C. Nuckolls, X. Roy, Nat. Rev. Mater. 5 (2020) 371–387.
[153] R. Chevrel, M. Sergent, J. Prigent, J. Solid State Chem. 3 (1971) 515–519.
[154] R. Hernández Sánchez, A.M. Champsaur, B. Choi, S.G. Wang, W. Bu, X. Roy, Y.-S. Chen, M.L. Steigerwald, C. Nuckolls, D.W. Paley, Angew. Chem. Int. Ed. 57 (2018) 13815–13820.
[155] A.M. Champsaur, A. Velian, D.W. Paley, B. Choi, X. Roy, M.L. Steigerwald, C. Nuckolls, Nano Lett. 16 (2016) 5273–5277.
[156] J.R. Long, L.S. McCarty, R.H. Holm, J. Am. Chem. Soc. 118 (1996) 4603–4616.
[157] O.M. Yaghi, M.J. Scott, R.H. Holm, Inorg. Chem. 31 (1992) 4778–4784.
[158] J.R. Long, A.S. Williamson, R.H. Holm, Angew. Chem. Int. Ed. 34 (1995) 226–229.
[159] M.W. Willer, J.R. Long, C.C. McLauchlan, R.H. Holm, Inorg. Chem. 37 (1998) 328–333.
[160] Z. Zheng, J.R. Long, R.H. Holm, J. Am. Chem. Soc. 119 (1997) 2163–2171.
[161] Z. Zheng, T.G. Gray, R.H. Holm, Inorg. Chem. 38 (1999) 4888–4895.
[162] H.D. Selby, Z. Zheng, T.G. Gray, R.H. Holm, Inorg. Chim. Acta 312 (2001) 205–209.
[163] B.K. Roland, H.D. Selby, M.D. Carducci, Z. Zheng, J. Am. Chem. Soc. 124 (2002) 3222–3223.
[164] B.K. Roland, W.H. Flora, N.R. Armstrong, Z. Zheng, C. R. Chim. 8 (2005) 1798–1807.
[165] R. Wang, Z. Zheng, J. Am. Chem. Soc. 121 (1999) 3549–3550.
[166] B.K. Roland, C. Carter, Z. Zheng, J. Am. Chem. Soc. 124 (2002) 6234–6235.
[167] H.D. Selby, B.K. Roland, Z. Zheng, Acc. Chem. Res. 36 (2003) 933–944.
[168] H.D. Selby, P. Orto, M.D. Carducci, Z. Zheng, Inorg. Chem. 41 (2002) 6175–6177.
[169] H.D. Selby, P. Orto, Z. Zheng, Polyhedron 22 (2003) 2999–3008.
[170] Y.M. Litvinova, Y.M. Gayfulin, K.A. Kovalenko, D.G. Samsonenko, J. van Leusen, I.V. Korolkov, V.P. Fedin, Y.V. Mironov, Inorg. Chem. 57 (2018) 2072–2084.
[171] G. Liu, A. Pinkard, S.M. Ciborowski, V. Chauhan, Z. Zhu, A.P. Aydt, S.N. Khanna, X. Roy, K.H. Bowen, Chem. Sci. 10 (2019) 1760–1766.
[172] M.L. Steigerwald, T. Siegrist, S.M. Stuczynski, Inorg. Chem. 30 (1991) 4940–4945.
[173] A.M. Champsaur, T.J. Hochuli, D.W. Paley, C. Nuckolls, M.L. Steigerwald, Nano Lett. 18 (2018) 4564–4569.
[174] D.A. Reed, T.J. Hochuli, N.A. Gadjieva, S. He, R.A. Wiscons, A.K. Bartholomew, A. M. Champsaur, M.L. Steigerwald, X. Roy, C. Nuckolls, J. Am. Chem. Soc. 144 (2022) 306–313.
[175] A.M. Champsaur, C. Mézière, M. Allain, D.W. Paley, M.L. Steigerwald, C. Nuckolls, P. Batail, J. Am. Chem. Soc. 139 (2017) 11718–11721.
[176] A.M. Champsaur, J. Yu, X. Roy, D.W. Paley, M.L. Steigerwald, C. Nuckolls, C. M. Bejger, A.C.S. Cent, Sci. 3 (2017) 1050–1055.
[177] X. Chia, A.Y.S. Eng, A. Ambrosi, S.M. Tan, M. Pumera, Chem. Rev. 115 (2015) 11941-11966.
[178] J. Wang, Y. Wang, D. Zhang, C. Chen, Z. Yang, A.C.S. Appl, Nano Mater. 4 (2021) 7698–7711.
[179] K. Hegetschweiler, T. Keller, H. Zimmermann, W. Schneider, H. Schmalle, E. Dubler, Inorg. Chim. Acta 169 (1990) 235–243.
[180] J.M. Garriga, R. Llusar, S. Uriel, C. Vicent, A.J. Usher, N.T. Lucas, M. G. Humphrey, M. Samoc, Dalton Trans. (2003) 4546–4551.
[181] R. Llusar, S. Uriel, C. Vicent, J.M. Clemente-Juan, E. Coronado, C.J. Gómez-García, B. Braïda, E. Canadell, J. Am. Chem. Soc. 126 (2004) 12076–12083.
[182] R. Llusar, S. Triguero, V. Polo, C. Vicent, C.J. Gómez-García, O. Jeannin, M. Fourmigué, Inorg. Chem. 47 (2008) 9400–9409.
[183] M.N. Sokolov, A.L. Gushchin, D.Y. Naumov, O.A. Gerasko, V.P. Fedin, Inorg. Chem. 44 (2005) 2431–2436.
[184] S. Duval, J. Marrot, C. Simonnet-Jégat, E. Cadot, Solid State Sci. 11 (2009) 56–60.
[185] M.N. Sokolov, A.L. Gushchin, K.A. Kovalenko, E.V. Peresypkina, A.V. Virovets, J. Sanchiz, V.P. Fedin, Inorg. Chem. 46 (2007) 2115–2123.
[186] Z. Ji, C. Trickett, X. Pei, O.M. Yaghi, J. Am. Chem. Soc. 140 (2018) 13618–13622.
[187] N.E. Horwitz, J. Xie, A.S. Filatov, R.J. Papoular, W.E. Shepard, D.Z. Zee, M. P. Grahn, C. Gilder, J.S. Anderson, J. Am. Chem. Soc. 141 (2019) 3940–3951.
[188] O. Salinas, J. Xie, R.J. Papoular, N.E. Horwitz, E. Elkaim, A.S. Filatov, J. S. Anderson, Dalton Trans. 50 (2021) 10798–10805.
[189] J.H. Gillen, C.A. Moore, M. Vuong, J. Shajahan, M.R. Anstey, J.R. Alston, C. M. Bejger, Chem. Commun. 58 (2022) 4885–4888.